République Algérienne Démocratique et Populaire
Ministère de l'Enseignement supérieur et de la Recherche Scientifique

Ecole Nationale Polytechnique
Département de Génie Mécanique
Laboratoire de Génie Mécanique et Développement

Thesis

Presented for obtaining the

Doctor's degree

In Mechanical Engineering

Option: Clean and Renewable Energy Mechanical Systems

Thermodynamic and Economic Study of Two Configurations of Solar Thermal Power Plants

---

by
Madjid Amani

Defended on September 28, 2021 before the jury members composed of:

Mr. Salah Larbi	Professor, ENP, Algiers, Algeria	Chair
Mr. Adel Ghenaiet	Professor, USTHB, Algiers, Algeria	Supervisor
Mr. Arezki Smaili	Professor, ENP, Algiers, Algeria	Co-Supervisor
Mr. Kamel Boughrara	Professor, ENP, Algiers, Algeria	Examiner
Mr. Rabah Dizene	Professor, USTHB, Algiers, Algeria	Examiner
Mr. M.Moundji Hadjiat	Doctor, CDER	Examiner

ENP 2021

10, Avenue des Frères Oudek, Hassen Badi, BP.182, 16200 El Harrach, Alger, Algérie
www.enp.dz

République Algérienne Démocratique et Populaire
Ministère de l'Enseignement supérieur et de la Recherche Scientifique

Ecole Nationale Polytechnique
Département de Génie Mécanique
Laboratoire de Génie Mécanique et Développement

Thesis

Presented for obtaining the

Doctor's degree

In Mechanical Engineering

Option: Clean and Renewable Energy Mechanical Systems

Thermodynamic and Economic Study of Two Configurations of Solar Thermal Power Plants

---

by
Madjid Amani

Defended on September 28, 2021 before the jury members composed of:

Mr. Salah Larbi	Professor, ENP, Algiers, Algeria	Chair
Mr. Adel Ghenaiet	Professor, USTHB, Algiers, Algeria	Supervisor
Mr. Arezki Smaili	Professor, ENP, Algiers, Algeria	Co-Supervisor
Mr. Kamel Boughrara	Professor, ENP, Algiers, Algeria	Examiner
Mr. Rabah Dizene	Professor, USTHB, Algiers, Algeria	Examiner
Mr. M.Moundji Hadjiat	Doctor, CDER	Examiner

ENP 2021

10, Avenue des Frères Oudek, Hassen Badi, BP.182, 16200 El Harrach, Alger, Algérie
www.enp.dz

République Algérienne Démocratique et Populaire
Ministère de l'Enseignement supérieur et de la Recherche Scientifique

Ecole Nationale Polytechnique
Département de Génie Mécanique
Laboratoire de Génie Mécanique et Développement

Thèse de Doctorat

En vue d'obtention du grade de

DOCTEUR

en Génie Mécanique

Option: Systèmes Mécaniques à Energies Propres Renouvelables

Etude Thermodynamique et Economique de Deux Configurations de Centrales Hybrides Solaire-Gaz

---

Présentée par
Madjid AMANI

Soutenue le 28 Septembre 2021 devant le jury constitué de:

Mr. Salah LARBI	Professeur, ENP	Président
Mr. Adel GHENAIET	Professeur, USTHB	Directeur de thèse
Mr. Arezki SMAILI	Professeur, ENP	Co-Directeur
Mr. Kamel BOUGHRARA	Professeur, ENP	Examinateur
Mr. Rabah DIZENE	Professeur, USTHB	Examinateur
Mr. M.Moundji HADJIAT	Maître de recherche A, CDER	Examinateur

ENP 2021

10, Avenue des Frères Oudek, Hassen Badi, BP.182, 16200 El Harrach, Alger, Algérie
www.enp.dz

Dedication

I would like to dedicate this modest work:

To my parents and my siblings, To Amani family, To Akkouche family, To Beldjenna family, To Akkache family, To Hassina Amrane, To my Ikouvaane village and To the guardians of Kabyle and Amazigh culture.

Tribute to A. Imache, F. Ali, S. Azem, M.A. Bessaoud, M. Mammerie, M. Haroun (Masin U Harun), A. Zamoum, A. Mohya, L. Matoub, F. Mehenni, L. Ait Menguellet, Idir, Y. Adli et al and JSK.
"Tamurt n Leqvayel"

In the memory of Sir. Isaac Newton,

The greatest scientist and theologian
whose concern was only to decode the mind of GOD, the Almighty.

1643-1727

"In the absence of any other proof, the thumb alone would convince me of God's existence"

Tanemmirt i vav igenwan, Illu-nney a Yiwen!

ACKNOWLEDGEMENTS

I would like to express my sincere gratitude to **Pr. Adel Ghenaiet** for his guidance and wisdom sharing during my whole Doctoral program. He was kind and courageous enough to accept me as a PhD student. I especially appreciate that he gave me the freedom to do my own research while, at the same time, guiding me in the right direction. I deeply appreciate the support from him, who continuously provided feedback on my work and helped me develop my research skills. I am very grateful to him for the quality of advises that he gave me. I am grateful to him for all the scientific and the pedagogical help that he gave me during the preparation of the present thesis: his availability and his valuable recommendations. **Pr. Adel Ghenaiet** schooled me the sense of analysis, without his deep experience research in thermodynamic field and without his precious support it would not be possible to conduct this research.

I would also like to express my sincere gratitude to **Pr. Arezki Smaili** for his continuous support of my Doctoral program and related research, for his patience, motivation, and immense knowledge. I am very grateful to him for the quantity and the quality of the scientific information he gave me mainly in solar and economic assessment. I am very grateful for his availability throughout the project, for providing me an excellent environment with the necessary material to achieve my research project. **Pr. Smaili** was my teacher in the mechanical engineering study and I received a valuable heat transfer courses and the quality knowledge that I found really useful along my Ph.D program. In addition, I should mention that I learnt two precious qualities from him, the first one is the **Notion of Time** and the second one is the **parallel work on different tasks** that I found as a perfect tool to face hard situations. His guidance helped me in all the time of research and writing of this thesis. I have to thank him for the opportunity he gave me to let me follow my Doctoral thesis while I am a full time worker in the industrial field, otherwise if he was not being understandable maybe this work could not be achieved. Consequently, I am deeply indebted to my **Pr. Arezki Smaili** for his fundamental role in my doctoral work.

I would also like to thank members of my thesis committee: Pr. Salah Larbi (Professor, ENP, Algiers), Pr. Kamel Boughrara (Professor, ENP, Algiers), Pr. Rabah Dizene (Professor, USTHB,

Algiers) and Dr. Mohammed Moundji Hadjiat (Doctor, CDER) for accepting to review and evaluate this thesis.

Special thanks to Mr. Slimane Hadioui (Ccix Sliman) for his good teaching. He was the first teacher of mine and along the primary school period without him maybe I am not who I am now.

I would like to thank Mr. Mohammed Amokrane Mahdi, Mr. Samir Ouchene and Mrs Nassima Gharsa with her husband Mr. Ahmed Said Ghalem (department heads at Algerian Petroleum Institute) for the quality of the scientific information that they gave me. Also, I thank the smart boy Daoud Bousnane my best friend at Algerian Petroleum Institute and my Ph.D friends at Polytechnic school include Zakaria Baka, Karim Kaced, Moussaab Bounabi and Choayb Bouhafs.

I thank all those who helped me and supported me from near or far,

Thank you very much to all.

Thanks GOD and Thanks Parents

Madjid (Mokrane)

ملخص

الهدف الأساسي من هذه الأطروحة هو دراسة الديناميكا الحرارية والاقتصادية لمحطتين حراريتين مختلفتين لتوليد الكهرباء بتهجين الغاز و الشمس (ISCC). تقوم المحطة الأولى بدمج تقنية الطاقة الشمسية المركزة باستخدام مرايا القطع المكافئ في دورة مركبة لتكوين نظام ISCC-PTC أين يتم إدخال الحرارة الشمسية في الدورة البخارية. أمّا المحطة الثانية فهو نموذج جديد مقترح تعمل بدمج نظام برج مركزي للطاقة الشمسية لتكوين محطة ISCC-SPT. وهذه الأخيرة تقوم بدمج الحرارة الشمسية كحرارة محسوسة لتسخين تيارات غازية ساخنة عادمة للاستفادة الخارجة من العنفة الغازية .بالتالي هذا الإدماج الشمسي ببرج مركزي يلعب دور إحتراق إضافي. يسجل تحليل الأداء الحراري قيم مردودية عامة عالية خلال النهار لكل من ISCC-PTC و ISCC-SPT وهما بنسب 59 ٪ و 64٪ أعلى بكثير من القيمة الليلية أو أثناء الأيام الملبّدة بالغيوم عندما تعمل المحطة في وضع CC. وزيادة على ذلك، فإنّ التقييم الاقتصادي لتكلفة الكهرباء المولدة و المعبّرة عنها بتكلفة الطاقة المستوية (LCOE) تبلغ 0.0222 دولار/ كيلوواط ساعي للنّظام ISCC-PTC و0.0301 دولار/ كيلوواط ساعي للنّظام ISCC-SPT. وهذه القيمتان يمكن تخفيضهما من خلال الإستمثال و تصبحان تنافسية عندما تكون تكلفة البيئة أخذت بعين الاعتبار. إضافة إلى ذلك، قمنا بمقاربة آنية وسنوية للأداء الحراري لهاتين التشكيلتين حيث كشفت النتائج التي تم الحصول عليها من خلال أداء المحطة ISCC-SPT كانت هي الأحسن من من ناحية الكفاءة و المردودية خاصة و التيّ تظهر تحسنات ملحوظة في مردودية تحويل الطاقة الشمسية إلى الكهرباء خلال السنة. أمّا من حيث المقاربة الاقتصادية، تُظهر كلتا المحطتين تقريبا نفس قيمة LCOE وهما بحوالي 0.0297 دولار/ كيلوواط ساعي و 0.0269 دولار/ كيلوواط ساعي للنّظامين ISCC-SPT و ISCC-PTC على التوالي. وعلاوة على ذلك، يمنح هاذين النظامين للمحطات الهجينة بحفظ الوقود بكمية كبيرة وتقليل الانبعاثات الملوثة خلال مدة التشغيل. لذلك في المجمل، تسمح لنا كل هذه النتائج باستنتاج أنّ تقنية تهجين الطاقة الشمسية المركزة في دورة مركبة يبدو خيارًا واعدًا، كونها من الناحية التقنية والاقتصادية قابلة للتطبيق طوال مدة الاستعمال.

الكلمات المفتاحية: محطة الطاقة الهجينة؛ برج الطاقة الشمسية؛ مولد بخار استرداد الحرارة؛ الأداء الحراري الاقتصادي؛ تكلفة الطاقة المستوية.

Résume

La présente thèse porte sur l'étude thermodynamique et économique de deux différentes centrales hybrides solaire-gaz (ISCC). La première centrale intègre la technologie à concentration solaire via les collecteurs cylindro-paraboliques (PTC) dans un cycle combiné (CC) pour constituer le système ISCC-PTC. Dans ce système, l'énergie solaire thermique est introduite dans le cycle à vapeur. La seconde centrale intègre le système à tour solaire (SPT) pour constituer la centrale ISCC-SPT. Cette dernière est une configuration nouvelle proposée qui intègre l'énergie solaire thermique comme une chaleur sensible pour chauffer les gaz d'échappement de la turbine à gaz. Par conséquent, cette intégration à tour solaire joue donc le rôle du poste de combustion supplémentaire. L'analyse des performances thermiques montre des valeurs élevées du rendement globale pendant la journée pour les deux systèmes ISCC-PTC et ISCC-SPT, qui sont respectivement d'environ 59 % et 64 %. Ces performances sont beaucoup plus élevées que celles de la nuit et les temps nuageux au moment que les centrales fonctionnent en mode CC. En outre, l'évaluation économique du coût de l'électricité exprimé par le coût actualisé de l'énergie (LCOE) est d'environ 0.0222 $/kWh pour l'ISCC-PTC et de 0.0301 $/kWh pour l'ISCC-SPT. Ces valeurs pourraient être réduites par une optimisation, et deviennent compétitives lorsque le coût environnemental est pris en considération. Ainsi, une étude comparative des performances instantanées et annuelles entre ces deux configurations d'ISCC est également réalisée. Les résultats obtenus révèlent que l'ISCC-SPT donne de meilleures performances par rapport à celles de la centrale ISCC-PTC et qu'elle montre des améliorations notables du rendement en terme de conversion du solaire en électricité tout au long de l'année. Tandis que la comparaison économique affiche des valeurs approximatives de LCOE, et qui sont d'environ 0.0297 $/kWh and 0.0269 $/kWh pour l'ISCC-SPT et l'ISCC-PTC respectivement. Ajoutant, ces deux centrales solaires thermiques offrent une importante économie de carburant et moins d'émissions polluantes pendant toute leur durée de vie. En conséquence, tous ces résultats permettent de conclure que l'intégration de la technologie à concentration solaire dans un CC est une option prometteuse, car techniquement et économiquement est viable tout au long de sa vie de fonctionnement.

Mots-clés: Centrale thermique hybride solaire-gaz; Tour solaire; Chaudière de récupération; Performances thermo-économiques; Coût actualise de l'énergie.

Abstract

The present thesis is concerned with thermodynamic and economic investigations of two different integrated solar combined cycle (ISCC) plants. The first plant integrates a parabolic trough collector (PTC) technology into a combined cycle (CC) to constitutem the ISCC-PTC system where solar heat is introduced in the steam cycle and the second one is integrating a solar power tower (SPT) system to compose the ISCC-SPT. The latter is a proposed configuration which integrates solar thermal energy as sensible heat to heat up the exhaust gases from the gas turbine, thus solar integration plays the role of supplementary firing. The thermal performances analysis shows high thermal efficiency values during the day for both ISCC-PTC and ISCC-SPT which are about 59 % and 64 % respectively much higher when they work as a CC mode during night or cloudy periods. In addition, the economic assessment for the electricity cost expressed by the levelized cost of energy (LCOE) are about 0.0222 $/kWh for the ISCC-PTC and 0.0301 $/kWh for the ISCC-SPT. These LCOE values could be reduced through an optimization and become competitive when the environment cost is taken into consideration. Also, a comparative study of instantaneous and annual performances between these two ISCC configurations is carried out. The obtained results reveal that ISCC-SPT performs better than ISCC-PTC and it shows noticeable enhancements in solar-to-electric efficiency throughout the year. In terms of economic comparison, both power plants show approximately the same LCOE value of about 0.0297 $/kWh and 0.0269 $/kWh for ISCC-SPT and ISCC-PTC respectively. Furthermore, these two solar systems permit an important fuel saving and less pollutant emission during the operating lifetime. All these outcomes allow concluding that integration of concentrating solar technologies into a CC is a promising option as it is technically and economically viable over the operating lifetime.

Keywords: Integrated solar combined cycle; Solar power tower; Heat recovery steam generator; Thermo-economic performance; Levelized cost of energy.

Table of Contents

List of Figures

List of Tables

List of Symbols

Nomenclature

A	Surface area [m^2]
C_L	Number of lines in the parabolic solar field
C_p	Specific heat [J/kg K]
$\overline{C_p}$	Mean specific heat [J/kg K]
DNI	Direct Normal Irradiation [W/m^2]
e	Fraction of air cooling
f	Ratio of the fuel and air mass flow rates
f_{clean}	Cleanliness factor
$f_{end\ loss}$	Geometrical end losses factor
f_{PTC}	Focal length of the parabolic trough collector [m]
$f_{row\ shadow}$	Shading factor
F_g	Gas property factor
h_{fc}	Forced convection coefficient [W/m^2 K]
h_{nc}	Natural convection coefficient [W/m^2 K]
h	Enthalpy [kJ/kg]
H	Height of the volumetric receiver aperture [m]
H_{sr}	Sunrise time [hour]
H_{ss}	Sunset time [hour]
$\vec{i}$	Unit vector from the center of the heliostat pointing to the target
I_{sc}	Solar constant [W/m^2]
I_{so}	Extraterrestrial radiation [W/m^2]
k	Thermal conductivity [W/m K]
k_{air}	Air conduction coefficient [W/m^2 K]
k_g	Gas unit cost factor [%]
k_s	Steam unit cost factor [%]
k_{sol}	Solar field cost factor [%]
K	Incidence angle modifier
L_{PTC}	Length of a single parabolic trough collector [m]

L_{space}	Distance between two parallel parabolic collectors [m]
$LMTD$	Log-Mean Temperature Difference [°K]
$\dot{m}$	Mass flow rate [kg/s]
M	Thermodynamic state point for mixture water/steam
n	Day number
$\vec{n}$	Unit normal vector of the heliostat surface
N	Number of heliostats
N_L	Number of collectors in each row of the parabolic solar field
Nu	Nusselt number and given as follows: $Nu = 0.0287 R_e^{0.8} Pr^{1/3}$
P_{fw}	Pressure of feed water [bar]
Pr	Prandtl number and given as follows: $Pr = \frac{C_p u}{k}$
Q	Thermal energy or duty [W]
Q_{cv}	Lower Heating Value of natural gas (kJ/kg)
Q_{fuel}	Power of fuel consumed by Gas turbine [W]
$Q_{PTC\ solar\ field}$	Total useful solar thermal energy gained by the parabolic solar field [W]
Q_1	Superheater duty [W]
Q_2	Evaporator duty [W]
Q_3	Economizer duty [W]
Re	Reynolds number
S_{helio}	Heliostat surface [m^2]
S_r	Volumetric receiver surface [m^2]
S_0	Distance between heliostat and receiver
Sol,el,rat	Solar electric ratio
T	Temperature [°K]
T_{hrsg1}	Exhaust gases inlet temperature into HRSG [°K]
T_{hrsg2}	Exhaust gases inlet temperature into the evaporator of the HRSG [°K]
T_{hrsg3}	Exhaust gases inlet temperature into the economizer of the HRSG [°K]
T_{hrsg4}	Exhaust gases outlet temperature from the HRSG [°K]
T_{s2}	Superheated steam outlet temperature from the HRSG [°K]
T_{w1}	Feed water inlet temperature into the economizer [°K]
T_{w2}	Feed water inlet temperature into the evaporator [°K]
T_1	Compressor inlet temperature [°K]
T_2	Compressor outlet temperature [°K]

T_3	Turbine inlet temperature [°K]
T_4	Turbine outlet temperature [°K]
U	Overall heat transfer coefficient [W/m^2 K]
UA	Product of U and surface area A [W/K]
V_w	Wind velocity [m/s]
W	Work or power [MW]

Greek symbols

α	Absorptivity
γ	Specific heat ratio
γ_{col}	Intercept factor of the parabolic trough collector
δ	Declination angle
H	Efficiency
η_b	Combustion efficiency
η_{cs}	Isentropic efficiency of the compressor
$\eta_{nominal}$	Nominal optical efficiency of the parabolic trough collector
η_m	Steam turbine mechanical efficiency
η_{pc}	Compressor polytropic efficiency
η_{pt}	Turbine polytropic efficiency
η_{ts}	Isentropic efficiency of the turbine
η_o	Optical efficiency for the parabolic trough collector
θ	Incidence angle
θ_z	Angle or zenith angle
ε	Receiver emissivity
μ	Exhaust gases dynamic viscosity [kg/m s]
μ_{air}	Air dynamic viscosity [kg/m s]
ρ_{air}	Air density [kg/m^3]
ρ_{col}	Reflectance of the clean parabolic trough collector
σ	Stefan–Boltzmann constant [W/m^2 K^4]
σ_{tot}	Dispersion of the reflected beam, mrad
σ_{solar}	Dispersion of sunlight, mrad
σ_{mirror}	Dispersion due to mirror slope error, mrad
σ_{track}	Dispersion due to tracking errors, mrad

π	Pressure ratio
τ_b	Atmospheric transmittance
τ_{cov}	Transmittance of the glass envelope for parabolic collector receiver
ϕ	Latitude
ω	Hour angle
ω_s	Sunrise hour angle
Subscripts	
a	Air or assumed
abs	Absorber or absorbed
atm	Atmospheric
ap	Approach point
b	Blade
c	Reflection or collection of Parabolic collector or heliostat field area
C	compressor
col	Collector
cool	Cooling
cos	Cosinus
d	Design
e	Electric
elec	Electric
f	Fuel or fluid
fc	Forced convection
f,in	Fluid inlet
f,out	Fluid inlet
g	Gas
helio	Heliostat
hrsg	Heat recovery steam generation
i	Inlet
loss	Losses
nc	Natural convection
o	Outlet
opt	Optical
p	Aperture area or pump

pip	Pipe
pp	Pinch point
r	Receiver
rad	Radiation
rec	Receiver
ref	Reflectivity
s	Steam, superheated steam or isentropic transformation
sat	Saturated
sb	Shading and blocking
sol	Solar
spill	Spillage
sr	Sunrise
ss	Sunset
ST	Steam turbine or Solar tower
t	Transfer
T	Turbine
tr	Transfer
th	Thermal
u	Useful
w	Water
z	Zenith

Abbreviations

ap	Approach point
C	Capital cost [$]
C_c	Concentration ratio
C_g	Specific cost of gas unit [$/kW]
C_s	Specific cost of steam unit [$/kW]
$C_{sol,Helio}$	Specific cost of heliostats field [$/kW]
$C_{sol,PTC}$	Specific cost of parabolic collectors field [$/kW]
$C_{sol,Tow}$	Specific cost for tower with receiver [$/kW]
CC	Combined cycle
CRF	Cost recovery factor
CSP	Concentrated solar power

DNI	Direct normal irradiation [W/m^2]
DNI_an	Annual direct normal irradiation [kWh/m^2 yr]
DSG	Direct Steam generation
GT	Gas turbine
HCE	Heat collector element
HLJ	Hottel, Liu and Jordan
HRSG	Heat recovery steam generation
HTF	Heat transfer fluid
ISCC	Integrated solar combined cycle
ISCC-PTC	Integrated solar combined cycle using parabolic trough collector technology
ISCC-SPT	Integrated solar combined cycle using solar power tower system
LCOE	Levelized Cost of Energy ($/kWh)
LMTD	Logarithmic mean temperature difference [K]
MWe	Megawatt electricity
MWth	Megawatt thermal
NTU	Number transfer unit
PTC	Parabolic trough collectors
O&M	Operation and Maintenance [$]
pp	Pinch point
PTC	Parabolic trough collector
PVF	Annual fuel cost [$]
P_{fw}	Feed water pressure [bar]
Pel_an	Annual electrical energy production [kWh]
R	Discount rate
SF	Solar fraction
SFC	Specific fuel consumption [kg/MWh]
SPT	Solar power tower
SSG	Solar steam generation
ST	Steam turbine
TES	Thermal energy storage

Introduction

As the world supply of fossil energy sources decreases, the need for energy conservation, efficient energy conversion and developing renewable energy technologies becomes ever more critical. Global energy consumption has increased very rapidly leads to the global warming which is largely the result of the emission of radiation-trapping gases, such as carbon dioxide and methane, into the atmosphere as a consequence an increase in the average global temperature [1]. A viable alternative to alleviate the situation is the integration of renewable sources such as concentrated solar thermal power (CSP) with combined cycles or steam cycles, resulting in reduced capital cost and continuous power supply. CSP technology includes parabolic trough collector (PTC), linear Fresnel collector (LFR), parabolic dish collector (PDC) and central receiver system (CRS) is the most likely candidate for providing the majority of this renewable energy, because it is among the most cost-effective renewable electricity technologies and because its supply is not restricted if the energy generated is transported from the world's solar belt to the population centres [1].

Parabolic trough collector (PTC) technology and central receiver system (CRS) have demonstrated their technical feasibility where the former at present is the most mature and proven CSP technology [1]. PTC technology is hybridized in numerous ways as it is integrated into a CC to constitute an Integrated Solar Combined Cycle (ISCC) power plant and several of such solar thermal power plants are commercialized and operating all around the world. Also, the integration of solar power tower (SPT) or the CRS in ISCC system is catching the attention of both researchers and power production experts since it is more attractive than stand-alone CSP technology in terms of solar conversion into electricity and cost. Some commercial SPT plants working in solar only are operating in different part of the world. The maturity level of the SPT technology is lower than that of the PTC and most of the ISCC plants in operation today employ the PTC technology with no known commercial ISCC that uses SPT system [2].

Algeria has planned to install about 7 GW of concentrating solar power plants by 2030. During the period of 2021-2030 [3], an annual capacity of 500 MW would be installed by 2023, and 600 MW per year after that [4]. Hence, these important investments require accurate selection of the most suitable technology that would be installed. According to the literature, very limited research was dedicated to the development of SPT coupled with CC

and most of ISCC power plants are still those using PTC technology, whereas SPT plants with Jülich concept are running in a solar-only plant [2].

The aim of the present work is thermal performance and economic investigations of two different ISCC configurations, one which adopts the PTC technology (ISCC-PTC) and the second which is driven by the SPT system (ISCC-SPT). The first configuration concerns the first ISCC plant installed in Hassi R'mel since the aim of this installation is to serve as a pilot project for further installations throughout the national territory; and most published works regarding this kind of ISCC layout have been devoted on thermal performances investigation with no economic assessment for the electricity production. Hence, a thermo-economic model is developed to simulate such kind of configuration in terms of thermal performances and solar to electric conversion with taking into account the economic aspect for the electricity generation expressed by the levelized cost of energy (LCOE). The second investigated ISCC plant is a new hybridization of SPT system with an open volumetric air receiver into a CC. This new proposed ISCC-SPT solar thermal power plant layout is to fill the existing lack related to the integration of a SPT system into a CC where very limited research has been consecrated to the development of such system [2]. We note that all SPT systems in operation today are in solar only plant with no commercialized ISCC driven by a SPT. Consequently, the investigation of the new ISCC-SPT plant from thermal performances and economic aspects is to prove its feasibility and viability; and assess the maturity level of such hybridization of SPT system into a CC.

The solar model adopted in this study is based on Hottel, Liu and Jordan model to evaluate the amount of the Direct Normal Irradiation (DNI) received by CSP at any geographic location. The thermodynamic analysis for Brayton and Rankine cycle is detailed to calculate the quantity of steam mass flow generated in the Rankine cycle in design and off-design modes using Ganapathy's method. Furthermore, the economic issue is considered to demonstrate their technical feasibility; thereby the levelized cost of energy (LCOE) model is adopted for the economic assessment. The thermodynamic and economic developed models both are running under MATLAB code. As a result, a comparison between the two different ISCC configurations is conducted in terms of performance to find out the most efficient system based on solar-to-electric efficiency and the maturity level with taking into consideration the cost of the electricity produced.

The work is described on five steps as follows:

First, an overview of CSP technologies is given to show how different concentrating solar systems convert solar radiation into electricity with current status of existing solar thermal

power plants. Thus, different configurations of solar thermal plants that integrate CSP technologies have existed, some are in operating all over the world and some are under development. Also, every CSP technology integrated with the thermodynamic power block is described in this section. **Secondly,** the state of the art for this type of solar thermal systems with various configurations is reported. In this section, several techniques of solar integration into thermodynamic blocks are presented with the main focus on the PTC and SPT technologies. Through the current status of solar thermal power plants, the most mature system is noticed and the lack of study due to limited research for some aspect is revealed. **Thirdly,** the first integrated solar combined cycle (ISCC) in Algeria is studied from thermal performances point of view and economic issue. The solar thermal power plant consists of a PTC solar field integrated to a CC plant. The latter is composed of two GTs with a capacity of 47 MW for each one and a Rankine power block of two HRSGs single pressure and a steam turbine. The solar thermal plant works as ISCC during the day while solar radiation is available and as CC during the night. This is one way to retain power dispatchability, and subsequently the thermal storage could be eliminated or significantly reduced for a solar hybrid plant. The thermal study of this configuration is simulated for the 21st of March under an average ambient temperature value of the day; therefore the solar and thermodynamic models are carried out in MATLAB programming. The results show high thermal performances during the day when solar radiation reaches its maximum at solar noon with a maximum of electricity production. Furthermore, the electricity cost of such ISCC configuration is assessed by using the LCOE method to demonstrate its viability and feasibility for further installations. The present solar thermal plant is registered among the ambitious renewable energy program of Algeria at the horizon 2030. Economic analysis of such span projects is required to demonstrate their technical feasibility and we note that most of published works related to this program are focused on thermal performance study. Consequently, the obtained results from this investigation can provide some guidelines and suggestions for future installations of such solar thermal power technology. **Fourthly**, a novel configuration of an ISCC based on SPT technology is proposed. The concentrated solar radiation onto the volumetric receiver is used as a supplementary firing which leads HRSG operate in fired mode. In contrast to solarized GT where major modifications are required to resist to pressure more than 15 bar, this configuration with an open volumetric air receiver has the advantage of simplicity as the flue gases from GT are at atmospheric pressure, and doesn't require a solar steam generator (SSG) between the Rankine and the solar power blocks. The gases are at low pressure and the temperature difference across receiver is not too high,

inducing less stress on the receiver. Since the system works as an ISCC during the day and as a CC during night, no Thermal Energy Storage (TES) is considered in this analysis. The thermodynamic analysis of the new ISCC layout with a SPT is investigated in details. Therefore, the analysis shows how the present technique of solar integration increases thermal performances and the efficiency of solar to electric conversion. Therefore, complete detailed solar and thermodynamic models are carried out under MATLAB. The economic issue to assess the electricity cost is considered to demonstrate the viability and the feasibility of the new ISCC solution. In addition, an optimization technique is used to set the optimal design and parameters to improve the thermal efficiency and reduce the total cost of such system. **Fifthly,** a comparative investigation between the two studied ISCC configurations is carried out in terms in terms of the maturity level for each solar integrated system while maturity is a vital aspect of any technology. Hence, a detailed thermodynamic model is presented to simulate the instantaneous and annual thermal performances for both plants. Furthermore, more attention is paid to solar-to-electric conversion as the latter is the key parameter to assess the solar integration technique in terms of thermal performances and electricity production. Consequently, the comparative investigation allows finding out the most efficient solar thermal plant system and the best solar integration technique based on the same solar field size for each plant. Assessment of the LCOE value for each ISCC system determines the configuration offering the lowest LCOE. Thereby, the simulation is reported under Hassi R'mel location (Algeria) and the variation of DNI during the day, ambient temperature, and wind speed this leads to off-design operation. The obtained results can be explored as guidelines for future projects of such solar thermal power plants type ISCC system over the Algerian territory.

Chapter 1

Concentrating Solar Power (CSP) Overview

1.1. Introduction

Since the world fossil energy sources have decreased, the need for efficient energy conversion and development of renewable energy technologies become ever more critical. Indeed, the global energy consumption has increased rapidly leading to the global warming as a result of emission of carbon dioxide and methane into the atmosphere [1]. A viable alternative to alleviate such a situation is integration of the solar energy using concentrating solar power technology (CSP) with the steam cycles or combined cycle (CC), resulting in less capital cost and a continuous power supply. One of the systems that will be further discussed is the ISCC based on the parabolic trough collector (PTC) technology and Solar Power Tower (SPT) system. By coupling the solar energy with the CC, the efficiency is further increased and CO_2 emission reduced [5]. Large numbers of CSP plants are under development over the world, and there are typically nine large commercial-scale solar power plants of 354 MW installed in the Mojave desert, in addition to several others of same technology operating in Italy, Iran and in North Africa.

Solar concentrating systems generate solar power by using mirrors or lenses to concentrate solar radiation onto a focal surface which is small area called receiver. The latter converts the concentrated solar energy into heat and transferred it to heat transfer fluid (HTF) to generate work in the power block which can be used for electricity generation.

Due to the features of being green, low cost and renewable, solar energy is widely recognized as one of the most competitive alternatives among all the renewable [6]. Using the energy source, CSP or solar thermal electricity (STE) is a technology that is capable of producing utility-scale electricity, offering firm capacity and dispatchable power on demand by integrating thermal energy storage or in hybrid operation [7]. Considering the high energy saving and high energy efficiency, CSP plants are predicted to produce a global electricity contribution of 7 % by the year 2030 and 25 % by the year 2050 [8]. It is envisioned that, with high levels of energy efficiency and advanced industry development, CSP could meet up 6 % of the world's power demand by 2030 and 12 % by 2050 [9]. Potential locations for CSP

plants around the world are generally being identified by using the global distribution of Direct Normal Irradiance (DNI) [10]. North Africa, the Middle East, the Mediterranean, and vast areas in the United States including California, Arizona, Nevada, New Mexico are known as the "Sun Belt" where greater solar radiation is available from the sun. Geographically, the Belt is suitable for CSP plants, as there are massive land areas with extraordinary solar irradiation, well suited to install a large number of solar-energy harvesting systems. By 2020, CSP is expected to be an economically competitive source of bulk power generation for peak and intermediate loads, and by 2025–2030 for base-load power [11, 12]. Commercially viable CSP plants should maintain a DNI of at least 2000–2800 kWh/m^2 yr. Present commercial CSP plants are being developed based on this level of irradiance [10]. However, it is also argued that a DNI value greater than 1800 kWh/m^2 yr is suitable for CSP plant development [13]. In the period of 1984-1991, the first commercial CSP plant was constructed in the Mojave Desert, California, and the USA by Luz International Ltd. However, due to a drop in the oil price at that time, the regulatory initiatives that supported the progress of CSP collapsed. In 2006, CSP plant development initiatives were pursued in Spain and in the United States. The policy in regard to solar power generation was amended in those countries, and feed-in tariffs were introduced in Spain [12]. As of March 2014, the California Energy Commission approved licenses for five CSP plants with a total installed capacity of 2284 MW [14]. In the United States, it has been assessed that CSP plants with a total capacity of 118 GW could be installed by 2030, and by 2050 the capacity could be increased further to 1504 GW [15]. As of 2015, the total installed capacity of CSP plants in Europe reached 5 GW, from 0.5 GW in the year 2006 [7].

1.2. Concentrating solar power (CSP) technology

In CSP power plants, electrical energy is generated by concentrating solar radiation. Generally, CSP plants consist of several components such as solar concentrators, receiver, steam turbine and electrical generator [16].

Solar thermal power plants with optical concentration technologies are important candidates for providing the bulk solar electricity needed within the next few decades. Four concentrating solar power technologies are today represented at pilot and demonstration-scale (Mills 2004): parabolic trough collector (PTC), linear Fresnel reflector (LFR), solar power tower (SPT) or central receiver system (CRS), and solar parabolic dish/engine system (SPD). All the existing pilot plants mimic parabolic geometries with large mirror areas and work

under real operating conditions. Reflective concentrators are usually selected since they have better perspectives for scale-up [1].

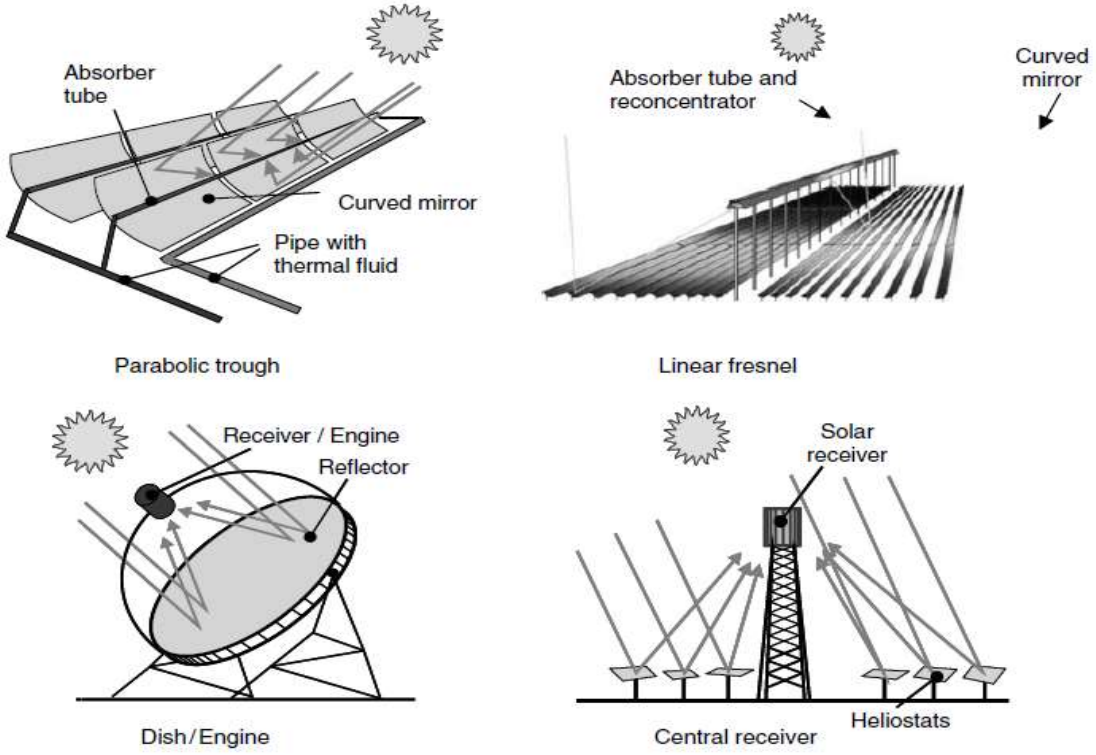

Figure 1.1. Various CSP technologies [1]

Depending upon their current power generation capacity, the plants are further classified into operational, under construction and under development. The CSP power generation systems use concentrators to focus sunlight onto a receiver that carries a working fluid which is heated up to a high temperature, and this heated fluid goes to a conventional steam turbine that is attached to a generator, thus electricity is produced [17,18]. Thermal energy storage (i.e. heat stored in a tank) is an integrated part of a CSP plant, where stored heat can be used for continuous operation of the CSP plant during the night, and on cloudy days. However, storage capabilities might not be present in all CSP plants. For instance, only 50 plants (around 40% of all plants) have the storage capacity in Spain [19]. In addition, other conventional fuels such as gas/oil are used as supplementary sources of energy [17, 20, 21]. Figure 1.1 shows the major parts of a CSP plant and Table 1.1 details the major characteristics of all CSP technologies.

The overall experience in CSP technology development has been positive and new opportunities are opening. At the R&D and demonstration level, many projects have been carried out. At the pilot and demonstration level, the projects PS10, PS20 and SOLAR TRES among others have provided valuable information for the development of the CSP

technology. They have offered excellent pattern to move CSP technology forwards [9]. Building on this experience, new pilot projects are underway or in the planning stage (ALSOL in Algeria). At the industrial and commercial plants of 50 MW to 400 MW power are underway or in operation in Spain, USA, Algeria, Egypt, Morocco, Mexico, Greece, Iran, India and China. The exploitations of these plants have been conclusive that there is a move to the deployment of large scale CSP plants [12]. Up to the year 2030, the market potential is estimated at least at 7 GW in the EU-MENA. This offers the opportunity to CO_2 reduction prospective of up to 12 million tons per year. These plants represent also a cost fall potential of 20 % compared to the last built 80 MWe SEGS IX plant in USA. According to ECOSTAR, there are three main drivers for cost reduction: scaling up, volume production and technology innovations. About 50 % of the intended reductions in costs of CSP plants will be from technology developments, and the other half from scale up and volume production [15]. In this context solar thermal power plants will be capable of delivering efficiently more than 3 % of the EU's electricity by 2020, and at least 10 % by 2030. Moreover, it offers the opportunity to generate about 50 % of the electricity needs of the EU-MENA region and supply over 10 % of the world's electricity by 2050 [12]. Advanced scenario by IEA, EU and DLR has anticipated that global CSP capacity will reach 1.5 TW at this year. The Figure 1.2 shows a data on CSP projects around the world that have plants that are either operational, under construction, or under development. CSP technologies include parabolic trough, linear Fresnel reflector, power tower, and dish/engine systems

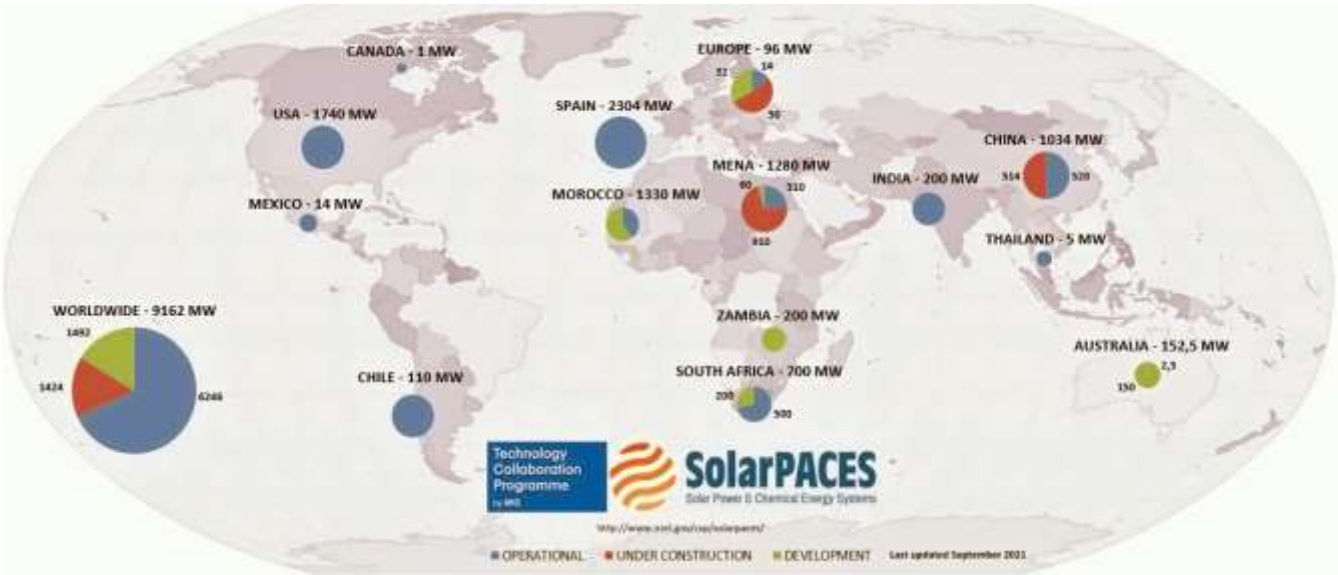

Figure 1.2. CSP projects around the world [22]

Table 1.1. Characteristics of CSP technologies [17, 22–28]

	PTC	**LFR**	**SPT**	**SPD**
Capacity (MWe)	10–200	10–200	10–150	0.01–0.4
Concentration ratio	25–100	70–80	300–1000	1000–3000
Solar efficiency max.	20 % (expected)	21 % (demonstrated)	20 % (demonstrated) 35 % (expected)	29 % (demonstrated)
Annual solar-to-electric efficiency	15 %	8–10 %	20–35 % (concepts)	20–35 %
Optical efficiency	Medium	Low	Medium	High
Receiver/absorber	Absorber attached to collector, moves with collector, complex design	Fixed absorber, no evacuation, secondary reflector	External surface or cavity receiver, fixed	Absorber attached to collector, moves with collector
Thermal efficiency (%)	30–40	–	30–40	30–40
Capital cost (US$/kW)	424	234	476	–
Operation and maintenance cost (US $/kW h)	0.012 − 0.02	low	0.034	0.21
Levelized cost of electricity (LCOE)[a] (USD/kWh)	0.26–0.37 (no TES) and 0.22–0.34 (with TES)	0.17–0.37 (6 h TES)	0.2–0.29 (6–7.5 h TES) and 0.17–0.24 (12–15 h TES)	–
Site solar characteristics/solar radiation required	Generally sites with annual sum of DNI larger than 1800 kWh/m^2			
Storage with molten salt	Commercially available	Possible, but not proven	Commercially available	Possible, but not proven
Operating temperature of solar field (°C)	290–550	250–390, possible up to 560° C	250–650	800
Power block cycle and fluid conditions	Superheated steam Rankine, steam @380 °C/100 bar	Saturated steam Rankine (steam @ 270 °C/55 bar), superheated steam Rankine (steam @ 380 °C/50 bar)	Superheated steam Rankine, steam @ 540 °C/100–160 bar	Stirling/Brayton
Heat Transfer fluid	Synthetic oil, water/steam (DSG), molten salt (demonstration), air (demonstration)	Water/steam	Water/steam, molten salt, air (demonstration)	Air, hydrogen, helium
Steam conditions (°C/bar)	Molten salt with lower melting points, air, steam, supercritical CO2[b] 380 to 540/100	260/50	540/100 to 160	Not applicable
Development status	Most proven	Demonstration	Mature	Demonstration

[a] Net present value of the unit cost of electricity over the lifetime of a generating asset is known as LCOE.
[b] SunShot Initiative is launched in 2011 by the United States Department of Energy that targets levelized cost of CSP generated electricity to be less than USD 0.06/kWh with cost of thermal storage less than USD 15/ kWht and exergetic efficiency greater than 95% by the year 2020

1.2.1. Parabolic trough collector (PTC)

In the PTC-CSP systems, large mirrors shaped like a giant U are used to reflect the solar radiation on to a receiver. The collector field comprises several hundred troughs that are placed in parallel rows aligned on a north-south axis. This configuration enables the single-axis troughs to track the sun from east to west throughout the day, ensuring that the solar radiation is continuously focused on the receiver pipes [29]. When the sun's heat is reflected off the mirror, the curved shapes send most of that reflected heat on to a receiver. The receiver or absorption tube is colored in order to achieve maximum absorption of the solar irradiation and a reduction in heat losses. The receiver tube is filled with the fluid; it could be oil, molten salt, or something that holds the heat well.

Different percentages of sodium nitrate, potassium, potassium nitrate are used for the molten salt. A high absorption coefficient of the absorption tube and its position in the focal point of the trough are the two important issues that need to be ensured for efficient heating of the working fluid. Depending on the concentration ratio, solar intensity, working fluid flow rate and other parameters, the temperature of the working fluid can reach 400 °C [30]. As the solar energy is concentrated 70–100 times in the system, the operating temperature reaches 350–550 °C. The solar-to-electric efficiency is 15 % for the system [31]. If a parabolic trough system is integrated with a steam turbine power plant then it is called direct steam generation technology. The super hot liquid heats water through a heat exchanger, the water turns into steam, that steam is used to rotate a turbine, and from there it works like a conventional power plant where a steam turbine turns the generator and electricity is produced. Once the fluid transfers its heat to water it is recycled and used again in the process, and the steam is also cooled, condensed and recycled again to repeat the process [12, 32].

One of the big advantages of the trough system is that the heated fluid can be stored and used later to generate electricity when sunlight is absent. Among the various solar harvesting technologies, this system ensures the best land use [17, 20, 23, 33-37]. Some parabolic trough plants use fossil fuel to supplement energy production during low solar radiation, and often the trough system can be integrated with conventional natural-gas-fired or coal-fired plants [29]. Compared to other CSP technologies, the parabolic trough system is more advanced [36]. Figures 1.3.a & 1.3.b shows some of the PTC plants in the world. The parabolic trough system is the most widely used CSP technology. The first parabolic trough system was developed in 1912 in Cairo, Egypt [23]. At present, globally, there are 77 operational parabolic trough power plants and most of them are located in Spain and the United States. Two plants are located in Morocco, two in Italy, two in South Africa, one in Canada, three

plants in India, one in Algeria, one in Egypt, one in the United Arab Emirates and one plant in Thailand.

Figure 1.3.a.160 MW NOORO I CSP, Morocco [38]

Figure 1.3.b. 140 MW ISCC Kuraymat, Egypt [39]

1.2.2. Linear Fresnel reflector (LFR)

LFR-CSP plants consist of an array of linear mirror strips as reflectors, with receivers, tracking system, process and instrumentation system, steam turbine and generator. The reflectors are the most important components in the system and the mechanism of the reflectors is the same as that of the Fresnel lens. The sun's rays are reflected by the Fresnel lens and focused at one point, generally on to a permanent receiver on a linear tower. In the daytime, the Fresnel reflectors are directed automatically toward the sun, and from there the reflected solar irradiation carries on to the linear tower where a receiver shaped like a long cylinder contains a number of tubes filled with water. With the high solar radiation the water evaporates and under pressure runs into the steam turbine that spins a generator that generates electricity [17, 40–42]. Figure 1.4 shows the major components of a LFR plant, and the 1.4 MW Puerto Errado 1 Thermosolar Power Plant. A LFR is made up of a number of linear mirror strips. This type of reflector can also resemble the dismantled reflector of a parabolic trough system. Using Fresnel reflector design, the capital cost of the reflectors becomes lower; however the efficiency is less than with parabolic trough reflectors [32, 43]. The capacities of the LFR CSP plants vary from 10 to 200 MW and the yearly solar-to-electric efficiency is estimated to be 8–10 % [44].

Figure 1.4. 1.4 MW Puerto Errado 1 Thermosolar Power Plant (PE1) at Calasparra, Spain [45]

1.2.3. Solar power tower (SPT)/Central receiver

SPTs are the CSP power generation system that employs large flat mirrors to reflect sunlight onto a solar receiver at the top of the centrally located tower [46]. The materials for the receiver are generally ceramics or metals that are stable at relatively elevated temperatures. The average solar flux impinging on the receiver varies from 200 kW/m^2 to 1000 kW/m^2, providing an opportunity to achieve a high working temperature [43]. In the receiver the temperature of the working fluid becomes high enough to produce steam, which eventually spins a conventional turbine to generate electricity. Water/steam, molten salt, liquid sodium or air can be utilized as the working fluid in the system for large plants with capacity of 100–200 MW [44, 47]. In the 1980s and 1990s, the United States Department of Energy Projects in California demonstrated that a SPT could collect and store heat, to generate utility-scale electricity all day round, 24 h a day. Today SPTs continue to help build a clean energy economy. In 2009, the Sierra Sun Tower, a modular two-tower system in the Mojave Desert, powered more than 5000 homes, and in 2010 construction began of the 392 MW three-tower system of the Ivanpah Solar Electric Generating System located in California, USA. In this plant there are about 175,000 mirrors. This California plant has created more than 1000 jobs and powers more than 350,000 homes [48]. Thousands of mirrors called heliostats reflect sunlight onto a receiver on top of a tower. Figure 1.5 shows the 10 MW PS-10 SPT CSP plant located at Seville, Spain. The heliostats are the major capital investment in a power tower CSP plant [25]. These computer-controlled mirrors move to maintain a focus from dawn to dusk. In the Sierra Sun Tower plant water is used as the working fluid, whereas at present

molten salt nitrate is widely used at power plants in the United States, as the fluid is not flammable, is non-toxic, and has better heat storage capacity than water. In the Jülich Solar Tower plant in Germany, the working fluid used in the plant is air.

Figure 1.5. 10 MW PS-10 solar power tower at Seville, Spain [49]

1.2.4. Solar parabolic dish (SPD) system

In the SPD-CSP system, a parabolic point-focus concentrator in the form of a dish is used in a system that reflects solar radiation onto a receiver at the focal point. The concentrators are placed in an assembly with a two-axis tracking system that follows the sun. At the focal point, for efficient power conversion, a Stirling/Brayton engine is placed with an electrical generator to utilize the concentrated heat on the receiver [50]. With a concentration ratio of approximately 2000 at the focal point of the SPDes, the temperature and pressure of the working fluid generally reaches around 700–750 °C and 200 bar, respectively [20-23, 33–35]. Generally, the diameter of the SPDes varies from 5 to 10 m and the surface area is 40–120 m^2. The shiny surface of the SPD is constructed of silver or aluminum which is coated on glass or plastic. However, higher performance can be attained when glass is used with a surface of silver having a thickness of 1 μm. In addition, to improve the reflection of the surface, a certain percentage of iron is used in the glass. In such a combination, the solar reflectance can reach 90–94 %. A single parabolic dish CSP system can have a power generation capacity varying from 0.01 to 0.5 MW [36, 51].

Figure 1.6. Parabolic dish CSP plant, Peoria, Arizona, United States [52].

1.3. Solar thermal power plant

Solar thermal power plants based on the idea to concentrate solar radiation to produce steam which can then be used for electricity generation. In other words, solar thermal electricity generation is very similar to conventional power plants; the only difference is the fuel. It is the sun. This makes obvious, that collecting the solar energy which has relatively low density is one of the main engineering tasks of solar thermal power plant development. For concentration most systems use glass or mirrors because of the very high reflectivity. Other materials are under development to meet the needs of solar thermal power plant systems. These systems can only use the direct radiation, but not the diffuse part of sunlight because it cannot be concentrated [53]. Because of their thermal nature, CSP technologies can be hybridized, or operated with fossil fuel as well as solar energy (Figure 1.7).

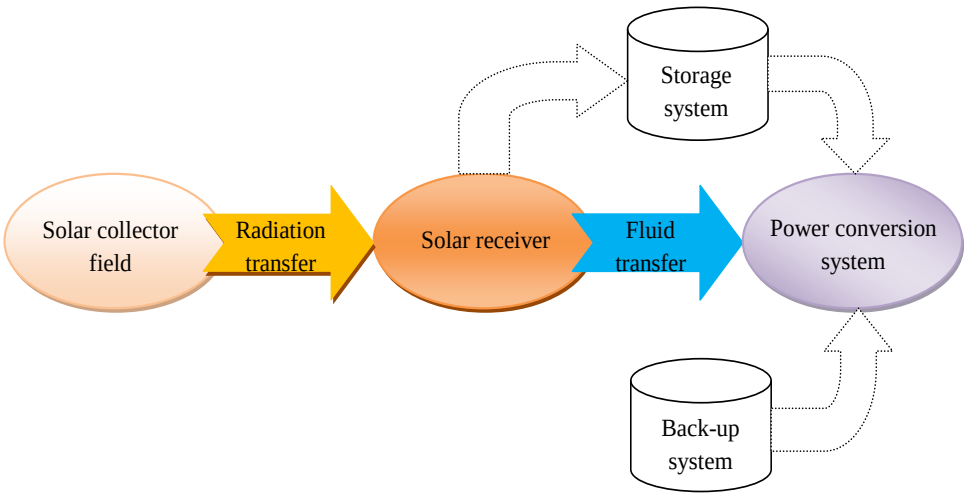

Figure 1.7. Basic configuration of solar thermal power plant

Parabolic trough and solar power tower plants are the most mature systems integrated into a power block for electricity generation [2] and are described in more detail below.

1.3.1. Parabolic trough collector system

Parabolic trough collectors (PTCs) are linear-focus concentrating solar devices that convert direct solar radiation into thermal energy with a good efficiency in the 150-400 °C temperature range, which makes this type of solar collector suitable to be coupled to a Rankine water/steam cycle for electricity production at large scales. The use of synthetic oil as a heat carrier medium between the solar field and the power block of a parabolic trough power plant is at present the most successful technology to produce electricity with solar thermal energy.

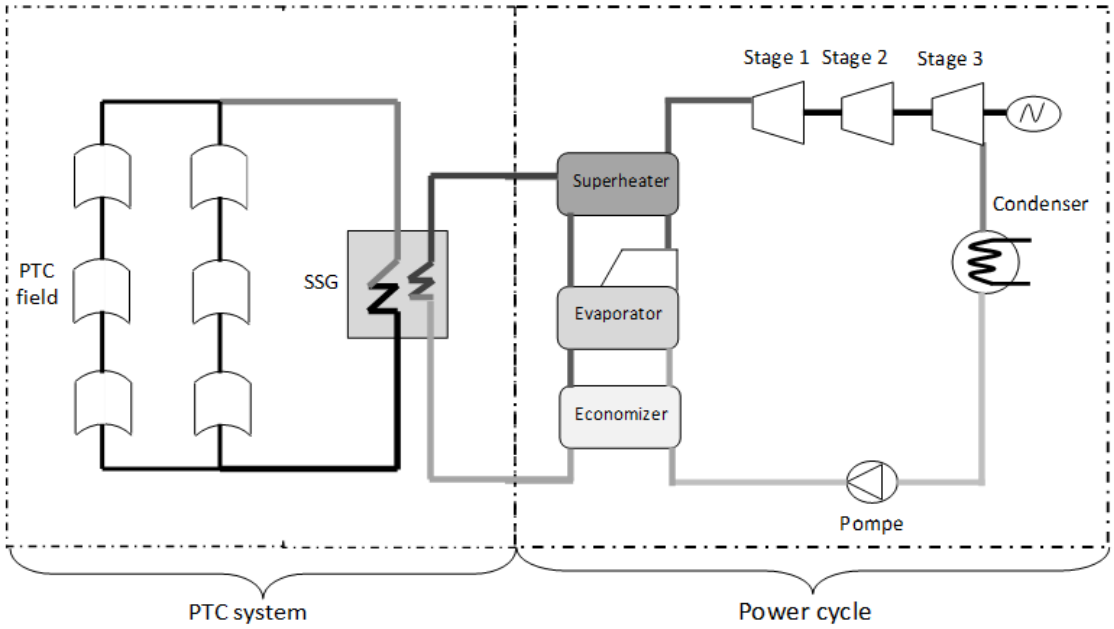

Figure 1.8. Simplified scheme of a solar power plant with parabolic trough collector

Parabolic trough concentrator (PTC) will focus radiation on a receiver much smaller than the reflector. A PTC, like the one represented in Figure 1.9, is basically made up of a parabolic trough shaped mirror that reflects direct solar radiation, concentrating it onto a receiver tube located in the focal line of the parabola. Concentration of the direct solar radiation reduces the absorber surface area with respect to the collector aperture area and thus significantly reduces the overall thermal losses. The concentrated radiation heats the heat transfer fluid circulating through the receiver tube, thus transforming the solar radiation into thermal energy in the form of the sensible heat of the HTF [54].

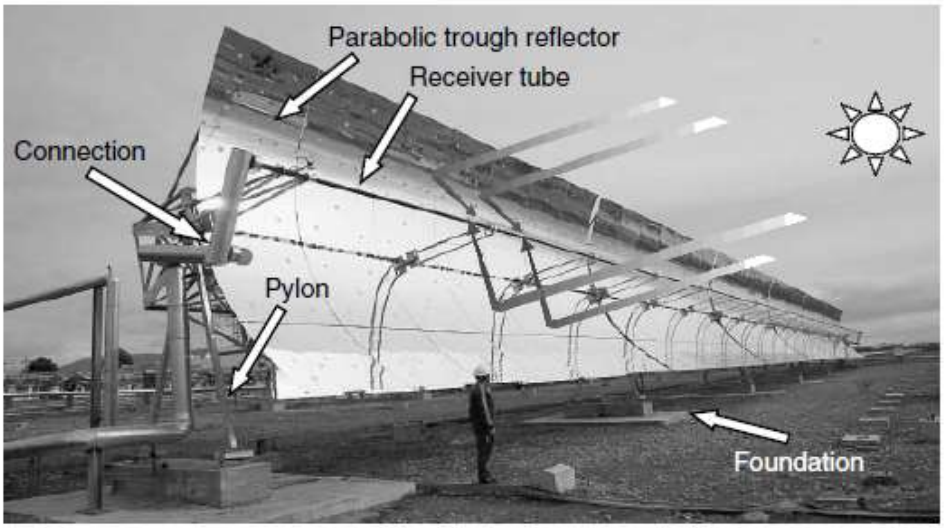

Figure 1.9. A typical parabolic trough collector [54]

The mirrors are made from a low iron float glass with a transmissivity of 98% that is silvered on the back and then covered with several protective coatings. The mirrors are heated on accurate parabolic molds in special ovens to obtain the parabolic shape. Ceramic pads used for mounting the mirrors to the collector structure are attached with a special adhesive.

1.3.1.1. Heat collector element

The heat collection element (HCE) or receiver tube consists of steel tube with a cermets selective surface, surrounded by an evacuated glass tube. The HCE incorporates glass-to-metal seals and metal bellows to achieve the vacuum tight enclosure. The vacuum enclosure serves primarily to protect the selective surface and to reduce heat losses at high operating temperatures [54].

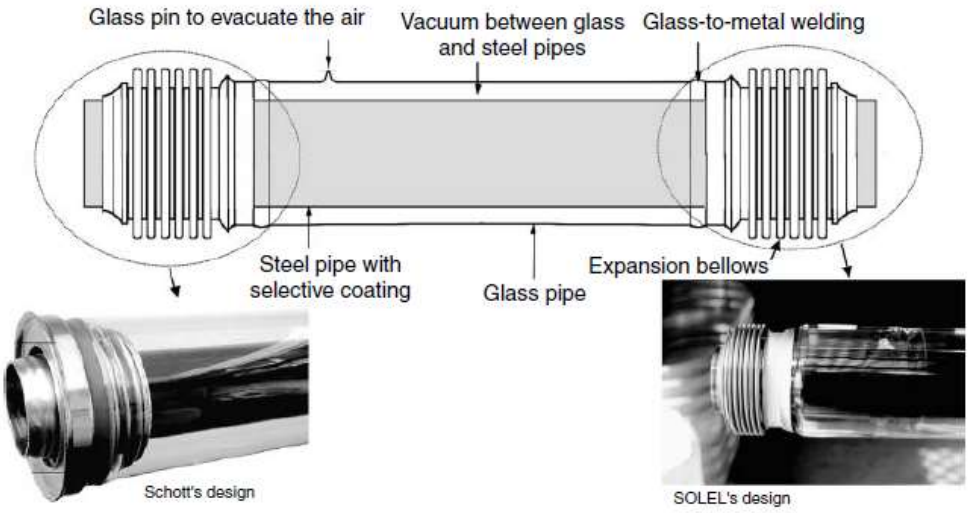

Figure 1.10. A typical receiver tube of a PTC [54]

The vacuum in the HCE is maintained at about 0.013 Pa. The outer glass cylinder has an antireflective coating on both surfaces to reduce reflective losses off the glass tube. Getters, metallic substances that are designed to absorb gas molecules, are installed in the vacuum space to absorb hydrogen and other gases that permeate into the vacuum space over time.

1.3.1.2. Parabolic Solar field

The solar field consists of a numerous parabolic trough collector (PTC), as shown in Figure 1.11 each parabolic trough collector has a linear parabolic shaped reflector that focuses the sun's direct beam radiation on a linear receiver located at the focus of the parabola. The collectors track the sun from east to west during the day to ensure that the sun is continuously focused on the linear receiver. A heat transfer fluid (HTF) is heated as it circulates through the receiver and returns to the solar heat exchanger to generate saturated steam [54].

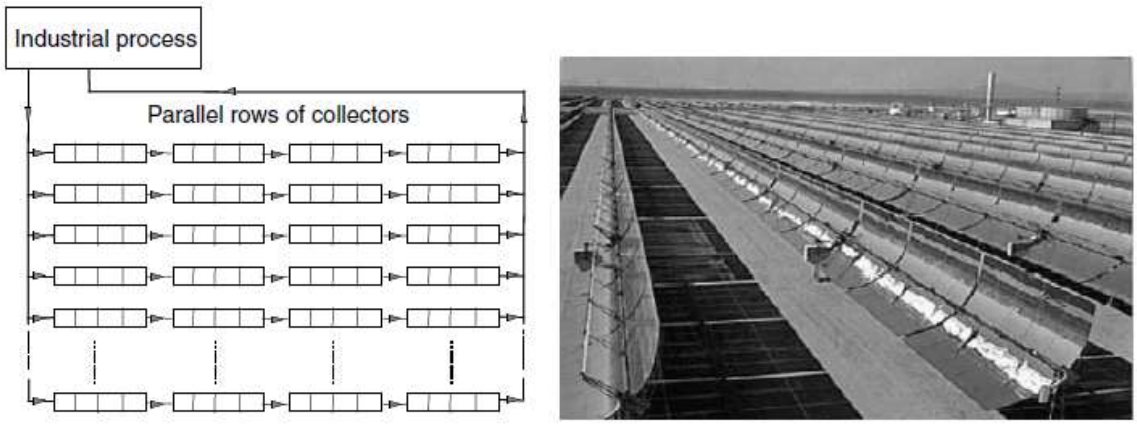

Figure 1.11. A typical solar field with parabolic trough collectors [54]

The solar field's basic component is the parabolic trough collector (PTC). As shown in Figure 1.12, each PTC is made up of parabolic reflectors (mirror), a metal support structure (pylon and support), a receiver tubes, glass cover and a tracking system that includes a drive, sensors and controls.

The Euro Trough (ET 150) collector consists of identical 12 m long collector modules. Each module comprises 28 parabolic mirror panels (7 along the horizontal axis between pylons and 4 in a vertical cross-section). Each mirror is supported on the structure at four points on its backside. This permits the glass to bend within the range of its flexibility without effect on the focal point. (ET 150) has less weight and less deformations of the collector structure due to dead weight and wind loading than the LS-3 collector. This reduces torsion and bending of the structure during operation and results in increased optical performance and wind

resistance. The weight of the steel structure has been reduced about 14% as compared to the available design of the LS-3 collector [55, 56].

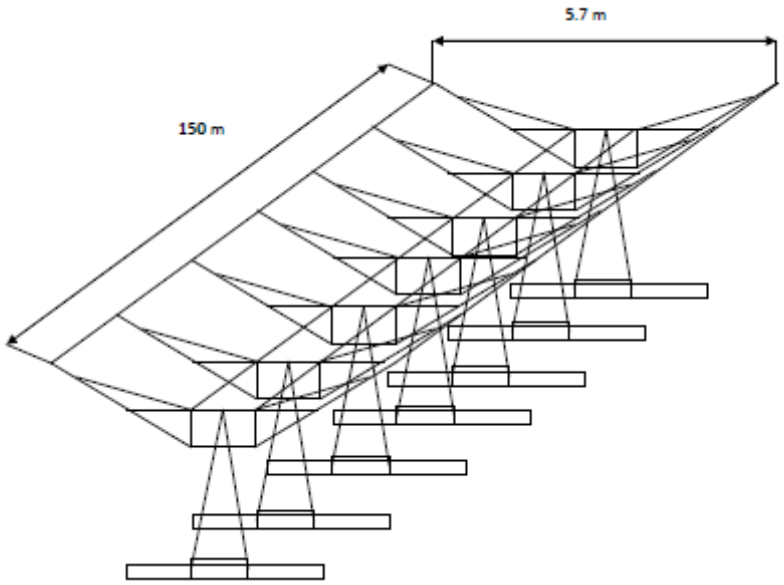

Figure 1.12. Euro Trough collector (ET150)

1.3.2. Solar Power Tower system

Solar Power tower (SPT) system which is also referred to Central Receiver System (CRS) uses a large number of heliostats, having dual axis control system (one about the vertical axis and the other about the horizontal axis). These heliostats reflect the solar radiation (impinging on their surface) to a stationary receiver located at the top of a tower. This concentrated solar energy incident on the receiver is converted to thermal energy, which is carried by the HTF passing through the receiver. The thermal energy of the HTF is transferred to the working fluid of the power cycle, thereby generating electricity.

The advantage of SPT is that a high geometrical concentration ratio ranging from 200 to 1000 can be achieved. Consequently, temperatures of the order of 1000°C can be reached with suitable HTFs. The high temperature leads to an increase in the power cycle efficiency. As a result of this, potentially, an overall solar to electric conversion efficiency of around 28 % can be achieved. As shown in Fig. 1.13, a typical central receiver system, also known as a solar power tower consists of three major subsystems, namely the heliostat field, the receiver and the power conversion system.

The heliostats and solar receivers are the key components of a solar tower where the heliostat field occupies the large part in the investment, about 60 % of the solar share [1].

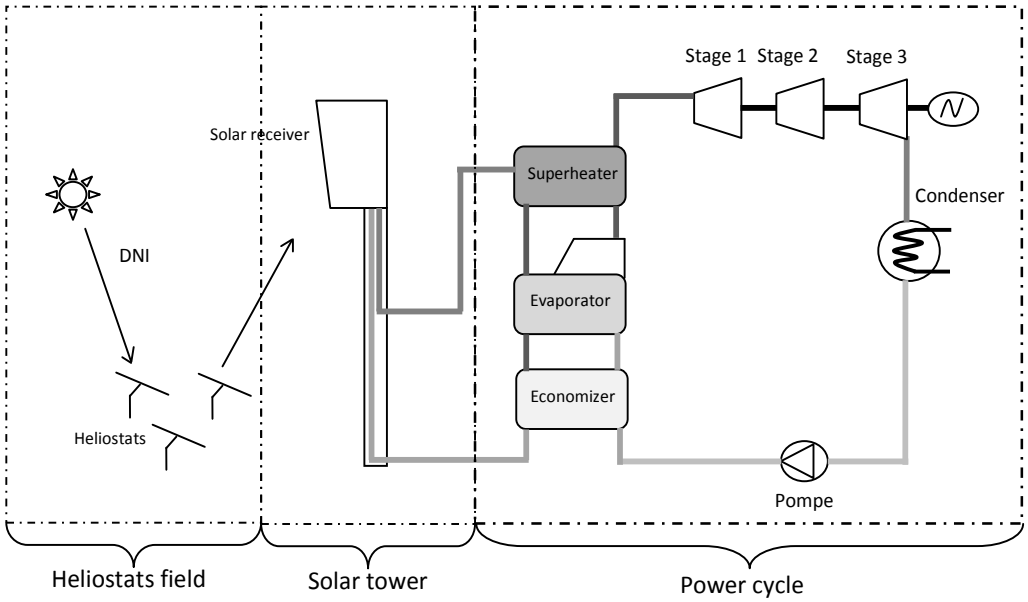

Figure 1.13. The three main subsystems of central receiver solar thermal power plant

The solar receiver is an essential subsystem even its investment impact is lesser (by 14 %) than the heliostat since the entire solar energy is focused on it [1].

1.3.2.1. Heliostats

Heliostats are conventionally flat or slightly curved mirrors mounted on a backup steel structure, which can be controlled or tracked about two axes, one horizontal and other vertical, so as to tilt the heliostats to reflect the solar rays to a fixed receiver on top of a tower. The aperture areas of the heliostats that have been used in various plants vary considerably from 1 m^2 to 120 m^2, but all heliostats within a plant have the same aperture area [57].

Figure 1.14. Heliostat [58]

1.3.2.2. Receivers

The receiver is one of the most important parts of tower plants. There are two types of receivers: tubular and volumetric. Tubular receivers are used for liquid HTF such as water, molten salt, thermic oil, liquid sodium and Hitec salt, and volumetric receivers use air or supercritical CO_2 as HTF. The type of receiver depends on the type of HTF and power cycle (Rankine or Brayton) used in the system. A brief description of the receivers is discussed as follows [57]:

1.3.2.2.a. Tubular Receivers

In tubular receivers, the HTF passes through a number of vertical tubes and gets heated by the radiant flux reflected from the heliostats. There are two types of tubular receivers: External cylindrical receivers and cavity receivers.

- External Cylindrical Receivers

In external cylindrical receivers vertical tubes are arranged side by side, in a cylindrical fashion and the radiant flux from the heliostats impinges from all directions. This is shown in Figure 1.15. Since the receiver is exposed to atmosphere, it is subjected to higher convection losses.

Figure 1.15. External Cylindrical Receiver used in Crescent Dunes Power Tower [57]

- Cavity Receivers

The cavity receiver consists of welded tubes kept inside a cavity in order to reduce convection losses. The heliostat field is arranged within the range of possible incident angles onto the receiver. Cavity receiver can be either a single or dual cavity type. A single cavity receiver

will have solar field on one side of the receiver while the dual cavity receivers will have solar field on either sides of the receiver. Figure 1.16 shows the single cavity receiver used in the PS 10 and Sierra sun tower plants.

Figure 1.16. Cavity Receiver used in PS-10 [57]

1.3.2.2.b. Volumetric Receivers

Which use air as HTF are made of porous wire mesh or metallic/ceramic foams. The solar radiation impinging on the volumetric receivers is absorbed by the whole receiver. Volumetric receivers are of two types: open volumetric and closed/pressurised volumetric. Figure 1.17 and Figure 1.17 give a schematic representation of them.

- Open Volumetric Receivers

In open volumetric receivers, ambient air is sucked through the porous receiver where air gets heated up by concentrated solar energy. The outer surface of the receiver will have a lower temperature than inside the receiver because the incoming air from the ambient cools the surface and avoids damage to the material. Jülich tower plant uses a porous silicon carbide absorber module as receiver. The air gets heated up to about 700˚C and is used to generate steam at 485˚C, 27 bar in the boiler to run the turbine. The schematic representation of the open volumetric receiver used in Jülich Plant is shown in Figure 1.17.

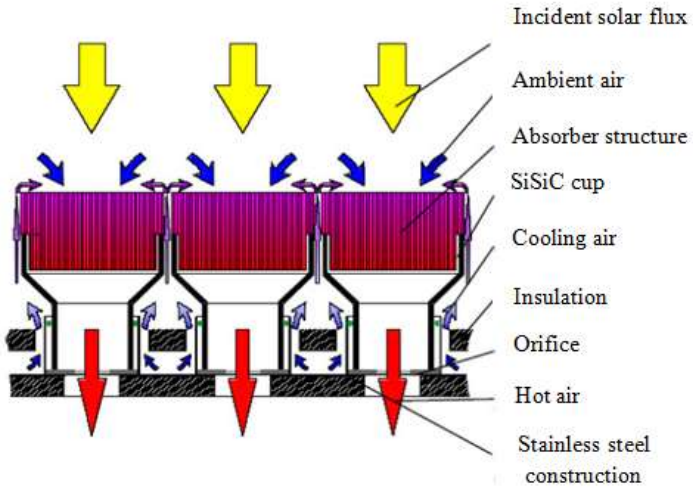

Figure 1.17. Schematic of Open Volumetric Receiver (HitRec Principle) [59]

- Closed Volumetric Receivers

Closed volumetric receivers are also called as pressurized volumetric receivers, in which the HTF (usually air) is mechanically charged through the receiver by a blower and the receiver aperture is sealed by a transparent window. The HTF will get heated up at the dome shaped portion of the receiver by the concentrated solar energy and the heated air will be used either in a Rankine cycle via heat exchanger or in a Brayton cycle for generating electricity. The schematic of a closed volumetric receiver is shown in Figure 1.18.

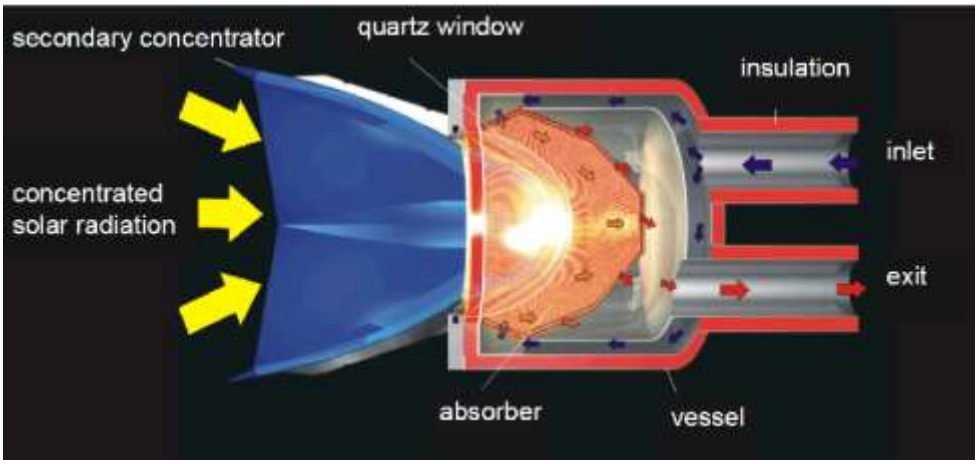

Figure 1.18. Schematic of the Pressurized Volumetric Receiver [60]

1.3.2.3. Current status

The central receiver solar power technology has show a fast development during recent years. The installed capacity is increasing day by day; this is due to the intensive R&D activities that have significantly improved the solar tower technology. Reducing initial costs and project

risks, and improving components performance are the major factors that have favored this deployment. The solar tower power components are mainly the heliostat field, the receiver and the power block, also is illustrated the technical data of the three main components of the power plants. It has been observed that most of the power plants are equipped with a steam tubular receiver that power a Rankine thermodynamic cycle. Different types of HTFs can be used in solar tower (ST) based on the type of receiver and power cycle employed in the system. The HTF used in the operational ST plants are water, molten salt and air. Other possible candidates are liquid sodium, Hitec salt and synthetic oil [57].

Concerning the heat transfer fluids (HTF), water/steam has initially been adopted in some solar towers such as PS10, PS20, Beijing Balading, Sierra and Yanqing. Molten salt is also a very commonly used HTF. It has been used for example in Gemasolar thermo-solar plant. Lately, there has been a big interest in developing air as a HTF.

Jülich solar tower is an example of this case. Depending on the receiver design and the heat transfer fluid, the working temperatures of the power conversion system range from 250°C, for water/steam cycles, to around 600°C with current molten salt design.

The development of Direct Steam Generation (DSG), which is currently in its early stage, as HTF is very promising for reducing costs and enhancing thermal efficiency by eliminating the heat exchangers network [61]. In 2006, the 11 MWe CRS power plant PS10 was built by Abengoa Solar in Sevilla Spain. It has been followed by the 20 MWe power tower plants PS20 in the same location, the 5 MW Sierra Sun Tower (in Lancaster, USA) and the 1.5 MW in Jülich Germany in 2009. Since 2011, the Gemasolar power plant, built in Spain as large as the PS 20 power plant, but with surrounded heliostat field and15 h storage, has been operating and delivering power around the clock [62]. After the three pioneer CSP countries, i.e., the USA, Germany and Spain, Chine.

vanpah solar electric generating system

Crescent Dunes Solar Energy Project

Planta solar 20&10

Jülich solar tower

Gema solar thermo solar plant

Sierra sun tower

Figure 1.19. Examples of Solar Power Tower Projects [google maps]

In the SPT plants using volumetric receivers, the concentrated solar radiation are absorbed deep inside a volume of highly porous structure, thereby air is used as a HTF. The selection of either an open or closed volumetric receiver considers some advantages of the air as it has no risk of freezing in addition to capability of reaching high temperatures of 850-1000 °C [1, 57]. Some operation SPTs using air volumetric receiver are shown below:

- Jülich Power Tower with 1.5 MWe capacity power tower in Germany is an experimental 60 m high tower plant. It uses a volumetric receiver with non-compressed air as the HTF. Due to the poor heat transfer coefficient of air, the efficiency of this plant is not so high. The working fluid is water. It also has 1.5 hours of storage capacity. It uses 2153 heliostats each of 8.2 m^2 area. The heliostats and tower are spread across a land area of 80000 m^2. It is a demonstration plant. This plant started operation in 2008 [63]. The air (HTF) is heated up to 700°C and is used to heat water (in the power cycle) up to 500°C at pressures of 100 bars.
- Solugas Plant This plant with 4.6 MWe capacity plant located in Spain. The construction for this plant was finished in early 2012. It is built over a land of area 60000 m^2 [64]. It uses 69 heliostats of 121 m^2 area each. It has a 75 m high tower. Since the area of each heliostat is high it is made up of 28 facets. The cavity receiver is located at a height of 65 m with an inclination of 35° with the horizontal. The diameter of the receiver is 5 m;

however, the sun's rays are concentrated to an area of 2.7 m diameter. The length of the receiver is 6 m and it has a cylindrical cavity region. [65].This plant uses a Brayton cycle and uses air as HTF [66].

- Themis Solar Tower This is a 2 MWe capacity tower constructed for research and development purposes. It is located in France. This ST plant is the refurbished and upgraded version of the tower initially built in the seventies to test 10 MWth scale electricity to concentrated solar energy production facility. It uses a new high performance, high precision heliostat tracking system which will allow the receiver temperature to reach 900°C. It has 201 mirrors to concentrate the solar energy on top of a concrete tower of 101 m height [67]. The HTF employed is compressed air [68]

1.4. Conclusion

This chapter provided a comprehensive outlook on the CSP technologies. Concentrating solar power (CSP) has received significant attention among researchers, power-producing companies and state policymakers for its bulk electricity generation capability, overcoming the intermittency of solar resources. The parabolic trough collector (PTC) and solar power tower (SPT) are the two dominant CSP systems that are either operational or in the construction stage. The USA and Spain are global leaders in CSP electricity generation, whereas developing countries such as China and India are emerging by aggressive investment. Solar thermal power technologies have distinct features that make them attractive energy options in the expanding renewable energy market worldwide. For these reasons, more and more countries are mandating that a part of the electric power be from renewable origin, in particular solar energy. As a result, renewable energy will become the world's second-largest source of power generation; delivering about 30% of the electricity needs by the year 2035. Nowadays, Concentrating Solar Power (CSP) technology implantation is growing faster than any other renewable technology and its hybridization with other thermal sources becomes more attractive than stand-alone CSP plant. Each year, hundreds of articles have been published on CSP in order to improve this technology and contribute alleviating global problems, i.e., climate change and associated shortage of energy, water and food.

Chapter 2

The Literature Review

2.1. Introduction

Concentrated solar power (CSP) is a technology for generating electricity by using thermal energy from solar radiation. Currently, four CSP technologies have found extensive application in the power industry: parabolic trough collector (PTC), linear Fresnel reflector (LFR), solar power tower (SPT) or central receiver system (CRS) (as sometimes called), and the parabolic dish concentrators (PDC). PTC and LFR systems operate within lower temperature ranges (300 °C ~ 400 °C) while SPT and PDC being capable of achieving up to 1000 °C or more [1]. A way of improving the power output of solar thermal systems is through hybridization of CSP technology with other thermal sources. Thus, integration of solar energy into a combined cycle (CC) using CSP technology to constitute the so-called Integrated Solar Combined Cycle (ISCC) is more attractive than stand-alone CSP plants [69]. The most operating ISCC solar thermal plants are those using PTC and SPT technologies and several layouts have existed which some are commercialized or underdevelopment through the world [1]. In this section, we review some works focusing on two kinds of solar thermal plants, one integrates PTC technology and other one adopts SPT system.

2.2. Parabolic trough collector power plants

Nowadays a large number of CSP plants with a majority for PTCs are now under development all over the world and installed in commercial plants, mainly the nine large commercial-scale solar power plants (SEGS) in California's Mojave Desert developed by Luz International Ltd are in operation and generating a power of 354 MW of where the first one was working since 1984 and several other plants with the same technology are operating in Italy, Iran and North African Countries.

In PTC technology the solar energy is concentrated and transferred to Heat Transfer Fluid (HTF) which is generally synthetic oil in the absorber tube, and then via an intermediate oil-to-water/steam heat exchanger is transmitted into the Rankine cycle. In addition, the steam can be generated directly into the absorber tube and this technique is called Direct Steam

Generation (DSG) as it is transmitted directly into the Rankine cycle. Consequently, several works have been carried out about this technology. Kalogirou [70] developed a detailed thermal model to analyze the PTC performances using an Engineering Equation Solver (EES). The thermal analysis is taken all modes of heat transfer include convection, conduction and radiation. Hence, the obtained results are validated with the existing collectors performances at Sandia National Laboratories and it showed a good agreement. A model for a small PTC is designed and simulated by Tzivanidis et al. [71] under different conditions to predict the thermal and optical efficiency. The simulation includes a parameters analysis those having an impact on PTC efficiency such as: the temperature distribution, the heat convection coefficient and the angle efficiency modifier. The results based on Solidworks software show that the PTC model performs efficiently with a validated calculation. Agagna et al. [72] proposed an improved model for predicting the thermal performances of a PTC. The model shows more accuracy compared to the previous published models with an average uncertainty of less than 0.50 %. It shows as well more accurate efficiency results than those obtained during the experimental tests of Sandia National Laboratory for all the cases. Thus, the proposed model could be an interesting tool for PTC thermal performance simulations. Also, Agagna et al. [73] combined between an experimental and numerical study to evaluate the optical efficiency and thermal performances of PTC of "MicroSol-R". The results from experimental tests are compared to the LS-2 collector at SNL platform while the three numerical developed models are compared to find out the most accurate one for predicting the PTCs performance.

PTC system is the most mature technology among CSP systems [71] and covers the 90 % of the total CSP power plants [74]. Giostri et al. [75] compared a PTC technology with a Linear Fresnel Reflector (LFR) in thermal power plant. The analysis using ''Thermoflex'', a commercial software shows that instantaneous and annual thermal performances of PTC are superior to those of LFR because of the latter is significantly affected by high incident angles of solar radiation. On other hand, the economic assessment of the electricity generation cost from LFR is competitive to that from PTC because of its reduced investment cost. Rady et al. [76] as well compared a PTC and LFR technologies based on some parameters such as power/land consumption ratio, optical and thermal efficiency at nominal conditions. It is found that PTC exhibits higher optical and thermal performances than LFR while the latter has a better use of the land. The availability of storage capacity plays an important role for the economic success of solar thermal power plants; Herrmann et al. [77] studied another Thermal Energy Storage (TES) concept using molten salt material that is incorporated in PTC

power plants. Thus, the investigation shows that there are no technical barriers to realize the molten salt storage since it is a feasible and viable concept from economic point of view that can improve the economy of PTC plants. Experimental study of thermal performances of a PTC thermal plant using the HTF type Therminol 55 as thermal energy storage is carried out by Kumaresan et al. [78]. It is seen that reducing heat loss like a performance parameter enhances the performances of the system, thus the PTC should be close to the storage and a proper insulation is required. Sivaram et al. [79] developed a numerical model to investigate a small-scale PTC employed for thermal energy storage system. The results of the performance parameters are validated with the experimental investigations and it is found a good agreement within 10 % deviations. Bataineh et al. [80] investigated the transient behavior and thermal storage capability of two candidate storage media based on the optimal design of the storage system. It is found that Dead Sea salt and Basalt rocks can be substitute the use of molten salt as storage material due to their cost advantages and easily handling. Implementation of CSP thermal plants at any place is based on some criteria like high solar radiation level, flat lands and sufficient water resources. Boukelia et al. [81] reviewed the potential installation of CSP plants in Algeria with more attention is paid to PTC power plants. It is found that Algeria has all the necessary requirements for the development of PTC thermal plants registered among the national Renewable energy program for the period 2011-2030. Al-Maliki et al. [82] developed a model to simulate a PTC power plant with thermal energy storage ‘’Andasol II”, thus APROS software tool is adopted. The comparison results between the measured data and simulation shows a good agreement, consequently this developed model could use for further such thermal plants and determine the best approach of a plant operation. In addition to some techniques of increasing the steam power cycles efficiency like preheat the working fluid before the boiler; Alsagri [83] investigated the feasibility of using solar PTC system for preheating process in the steam power cycle. Therefore, a thermodynamic analysis of different considered scenarios is carried out. The results shows a significant improvement in the steam power cycle efficiency for the different chosen scenarios and concluded that integrating a PTC into steam cycle as the preheating unit is the best choice technically.

Various techno-economic studies of ISCC based on PTC have been conducted. Dersch et al. [84] found that integration of PTC technology with CC power plant provides an interesting way for solar electricity generation and has potential environmental and economic benefits. Montes et al. [85] showed the benefit of coupling the solar field to CC which is more evident in hot and dry climate such as for Las-Vegas and Almeria conditions. Even the negative

impact of the hot weather of Las-Vegas on the CC performances, the good coupling of solar thermal power with CC makes the ISCC operates efficiently. Antonanzas et al. [86] found that the solar hybridization with CC installed through Spain has increased electricity production in peak hours as well as the overall efficiency and has reduced CO_2 emission. During the period of high ambient temperatures which generally coincide with the period of higher normal irradiation, it is possible to integrate the steam produced by the solar thermal collectors. Consequently, it permits to alleviate the drop in electricity production of CC during the peak demand periods and to improve overall efficiency and reduce the levelized cost of energy (LCOE). Zhu et al. [87] examined the thermodynamic impact of integration of solar energy into CC power plant operating with two gas turbines, one steam turbine and two heat recovery steam generators (HRSG) with an optional duct burner to boost the overall power. They concluded that with a thermal solar input of 200 MW into HRSG, the output can be boosted from 475 MWe to about 558 MWe which has a benefit on fuel saving and pollution reduction. With the competitive PTC technology, the solar energy is transferred to a circulating fluid in the absorber tubes which is generally synthetic oil. In this case, an intermediate oil-to-water/steam heat exchanger is needed to transmit the solar energy carried by oil to water/steam in Rankine cycle, resulting in the so called heat transfer fluid (HTF) technology. Another configuration is the direct steam generation (DSG) technology used to increase the power output during the sunny periods. Nezammahalleh et al. [88] considered three configurations of ISCC system which are (ISCC-DSG) technology, an (ISCC-HTF) technology and a solar electric generating system (SEGS). This study has revealed that both ISCC-DSG and ISCC-HTF present a high heat electricity net efficiency, but ISCC-DSG is the best option due to high temperature superheated steam produced in the receiver pipes. Furthermore, it is found that ISCC-DSG economically is viable because no additional investment is required compared to the one using oil as HTF. Also, Behar et al. [89] has reviewed the different hybridization of solar energy in ISCC-PTC systems and it was observed that ISCC system using DSG offers more performances than those using HTF. Derbal-Mokrane et al. [90] and Behar et al. [91] have investigated thermal performances of the first ISCC thermal power plant under Algerian climate. It results that global thermal performances during the day reach a high value at midday with an electricity production value of 157 MW corresponding to an efficiency of 67 %. Rovira et al. [92] compared ISCC technology using HTF with DSG and showed that the performance of ISCC using DSG is improved compared to that technology with HTF.

Another promising technology of concentrating solar energy is the solar tower which is expected to lead in the future. A comparative study [93] between solar Rankine cycle (SRC) and ISCC plants both coupled to a solar field based on PTC/solar tower system is carried out. In this study, molten salt is used to transfer heat to the water loop in SRC and synthetic oil (Therminol VP-1) is used for the ISCC. As a result, with the same the solar field aperture area, the coupling with PTC causes low performances due to the less quantity of solar energy intercepted by its solar field compared to heliostats field of the solar tower. Abdel Dayem et al. [94] simulated the Kuraymat (Egypt) ISCC using TRNSYS, and compared (with a good agreement) the predicted thermodynamic performances with the measured data under the same conditions of design specifications and weather. Aldali et al. [95] studied the thermodynamic performance of a proposed ISCC under Libyan weather based on fuel saving and power boosting modes. The obtained results for the fuel saving mode show a reduction in fuel consumption and CO_2 emission.

Besides to technical study, the economic assessment is required from the point of view of feasibility and viability for electricity production. Price et al. [96] quantified the cost reduction potential of LCOE for different configurations of solar energy integration. Therefore, a comparative investigation to a reference 50 MW power plant with the solar-only mode without storage has revealed that substitution in the same power by ISCC can reduce the cost of electricity by 33 % (0.11 to 0.073 $/kWh), and the increase of concentrator size from 50 m to 150 m reduces the cost from 0.11 to 0.10 $/kWh. Horn et al. [97] investigated the technical and economical of ISCC installation in Egypt; thereby a comparative study between ISCC using PTC technology and SPT is carried out. Hosseini et al. [98] assessed the technical and economic study for six different sizes of ISCC power in Iran. The obtained LCOE when environmental effect is considered, ISCC using 67 MW integrated to a CC is the best choice for the construction of the first solar power plant in Iran. Mokheimer et al. [99] have conducted a techno-economic comparative study of three types of CSP technologies (PTCs, LFR and Solar Tower) adopting a conventional gas turbine (GT) cogeneration plant under Dhahran (Saudi Arabia) weather conditions. Thus, THERMOFLEX with PEACE software was used for this integration with different GT 50-150 MW. The simulation results found that LFR technology is the optimal configuration of solar integration with the steam side of a GT cogeneration with 50 MWe and Jazan city is the suitable location for such hybridization. Duan et al. [100] proposed a novel solar integration with a CC using PTC technology. In such configuration, a part of a compressed air from the GT compressor is used as the HTF through the receiver of solar PTCs field with size of 30 MW; while the solar

energy carried by the compressed air is used to generate steam in the HRSG with two pressure levels. It results that the novel ISCC using compressed air has more advantage in terms of performance and economy compared to ISCC using oil as HTF. Li et al. [101] presented a novel integration of solar energy into CC with two different pressure and temperature levels in HRSG part. The solar integration is based on concentrating and non-concentrating solar systems which are PTCs using DSG system and evacuated tube (ET) respectively, both are simultaneously coupled with a CC. It has shown that the integration of both solar technologies in a temperature cascade way contributed positively in terms of solar heat conversion efficiency and a lower LCOE cost achieved compared to ISCC-DSG system power plant.

In the ISCC system with Hassi R'mel concept which is designed by Abener and Abengoa Solar [89], one part of feed water is withdrawn from HRSG single pressure and converted into saturated steam by solar steam generator (SSG) working in parallel to HRSG and then returned to the latter where it is mixed and superheated. Hence, Achour at al. [102] investigated the thermal performances of such ISCC system under southern Algerian climate. The thermodynamic simulation model exhibits high thermal efficiency with a good conversion of solar energy to electricity. It permits also to conclude that this kind of thermal power plants integrating a PTC with HTF into a conventional CC is the most efficient system. Abdelhafidi et al. [103] as well proposed an innovative model to predict thermal performances for the same ISCC Hassi R'mel concept for the future installation. Validation of this model is carried out with the first ISCC installed in Hassi R'mel (Algeria) which shows a good agreement with the experimental results. Also, a sophisticated dynamic model for performances simulation of an ISCC system has been developed and detailed by Temraz et al. [104] as the purpose of investigation and improvement of such system limitations and capabilities. The simulation model is based on APROS software model and Kuraymat ISCC power plant is the case study where results validation showed high accuracy with actual measurements of the plant. Wang et al. [105] proposed a novel ISCC using DSG where a hot water heater is added at the end of HRSG to decrease more the exhaust gas temperature outlet from the latter and increase its efficiency. The thermal performance of such new plant configuration was carried out including a parametric and optimal analysis with taking into account the economic issue. Rovira et al. [106] have also studied a novel ISCC with partial recuperation in gas turbine power block and thermal performances of such new layout are compared to the conventional ISCC proposed previously. Khoshgoftar Manesh et al [107] improved the combined cycle power plant by introducing the concentrated solar energy via PTC system. The solar thermal plant was investigated with multi-analysis include energy,

exergy, exergoeconomic, exergoenvironmental, emergoeconomic, emergoenvironmental analyses described as (6 E) and also an optimization technique was applied to find out the optimum configuration for such improved thermal power plant. Zhang et al. [108] investigated the integration of solar energy into an ISCC and generalized model is proposed with respect to fuel-savability. Therefore, different configurations have been conducted to assess the impact of solar energy integration at different level on the plant performances based on the exergy balance. Dabwan et al. [109] have proposed an innovative integration of solar energy into a gas turbine (GT). The system consists of a parabolic solar field that used to preheat the compressed air before entering the combustion chamber of a GT with the use of an intercooled system. The thermodynamic investigation and economic assessment showed more improvements over the conventional solar preheating GT

According to the published works, investigations of an ISCC based on PTC technology (ISCC-PTC) with Hassi R'mel concept have been focused on thermal performances analysis only and no economic assessment has been considered to demonstrate the feasibility and competitiveness of such system. To fill this lack, techno-economic assessment of the first ISCC plant in Algeria is carried out in this study. The economic issue is evaluated based on the levelized cost of energy (LCOE) method to evaluate the cost of electricity including the fuel saving cost and emission reduction throughout the lifetime of operation. The results can provide some guidelines and suggestions for the development of such typical ISCCs among the ambitious renewable energy program of Algeria at the horizon 2030.

2.3. Solar Power Tower technology

In solar electricity generation the parabolic trough collectors have been the most mature technology among the CSP. On the other hand, the SPT system or CRS using the heliostat field to concentrate the solar radiation onto a receiver located on the top of a tower has demonstrated its technical feasibility and it is under commercialization [1]. Actually, the most promising SPT technologies are those using molten salt, saturated steam and volumetric air receiver. Planta Solar 10 (PS10) uses the saturated steam, Gemasolar uses the molten salt and Jülich and Themis use air as HTF in the volumetric receiver. In the SPT plants equipped with volumetric receivers, the concentrated solar radiation is absorbed deep inside a volume of highly porous structure. The selection of either an open or closed volumetric receiver considers some advantages of the air as it has no risk of freezing in addition to capability of reaching high temperatures of 850-1000°C [1, 57].

The heliostat and the solar receivers are the key components of the SPT technology of which the heliostat field occupies the large part in the investment, with 60 % of the solar share. The solar receiver is an essential subsystem even its investment impact is lesser (by 14 %) than the heliostats since the entire solar energy is focused on it [1]. The heliostat field optical efficiency depends on the cosine effect, atmospheric attenuation, interception efficiency and shading and blocking efficiency. Accordingly, there were several studies carried out to design efficiently the heliostats, the receivers and the power blocks [110-112]. The heliostat field optical efficiency has the major impact on the solar tower plant performance. Besaratiet al. [110] have proposed a novel simple approach to evaluate the optical efficiency of the heliostat field and found out the optimal heliostat field layout. Lee et al. [111], based on the Monte Carlo ray-tracing method, have simulated the optical efficiency of the first CRS power plant in Daegu Korea and found some improvements in the performance. Eddhibi et al. [112] dealt with the design and analysis of a preliminary heliostat field layout with reducing optical losses caused by the blocking and shading effects.

The concentrated sun radiation reflected from the heliostats is focused onto the receiver (absorber) and transferred to HTF. According to HTF, the receivers are either a tubular receiver using water, molten salt, synthetic oil and liquid sodium [57] or a volumetric receiver using air as HTF, which may be an open volumetric receiver or a closed volumetric receiver. The absorber is made of porous wire mesh or metallic/ceramic foams, reaching high temperatures between 700-1000°C [57**].** Hoffschmidt et al. [113] investigated the performance of an improved High Temperature Receiver II (HiTRec II) which consists of a ceramic material and where the air instability due to high temperatures is attenuated. Marcos et al. [114] assessed the Air Return Ratio (ARR) and optimized it for different receiver configurations (external, semi-cavity, cavity and receiver with secondary concentrator) under different operating conditions. Hischieret al. [115] compared the thermal performance of pressurized air receiver integrated in three different configurations of a solar tower power plant of 50 MWe namely: Brayton, recuperated Brayton and combined Brayton-Rankine cycles.

Several studies of SPT thermal plants using a volumetric receiver are carried out to design the efficient systems where some of them are commercialized or under development. Schwarzbozl et al. [116] investigated both the technical and economical aspects of optimized design of solarized GT systems with a solar tower using pressurized air receiver. As found the investment cost depends on the power level and solar share. Spelling et al. [117] made a thermo-economic optimization to determine the trade-off between LCOE and the initial

investment costs, thus permitting the plant to be most efficient and economic. Xu [118] et al. investigated the SPT plant using a molten salt based on the energy and exergy analysis. The results show the locations of different components where energy and exergy losses occur more. It is found also; that the overall performances and efficiency of SPT system could be increased by integrating some solutions like reheat Rankine cycles and supercritical Rankine cycles. Luo et al. [119] developed an optimization code to design and obtain the minimum levelized cost of electricity of a SPT power plant. Consequently, the called Sobol'-Simulated Annealing algorithm is carried out where the optimization code is a combined Sobol' method with the Simulated Annealing (SA) algorithm. The obtained results show that this proposed optimization method could reduce the number of optimization steps compared with that of the global algorithm and exhibits much more accurate optimal design. Xu et al. [120] built a mathematical model for a dynamic simulation of thermal energy storage (TES) system intended to SPT plant. It is found that recharge and discharge processes of the storage system could be used as a reference for further integrations of TES in a SPT power plants. Rovense et al. [121] proposed a SPT using closed Joule-Brayton cycle integrating a molten salt thermal storage; hence a thermo-economic analysis is carried out. The annual simulation of the thermal plant reveals noticeable energy production which is competitive with conventional energy production systems. Also, the economic assessment of the electricity cost demonstrated its feasibility and viability compared to the commercial plants.

Beaujardiere et al. [122] adopted Jülich SPT concept with different configurations of HRSG to transfer heat from air to water/steam cycle in a solar tower power plant with an open volumetric receiver. The analysis has shown that the highest conversion of solar energy is exhibited by the air return with a reheated HRSG dual pressure. Yamani et al. [123] compared the thermal performance of a solar tower technology using Brayton cycle based on an open volumetric receiver with the one based on Rankine cycle and a tubular water/steam receiver. Their conclusion is that the volumetric air receiver is strongly affected by the solar radiation intensity compared to tubular receiver, and the solar tower with Rankine cycle from the economic point of view is more competitive for the Algerian climate.

Stein et al. [124] discussed advanced power cycles driven by (CSP) technology with more attention to Brayton cycles based on the closed loop supercritical carbon dioxide (S-CO2) and air turbine CC. The solarized GT and closed cycle GT based on S-CO_2 offer high efficiency and may substitute the molten salt solar towers [124, 125]. There are mainly two versions for the integration of S-CO_2 Brayton cycles into SPT system: the direct-heated and the indirect-heated S-CO_2 Brayton power plant cycles. Wang et al. [126] investigated the highest overall

exergy efficiency of a molten salt solar tower coupled with S-CO_2 recompression Brayton cycle with thermal storage system. Therefore, the study is based on the optimum thermodynamic parameters including salt, temperature, and pressure cycle. Zhu et al. [127] integrated SPT in a topping cycle of direct-heated S-CO_2 Brayton cycles. Based on thermodynamic investigation of five different configurations including simple, pre-compression, recompression, partial-cooling and inter-cooling, the results have shown that the highest overall thermal efficiency is attributed to the inter-cooling S-CO_2 cycle followed the recompression. Kang et al. [128] simulated the performance of a solar tower coupled to a CC with solar integration in the topping air Brayton cycle. The study has shown that overall efficiency using particle suspension exceeds 48 % in a fully combined hybrid Brayton air-steam Rankine concept. Li et al. [129] studied the thermal performance of the so-called solar tower aided coal-fired power system, where three different schemes of solar integration were examined with saving fuel and power boosting modes. As a conclusion, the boiler and the solar field exhibit the highest exergy loss with lower coal consumption rate in the fuel saving mode for all three proposed schemes compared to the power boosting mode.

In the concept of ISCC system, solar heat is introduced in the bottoming Rankine cycle, therefore a SSG is generally added, and such a system offers several advantages over solar-only electric generation system or Rankine cycle [2, 130]. KRIBUS et al. [131] studied the feasibility of a new concept of solar thermal power plant which integrates a central receiver offering high temperatures to drive a combined cycle; thereby it is found that this new concept offers an advantage in solar-to-electric conversion with lower cost of electricity production. Stephan Heide et al. [132] proposed a concept of ISCC driven by CRS to increase the solar share where solar heat is injected into the GT between the compressor and the combustion chamber to achieve the high temperature for the pressurized air. Franchini et al. [93] have compared with ISCC-PTC the performances of SPT technology integrated into a CC using both oil as HTF to carry solar heat to the bottoming cycle. It is shown that the high annual solar-to-electric conversion is attributed to the ISCC with SPT. Zare et al. [133] proposed a novel configuration of a CRS integrated into a CC. The system consists of SPT with a closed Brayton cycle using helium as a working fluid and two organic Rankine cycles. The parametric study of energy and exergy examination shows that heliostat field is the largest source of losses and proposed cycles exhibit high efficiency and the new system performs better than Rankine and supercritical CO_2 cycles.

Okoroigwe et al. [2] reviewed ISCC driven by SPT system and compared to that based on PTC technology. It was concluded that the former is still immature. Zaversky et al. [134]

studied an innovative ISCC which consists of an open volumetric air receiver drives a conventional CC. The solar energy from the receiver heats up the compressor's air of GT via an air-air regenerative heat exchanger, and the results showed an improvement in solar-to-electric conversion compared to two different solar receivers. Khatoon et al. [135] have integrated a SPT using a molten salt as HTF with a CC plant. The latter consists of S-CO_2 topping cycle with a Rankine bottoming cycle. The performances investigation shows that this suggested plant could be a promising system for solar-to-electric conversion. Behar et al. [136] designed a solar receiver technology using the fluidized particle integrated into a combined cycle. It consists of solarized gas turbine using a solar tower, a Rankine cycle and thermal energy storage; thereby three operation modes of the present solar thermal plant were examined in terms of thermal performances and efficiency. The obtained results show that solar-to-electric efficiency reaches the value of 25.80 % for the hybrid mode while it varies from 21.16 % to 24.7 % for the solar-only operation mode. Besides, the methodology adopted in this study could be used to design large commercial scale of such thermal plant. Zoghi et al. [137] proposed a proposed a novel configuration of a solar tower system integrated into gas turbine cycle (GTC) and air bottoming cycle (ABC) with additional of subsystems for improving the thermodynamic performances. Thus, parametric investigation based on energy, exergy, exergoeconomic, and environmental analyses to assess the performances of such trigeneration system. Javadi et al. [138] have studied as well a double flash geothermal hybridized with a solar power tower (SPT) for multigeneration purposes. Thus, energy, exergy, and exergy-economy investigation based on the important parameters that have an impact on the system performance have been conducted. It is found that the integration of solar energy via the SPT technology into a geothermal power plant improves the overall thermal performances and it is more economic when compared to the same production capacity of the reference geothermal plant as expressed by the less use of geothermal extraction fluid. Boukelia et al [139] as well proposed a new design of solar tower plant (SPT) using molten salt hybridized with a binary geothermal power plant (BGPP). The BGPP based bottoming organic Rankine cycle (ORC) recovers the waste heat from SPT used for power generation and from thermodynamic analysis of such hybridization of SPT with a geothermal plant exhibits a significant improvements in term of performances when compared SPT stand-alone plant.

Very limited research effort has been consecrated for the development of solar tower coupled with a CC, while SPT plants with Jülich concept are running in a solar-only plant [95]. From

thermodynamic perspective, the SPT with volumetric receiver has a potential to be integrated in ISCC system due to the high working temperatures and economic perspective as well.

2.4. Conclusion

Integration of solar energy into a CC using CSP technology to constitute the ISCC is more attractive than stand-alone CSP plants. According to the literature, most of the ISCC power plants in operation today employ PTC technology (ISCC-PTC) with no known commercial ISCC plant at present driven by a SPT system (ISCC-SPT). This is because; the maturity level of the SPT technology is lower than that PTC. Furthermore, very limited research has been directed toward the development of the ISCC-SPT where the existed SPT plants are operating in solar-only mode. Consequently, thermodynamic and economic investigations of PTC and SPT systems integrated into a CC are carried out in the next sections. The first plant is an ISCC-PTC with Hassi R'mel concept where the solar heat from parabolic collectors introduced in the steam cycle. The second plant is an ISCC-SPT which is a new hybridization of SPT into CC. where solar heat from the tower receiver is injected into the flues gases from the GT before entering HRSG. The obtained results are compared between these two ISCC configurations to find out the most efficient solar thermal power plant.

Chapter 3

Thermo-economic Assessment of the first Integrated Solar Combined Cycle System in Algeria

3.1. Introduction

PTC technology is the most proven and lowest cost large-scale solar power system available today, primarily because of the nine large commercial-scale solar power plants that are operating in the California Mojave Desert. The Luz collector technology has demonstrated its ability to operate in a commercial power plant environment like no other solar technology in the world [1]. Hybrid solar thermal power plants with parabolic trough solar collectors, featuring gas burners and Rankine steam cycles have been successfully demonstrated by California's Solar Electric Generating System (SEGS). The particular interest is the integration of PTC technology with CC power plant. This configuration is referred to Integrated Solar Combined Cycle (ISCC) system.

Large numbers of CSP plants using PTCs technology are under development over the world, and there are typically nine large commercial-scale solar power plants of 354 MW installed in the Mojave desert, in addition to several others of same technology operating in Italy, Iran and in North Africa.

The aim of this section is to assess thermodynamically and economically the first ISCC power plant in Algeria integrating solar thermal energy into a CC. The solar heat collected by HTF through PTC solar field is integrated in the Rankine cycle via a Solar Steam Generator (SSG) and used as latent heat to generate saturated steam. SSG is working as a boiler (evaporator) in parallel to that one from HRSG to enhance the quantity of generated steam flow rate during the sunny periods. This ISCC configuration makes the solar integration use one heat exchanger which is the boiler and avoiding preheating and superheating exchangers. During daily light the power plant operates as ISCC whereas during night or cloudy days it operates as a conventional CC. The heat exchangers network is a critically important subsystem of the

power plant configuration, which the main purpose of analysis is to estimate steam turbine inlet temperature and steam mass flow rate; hence the method of pinch point and approach point are used in the thermodynamic modelling. Present numerical simulations are under different operations with solar irradiation varying during the day, and for economical issue LCOE is evaluated. Simulations results of such a complex plant under the Saharan climate allowed seeing the feasibility of such technology and how it is efficient, and may support future installations using parabolic troughs.

3.2. Mathematical model of a parabolic through collector

Parabolic trough collector (PTC) will focus radiation on a receiver much smaller than the reflector. A PTC, like the one represented in Figure 1.9, is basically made up of a parabolic trough shaped mirror that reflects direct solar radiation, concentrating it onto a receiver tube located in the focal line of the parabola. Concentration of the direct solar radiation reduces the absorber surface area with respect to the collector aperture area and thus significantly reduces the overall thermal losses. The concentrated radiation heats the Heat Transfer Fluid (HTF) circulating through the receiver tube, thus transforming the solar radiation into thermal energy in the form of the sensible heat of the HTF. This section treats the optical and thermal performances of these collectors [1,140-142].

3.2.1. Collector's optical performances

The PTC solar field reflects the Direct Normal Irradiation (DNI) onto the receiver where solar heat is transferred to Therminol VP-1 HTF. The analyzed PTC is LS-3 type for Schott's 2008 PTR70 parabolic trough receiver.

The useful solar energy gained by the Heat Collector Element (HCE) or PTC receiver that is transferred to HTF is calculated as follows:

$$Q_u = Q_{abs} - Q_{loss} \tag{3.1}$$

Where:

$$Q_{abs} = \eta_0(\theta) A_c DNI \tag{3.2}$$

Q_{loss} is the sum of heat losses from PTC receiver $Q_{loss,rec}$ and from piping $Q_{loss,pip}$:

$$Q_{loss} = Q_{loss,rec} + Q_{loss,pip} \tag{3.3}$$

With [102, 142]:

$$Q_{loss,rec} = a_0 + a_1\left(T_f - T_a\right) + a_2\, T_f^2 + a_3\, T_f^3 + a_4\, DNI\, K(\theta)\, cos(\theta) T_f^2 + \sqrt{V_w}\left(a_5 + a_6\, \Delta T_f\right) \tag{3.4}$$

The coefficients of the heat loss correlation for the 2008 PTR70 heat collection elements for LS-3 collector type are given by the Table 3.1 below [141, 142]:

Table 3.1. 2008 PTR70 heat loss coefficients

Coefficient	a_0	a_1	a_2	a_3	a_4	a_5	a_6
Value	4.05	0.247	−0.00146	$5.65\ 10^{-6}$	$7.62\ 10^{-8}$	−1.70	0.0125

The heat losses due to piping $Q_{loss,pip}$ are given by the following equation in a function of temperature in a polynomial form:

$$Q_{loss,pip} = 1.693\ 10^{-2}\Delta T - 1.683\ 10^{-4}\Delta T^2 + 6.78\ 10^{-7}\Delta T^3 \tag{3.5}$$

With ΔT is the difference between the average field temperature and the ambient air temperature as given below [141, 102]:

$$\Delta T = \frac{T_{f,out} + T_{f,in}}{2} - T_a \tag{3.6}$$

The optical efficiency $\eta_0(\theta)$ is given by the following equation [140]:

$$\eta_0(\theta) = \eta_{nominal}\, K(\theta) f_{row\ shadow}\, f_{end\ loss}\, f_{clean} \tag{3.7}$$

Where $\eta_{nominal}$ is the nominal optical efficiency and $K(\theta)$ is the incidence angle modifier [140, 143]:

$$\eta_{nominal} = \rho_{col}\tau_{cov}\alpha_{abs}\gamma_{col} \tag{3.8}$$

ρ_{col} is the reflectance of the clean collector, τ_{cov} is transmittance of the glass envelope, α_{abs} is absorptance of the absorber surface coating, γ_{col} is the intercept collector.

It is necessary to use the incident angle modifier which gives the error in the concentration counter due to using the sun tracking system:

$$K(\theta) = 1 - 2.2307\ 10^{-4}\theta - 1.1\ 10^{-4}\theta^2 + 3.18596\ 10^{-6}\theta^3 - 4.85509\ 10^{-8}\theta^4 \tag{3.9}$$

The shading factor caused by tracking of the collectors to the sun is defined as the ratio of the effective mirror aperture area, i.e. the illuminated area of mirror, to the total aperture area [140, 143]:

$$f_{row\ shadow} = min\left(max\left(0.0; \frac{L_{space}}{W_a}\frac{\cos\theta_z}{\cos\theta}; 1.0\right)\right) \tag{3.10}$$

The collector geometrical end losses can be formulated as [141,144]:

$$f_{end\ loss} = max\left(0; 1 - \frac{f_{PTC}}{L_{PTC}}\left(1 + \frac{W_a^2}{48 f_{PTC}^2}\right)\tan\theta\right) \tag{3.11}$$

f_{clean} is the cleanliness factor which is equal to 1 for a clean surface.

This thermal balance is represented by the Figure below.

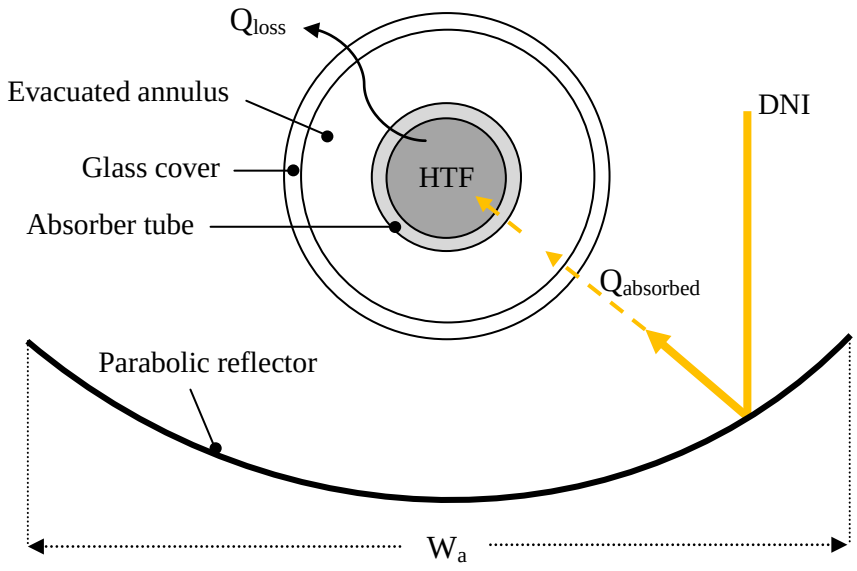

Figure 3.1. Schott's 2008 PTR70 Parabolic Trough Receiver for LS-3 collector type

3.2.2. PTC solar field

The solar field consists of a numerous PTCs, as shown in Figure 1.10 each collector has a linear parabolic shaped reflector that focuses the sun's direct beam radiation on a linear receiver located at the focus of the parabola. A HTF is heated as it circulates through the receiver to collect the solar heat and returns to the SSG heat exchanger to generate saturated steam [1].

The solar field's basic component is the parabolic trough collector (PTC). Each PTC is made up of parabolic reflectors (mirror), a metal support structure (pylon and support), a receiver tubes, glass cover and a tracking system that includes a drive, sensors and controls.

The total useful energy gained by HTF in the PTC solar field is given by [103]:

$$Q_{PTC\ solar\ field} = N_L C_L Q_u \tag{3.12}$$

where N_L, C_L are respectively, the number of collectors in each row and the number of lines in the solar field.

Total HTF mass flow rate $\dot{m}_{HTF}$ is calculated as follows [141]:

$$\dot{m}_{HTF} = \frac{Q_{PTC\ solar\ field}}{C_{p,HTF}\left(T_{HTF,o} - T_{HTF,i}\right)} \tag{3.13}$$

The solar field efficiency is the ratio of the net useful energy gained by the solar field and the total quantity of solar beam reaching the mirrors [140]:

$$\eta_{PTC\ solar\ field} = \frac{Q_{PTC\ solar\ field}}{N_L C_L A_c DNI} \tag{3.14}$$

HTF that used in the solar field is Therminol VP-1 with a specific heat is given in a function of temperature in a polynomial form [145]:

$$C_{p,HTF} = 0.002414\,T - 5.9591\,10^{-6}\,T^2 - 2.9879\,10^{-8}\,T^3 + 4.4172\,10^{-11}\,T^4 + 1.498 \tag{3.15}$$

3.3. Modeling of the first Integrated Solar Combined Cycle Systems in Algeria

The first Integrated Solar Combined Cycle (ISCC) system installed in Hassi R'mel (Algeria) is a new design that integrates a PTC field with a modern CC power plant. This ISCC configuration was proposed and designed by Abener and Abengoa Solar and consists of two GT units of 47 MW, a ST unit with a capacity of 80 MW, and a PTC solar field of 183120 m^2 to produce an estimated capacity about 150 MW [89]. This solar integration provides a great flexibility of management and control that were difficult to realize in the traditional solar power stations. The adjustment of the solar power station can be done by the flexibility of the GTs or by the solar concentrators. The ISCC has generated much interest because it offers an innovative way to reduce cost and improve the overall solar to electric efficiency. This power plant operates at the CC mode during non solar periods, and then the output would increase when solar energy is available. The initial concept was simply to increase the size of the steam turbine (ST), use solar energy to generate steam, and use the waste heat from the gas turbine to preheat and superheat the steam. A number of recent studies have looked at the best approaches for this integration. Most designs have looked at oversizing the steam turbine. ISCC plants typically have very low solar contributions, on the order of 1 % to 15 % of annual output for a base load combined cycle plant.

In the concept of this first ISCC plant located Hassi R'mel, due to the high DNI available in that region, a simple pressure level is proposed. During sunny periods, one part of feed water is withdrawn from the HRSG converted to saturated steam in the SSG. This saturated steam is returned to the HRSG where it is mixed and superheated. At night and during cloudy periods the ISCC system operates as a CC. A process flow diagram for the present ISCC is shown in figure 3.5.

3.3.1. Thermodynamic modelling

As shown by figure 3.5, ISCC of Hassi R'mel consists of two GT units, a ST unit, two HRSG with simple pressure level, a SSG working in parallel with HRSG evaporators and a solar

field without storage or back-up system. During the sunny periods one part of feed water is withdrawn from HRSG and converted to saturated steam in SSG and then returned to HRSG where it is mixed and superheated. The supplement of solar thermal energy provides an increase in steam mass flow of the Rankine cycle. In the other side, during cloudy periods and nights ISCC plant operates as a conventional CC. Based on the pinch and approach points, the flue gases and steam mass flow rates and temperatures are the key parameters.

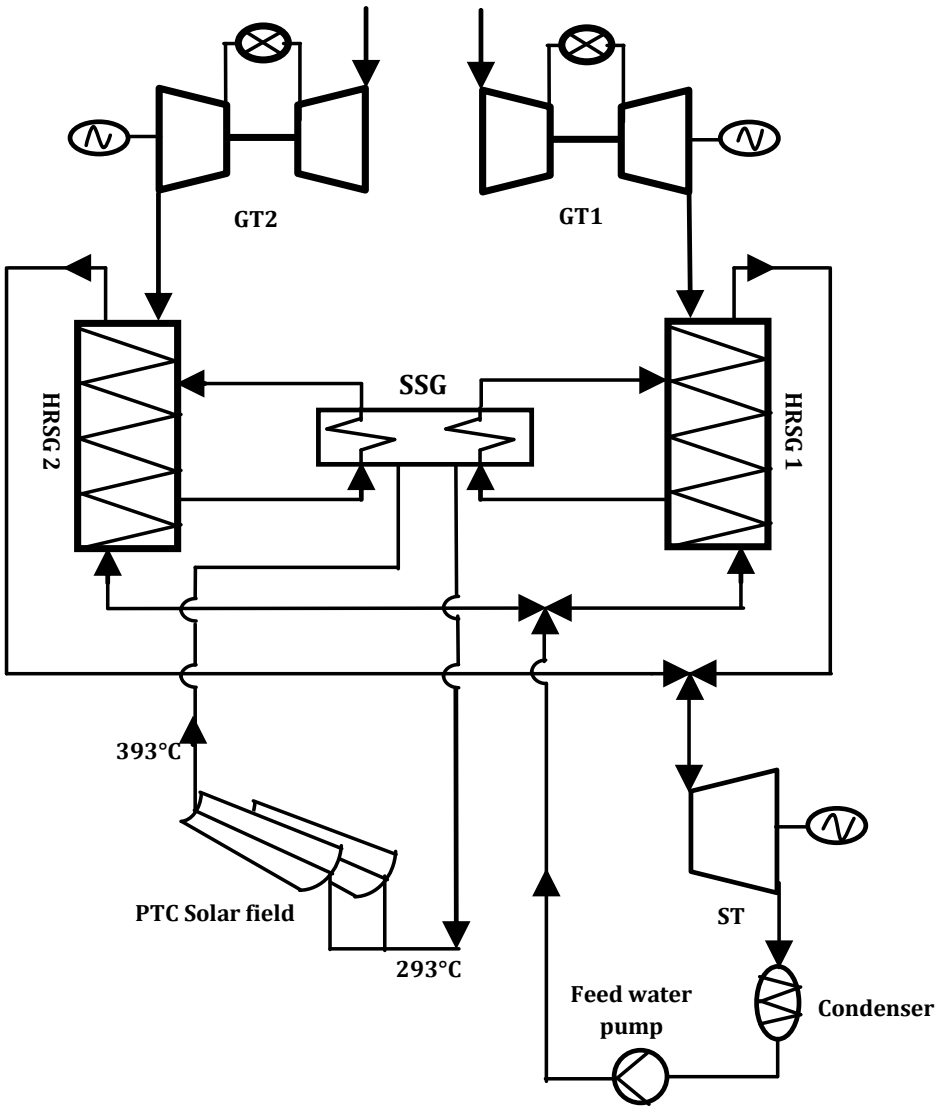

Figure 3.2. Schematic of ISCC Hassi R'mel power plant

3.3.1.1. PTC Solar Field

The solar field is divided in two parts; both consists of a numerous PTCs oriented north–south to maximize solar energy collection. The collectors track the sun from east to west during the day to ensure that the sun is continuously focused on the linear receiver and reflect the solar

direct irradiation (DNI) onto the receiver where solar heat is transferred to Therminol VP-1 HTF.

The solar field parameters and specifications are given in the Table below:

Table 3.2. PTC parameters

Parameters	Values
PTC LS-3 collector type specifications	
Aperture area (m^2)	545
Aperture (m)	5.76
Length (m)	99
Intercept factor γ (%)	96
Absorptivity α (%)	95
Reflectivity ρ (%)	98
Transmissivity τ (%)	97
Concentration ratio Cc	82
Solar field operation parameters	
Number of collectors in each row	6
Number of lines	56
HTF inlet temperature (°C)	293
HTF outlet temperature (°C)	393
Solar field area (m^2)	183120

3.3.1.2. GT model

The current GT used in the present work doesn't require any modification when it is coupled to SPT system where the open volumetric air receiver is used to heat up the flue gases from the GT at atmospheric pressure; in contrast to solarized GT in which some modifications on GT and volumetric receiver to resist at a pressure of 15 Bar are required. In modern and currently technology GT the polytropic efficiency for the compressor and turbine are about 0.9, considered constant during the calculation [146]. The cooling evaluation is based on references [147]. The mechanical and electrical efficiency are in the range 97 %-99 % while the combustion chamber efficiency is about 98 %-100 % [148]. Moreover, the typical value of pressure drop in the combustion chamber and HRSG are 2 %-6 % [149] and for filtration is 0.005-0.015 bar [150].

The gas turbine power plant can be described by considering air flowing into the compressor, getting heated in the combustor, and producing power by interacting with the turbine blades. Air is considered to be the working fluid where it is compressed in the compressor, receives heat from an external source in the combustor, and expands in the turbine.

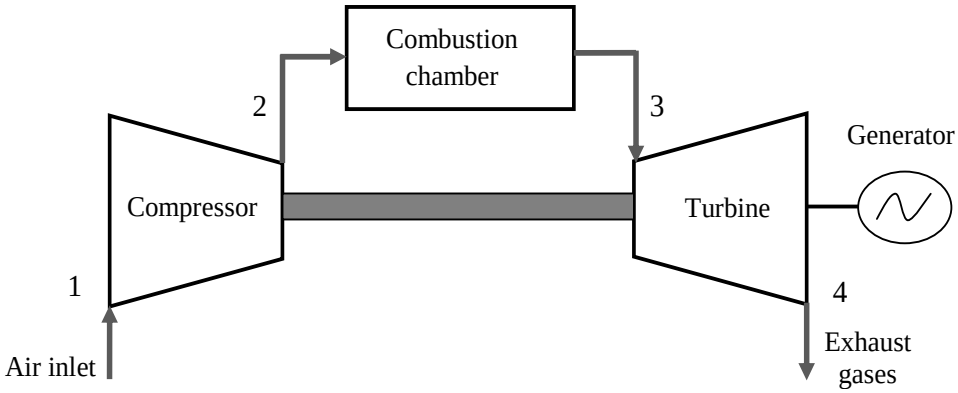

Figure 3.3. Schematic for a gas turbine cycle

As shown in the following figure, the thermodynamic cycle of the ideal gas turbine, known as the ideal Brayton cycle, consists of four processes: isentropic compression, constant pressure heat addition in the combustion chamber isentropic expansion and constant pressure heat rejection.

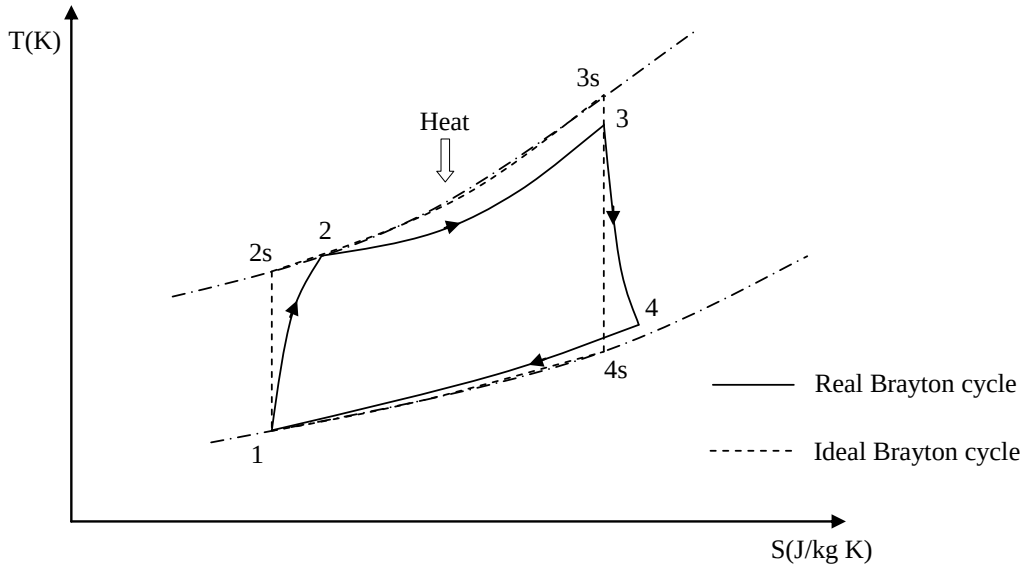

Figure 3.4. Brayton cycle

The difference between ideal and real Brayton cycle represents the energy and the exergy losses including adiabatic compression, pressure drop within heat adding process and adiabatic expansion

The thermodynamic process of the Brayton cycle is formulated with the same detailed model given by the reference [151]:

The compressor consumed power is given by:

$$W_C = \dot{m}_a \overline{C_{pa}} (T_2 - T_1) \tag{3.16}$$

T_2 computed from isentropic efficiency via polytropic efficiency and pressure rise and obtained iteratively.

$$\eta_{cs} = \frac{\pi_c^{\frac{\gamma_c - 1}{\gamma_c}} - 1}{\pi_c^{\frac{\gamma_c - 1}{\eta_{pc}\gamma_c}} - 1} \tag{3.17}$$

An experimental mean specific heat of air at constant pressure in the compressor section, with a, b, c, d are constants given in Table 3.5 [152].

$$C_{pa} = a + bT + cT^2 + dT^3 \tag{3.18}$$

The output power of the expansion gases in the gas turbine equals:

$$W_T = \dot{m}_g \overline{C_{pg}} (T_3 - T_4) \tag{3.19}$$

T_4 obtained iteratively from isentropic efficiency definition and polytropic efficiency and expansion:

$$\eta_{Ts} = \frac{1 - \pi_t^{-\frac{\gamma_t - 1}{\gamma_t}\eta_{pt}}}{1 - \pi_t^{-\frac{\gamma_t - 1}{\gamma_t}}} \tag{3.20}$$

An experimental estimate the mean specific heat at constant pressure in the turbine section, for exhaust gases compositions parameters a_i, b_i, c_i, d_i are given in Table 3.5 [152].

$$C_{pg} = a_i + b_i T + c_i T^2 + d_i T^3 \tag{3.21}$$

In case the expansion work of air cooling in the turbine section is taking into account, after the compression process some air is extracted for the air cooling system. The extracted air is used for the internal cooling system of the turbine blades. Thus the mass flow rate of the cooling system is estimated by an experimental correlation as follows:

$$\dot{m}_{cool,a} = \dot{m}_a [0.02 + 0.00032\ (T_3 - T_b)] \tag{3.21}$$

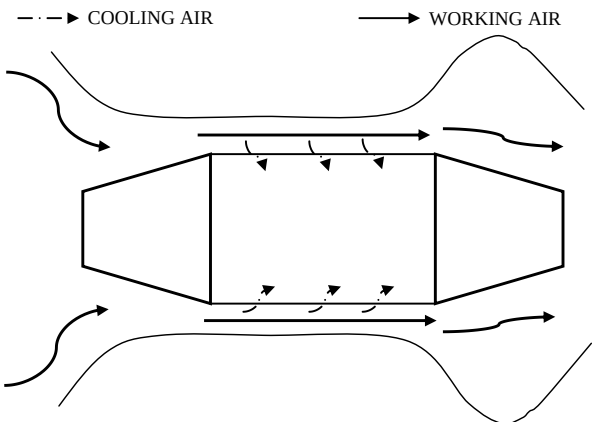

Figure 3.5. Air flow into the gas turbine

The expansion work $W_{T,g}$ taking into account the effect of cooling air system is:

$$W_{T,g} = W_T - \Phi Q_R \tag{3.22}$$

The relative quantity of extraction heat in the cooling system is:

$$Q_R = \dot{m}_{cool,a}(h_{cool,a} - h_2) \tag{3.23}$$

With:
$$\Phi = 1 - \left(\frac{T_4}{T_3}\right) \tag{3.24}$$

The air cooling temperature at the end of the cooling process is given by:

$$T_{cool,a} = T_2 + (T_b - T_2)\, \varepsilon_{cool,a} \tag{3.25}$$

Where $\varepsilon_{cool,a}$ is the cooling system effectiveness its typical value 0.42.

The expansion ratio for cooling air within the turbine is then evaluated:

$$\pi_{cool,a} = \left(1 - \xi_{cool,a}\right)\pi_t \tag{3.26}$$

Where: $\xi_{cool,a}$ is the expansion coefficient of cooling air, its typical value 0.35.

Then the cooling air temperature at the end of the expansion process $T_{4,cool,a}$:

$$T_{4s,cool,a} = T_{cool,a}\left(\pi_{cool,a}\right)^{\frac{1-\pi_t}{\pi_t}} \tag{3.27}$$

thus:
$$h_{4,cool,a} = h_{cool,a} + \eta_{Ts}\left(h_{cool,a} - h_{4,cool,a}\right) \tag{3.28}$$

The work of the cooling air expansion in the gas turbine is calculated:

$$W_{cool,a} = \dot{m}_{cool,a}\left(h_{cool,a} - h_{4,cool,a}\right) \tag{3.29}$$

The turbine power is summed from the expansion of gases and cooling air:

$$W_T = W_{T,g} + W_{cool,a} \tag{3.30}$$

The net power of GT is thus estimated according to:

$$W_{GTnet} = \dot{m}_a \eta_e \eta_m \left[(1 + f + e)\overline{C_{pg}}(T_3 - T_4) - \overline{C_{pa}}(T_2 - T_1)\right] \tag{3.31}$$

Where $f = \dot{m}_f / \dot{m}_a$ designates the ratio between the fuel and the air mass flow rates, and *e* is the fraction of air in cooling.

The fuel mass flow rate is obtained by utilizing the energy balance of the combustion chamber for the natural gas.

$$f = \frac{C_{pg}T_3 - C_{pa}T_2}{\eta_b Q_{cv} - C_{pg}T_3} \tag{3.32}$$

The GT unit efficiency is equal to the net output divided by the energy input to the thermal cycle. The fuel mass flow rate is obtained by utilizing the energy balance of the combustion chamber for natural gas.

$$\eta_{GT} = \frac{W_{GTnet}}{\dot{m}_f Q_{cv}} \tag{3.33}$$

The thermodynamic GT model developed in this study is validated upon Siemens SGT 800 [155]. GT power, efficiency and exhaust gases mass flow rates and temperature are validated (Table 3.4) for the design ambient temperature and a good agreement is achieved.

Table 3.3. Gas turbine data

Parameters	Symbols	Values	Units
Ambient temperature	T_a	21	°C
Atmospheric pressure	P_a	1.013	bar
Turbine inlet temperature	T_3	1200	°C
Pressure ratio	π	19.9	---
Turbine blade temperature	T_b	850	°C
Cooling system effectiveness	ε_R	42	%
Compressor polytropic efficiency	η_{pk}	90	%
Turbine polytropic efficiency	η_{pT}	91	%
Combustion efficiency	η_b	98	%
Mechanical efficiency	η_m	98	%
Electrical efficiency	η_e	98.5	%
Compressor inlet pressure losses	δP_1	0.5 %	%
Combustion pressure losses	δP_2	2 %	%
Pressure losses in HRSG	δP_3	2 %	%
Natural gas calorific value	Q_{cv}	46595	kJ/kg
Gas turbine output	W_{GTnet}	47	MW

Table 3.4. GT validation [93, 153]

Parameters	SGT-800	Predicted	Error (%)
Compressor air mass flow (kg/s)	129	126.16	2.2
Exhaust gases mass flow (kg/s)	131.5	129.02	1.8
Exhaust gases temperature (°C)	548	544.33	0.66
Gas turbine efficiency (%)	37	35.69	3.54

The specific heat of the air or gases is a function of temperature where the mean value is used at any section [152]:

$$\overline{C_{pg}} = \frac{\int_{T_i}^{T_o}(a + bT + cT^2 + dT^3)\,dT}{(T_o - T_i)} \tag{3.34}$$

The chart (Fig.3.6) shows an iterative calculation for the specific heat of exhaust gases through inlet to outlet the heat exchange section (GT and HRSG sections) by using Eqs. (3.34) and (3.35).

$$Q = \dot{m}_g \overline{C_{pg}}(T_o - T_i) \text{ then } T_o = \frac{Q}{\dot{m}_g \overline{C_{pg}}(T_o)} + T_i \text{ with } f\left(\overline{C_{pg}}(T_o)\right) = \frac{Q}{\dot{m}_g \overline{C_{pg}}(T_o)} + T_i \tag{3.35}$$

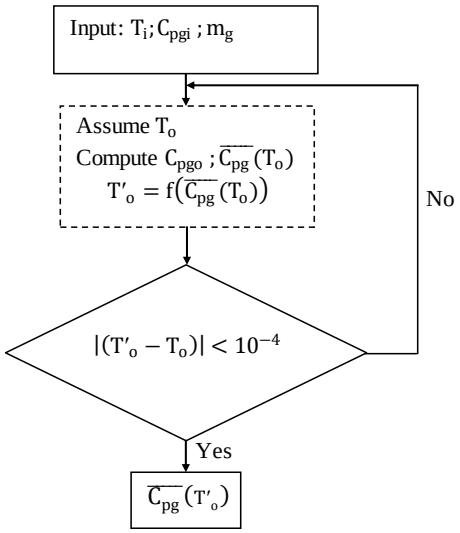

Figure 3.6. Determination of specific heat of gases

Here below, the constants of gases composition for determination of specific heat of gases at any section.

Table 3.5. Gases compositions and parameters [152]

Exhaust gases	Mass fraction C_i	M (kg/K.mol)	r (kj/kg.K)	a	b ($/10^{-2}$)	c ($/10^{-5}$)	d ($/10^{-9}$)
O_2	13.16	31.999	0.2598	25.48	1.52	-0.7155	1.312
N_2	74.514	28.013	0.2968	28.90	-0.1571	0.8081	-2.873
H_2O	7.893	18.15	0.4615	32.24	0.1923	1.055	-0.3593
CO_2	3.537	44.010	0.1889	22.26	5.981	-3.501	7.469
Others	0.896	-	-	-	-	-	-

3.3.1.3. Rankine Model / Steam generation

As first solar beam appears the plant works as ISCC. The amount of steam generated in the heat exchangers network (HRSGs+SSG) which is double enhances electricity production. Such of solar thermal plant uses an oversized ST because of the increased rate of superheated

steam generated due to solar thermal addition during the day. An oversized ST offers two advantages as the incremental cost for a larger ST is lesser than the overall unit cost in a solar-only plant, and also the integrated plant does not suffer from the thermal inefficiencies associated with the daily startup and shutdown of the steam turbine [154]. To recover some heat from the solar field, a SSG is used and the HRSG made up of three heat exchangers: superheater, evaporator and economizer.

While solar irradiation is available, one part of feed water is withdrawn from HRSG and converted into saturated steam by SSG and then returned back to HRSG where it is mixed and superheated as displayed by the Fig.3.7 The steam power block consists of two similar HRSGs and one SSG, thus we represent only one side for the steam generation process.

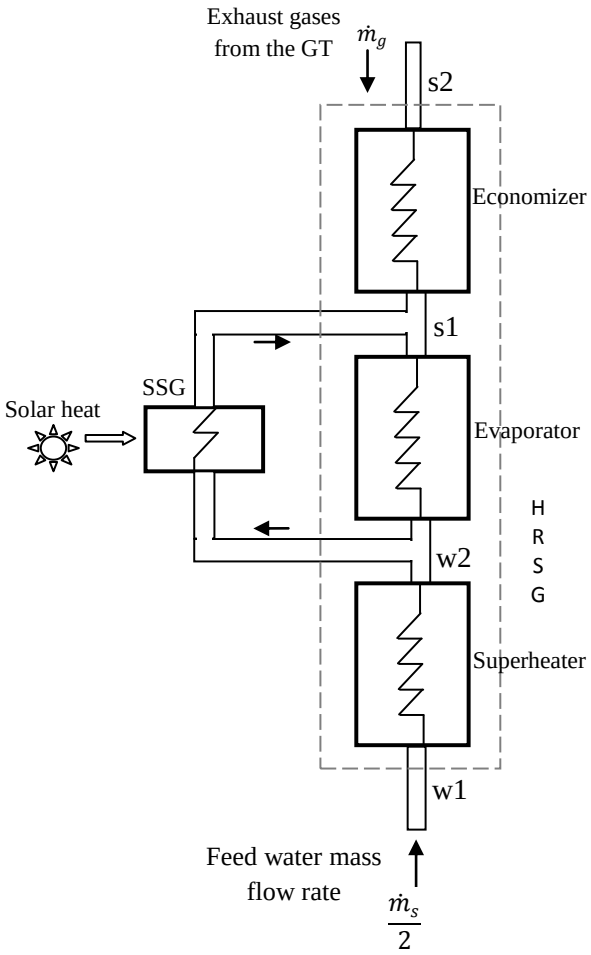

Figure 3.7. Heat exchangers network

The Rankine thermodynamic cycle for steam generation process is shown in the diagram T-S as displayed by the Figure below

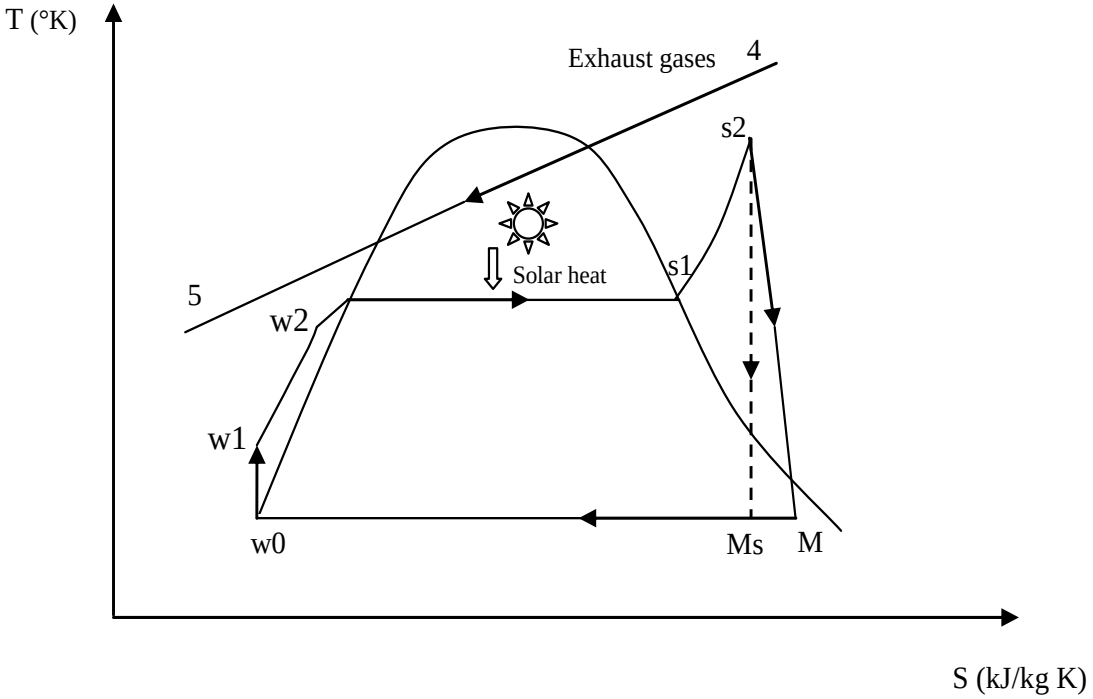

Figure 3.8. Rankine-Hirn cyle

In the design mode one can determine the gas–steam temperature profiles, the duty of each component and the mass flow rate of steam generation. Design condition is typically that of design mode of HRSG operation when the ISCC system operates as a conventional CC. This is done by simply selecting the pinch and the approach points at each evaporator level. In the low gas temperature heat recovery systems, the steam pressure and the pinch point play a crucial role in determining the gas–steam temperature profiles, and the exit gas temperature from the economizer cannot be arbitrarily assumed [155]. A temperature profile analysis is performed to evaluate the steam generation. The exhaust gases parameters are exported to CC thermal cycle with the principle input parameters of HRSG are the gas temperature outlet (from GT) $T_{hrsg1}$and the gas mass flow $\dot{m}_g$.

In this section, a thermodynamic method developed by Ganapathy is adopted to evaluate the HRSG performances and the quantity of steam generated in design and off-design modes [155, 156]. The two HRSG and are typically the same and the solar field is divided on two equal parts, thus the analysis of one HRSG and solar heat coming from one part of solar field is carried out then the evaluated steam mass flow value $\dot{m}_s$ is doubled. The determination of the steam generated during night or cloudy periods (design mode) is carried out according to this following procedure:

- Design mode

In the design mode, the gas–steam temperature profiles (Fig.3.9), each component duty, steam generation and exit gases temperature are determined by simply selecting the pinch point and the approach point at each evaporator level.

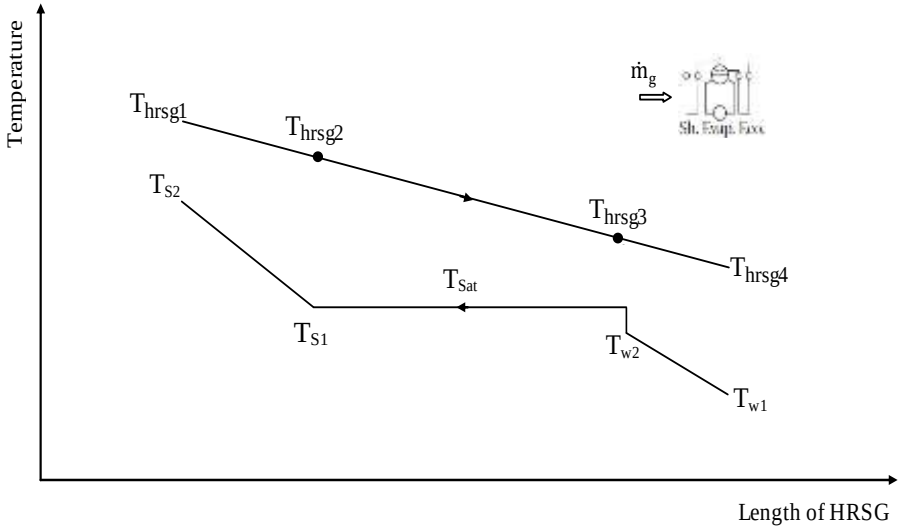

Figure 3.9. Deign mode gas-steam temperature profiles

Based on the reference [155] the proposed values of pinch point $\Delta T_{pp} = T_{hrsg3} - T_{sat}$ and approach point $\Delta T_{ap} = T_{sat} - T_{w2}$ are defined in Table 3.6.

Table 3.6. Pinch point and approach point [155]

Evaporator type	Plain tubes	Finned tubes	For both
Gas inlet temperature (°C)	Pinch point (°C)	Pinch point (°C)	Approach point (°C)
650-900	60 - 85	20-35	20-40
375-650	40-60	5-20	5-20

The determination of the steam generated at the design point during the night or cloudy periods is as follows:

From the energy balance of the superheater and evaporator including the heat loss factor and blow down:

$$0.99\,\dot{m}_{g,d}\overline{C_{pg}}\left(T_{hrsg1} - T_{hrsg3}\right) = \dot{m}_{s,d}(h_{s2} - h_{w2}) + 0.01\,\dot{m}_{s,d}\left(h_{w,sat} - h_{w2}\right) \quad (3.36)$$

With:

$$T_{hrsg3} = T_{sat} + \Delta T_{pp} \quad (3.37)$$

$$\dot{m}_{s,d} = \frac{0.99\,\dot{m}_{g,d}\overline{C_{pg}}(T_{hrsg1} - T_{hrsg3})}{\left((h_{s2} - h_{w2}) + 0.01\,\left(h_{w,sat} - h_{w2}\right)\right)} \quad (3.38)$$

Energy balance of economizer:

$$\dot{m}_{g,d}\overline{C_{pg}}\left(T_{hrsg3} - T_{hrsg4}\right) = 1.01\,\dot{m}_{s,d}(h_{w2} - h_{w1}) \quad (3.39)$$

$$T_{hrsg4} = T_{hrsg3} - \frac{1.01\,\dot{m}_{s,d}(h_{w2} - h_{w1})}{\dot{m}_{g,d}\overline{C_{pg}}} \tag{3.40}$$

The factor $(UA)_d$ of each section of HRSG is calculated from the heat transfer relation using Log-mean temperature difference $LMTD$:

$$(UA)_d = \left(\frac{Q}{LMTD}\right)_d \tag{3.41}$$

A subprogram of steam cycle in enthalpy-entropy diagram interpolates between the tabulated values of enthalpy and entropy of water/steam at each points including the steam quality x and specific volume v at design and off-design modes.

- *Off-design operation*

When the solar radiation and ambient temperature are changing during the day, the exhaust gas flow rate, temperature conditions or any of steam parameters also change this lead to an off-design and thus the new properties are evaluated at each section from an iterative procedure. The solar energy is injected as latent heat in parallel to the HRSG evaporator via a SSG as shown by Fig.3.10, and then the SSG and HRSG evaporator constitute a one block as they generate in parallel the saturated steam.

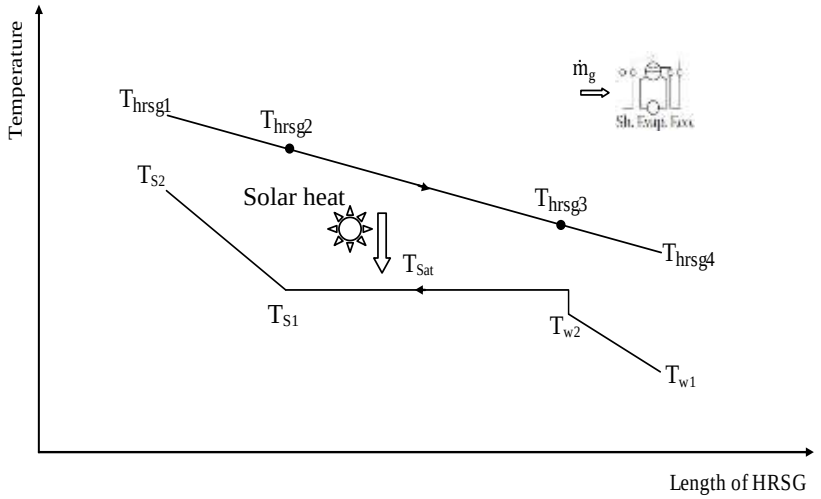

Figure 3.10. Off-design gas-steam temperature profiles

Once the design mode is established, in order to predict HRSG performance under DNI and temperature variation, several guessed values and iterations steps are required before arriving at the final heat balance, steam flow generation and duty. The heat loss factor and the blow down for HRSG and SSG are also considered in off-design.

The off-design value of UA is obtained by using correction factors for gas flow and steam flow [155]:

$$UA = (UA)_d \left(\frac{\dot{m}_g}{\dot{m}_{g,d}}\right)^{0.65} \left(\frac{F_g}{F_{g,d}}\right) \left(\frac{\dot{m}_s}{\dot{m}_{s,d}}\right)^{0.15} \quad (3.42)$$

The steam flow correction $\left(\frac{\dot{m}_s}{\dot{m}_{s,d}}\right)^{0.15}$ is not required for evaporator and economizer and $\left(\frac{F_g}{F_{g,d}}\right)$ is the correction factors for gas flow and taken with a value of 0.99 where the gas property factors $F_g = \frac{{c_p}^{0.33} k^{0.67}}{\mu^{0.32}}$. The procedure of evaluating the steam generated through HRSG in off-design is completely iterative as shown by the flowchart in Fig.3.11 and detailed below by the principle calculation. In these calculations, several trial and error steps are required before arriving at the final heat balance, duty and steam flow generation. In off-design the steam flow $\dot{m}_s$ is assumed at first, and iterations are required to arrive at the final result. From the relation between design value $(UA)_d$ and off-design value (UA) and equation $Q = (UA)LMTD$ the duty in off-design is obtained and subsequently the generated steam.

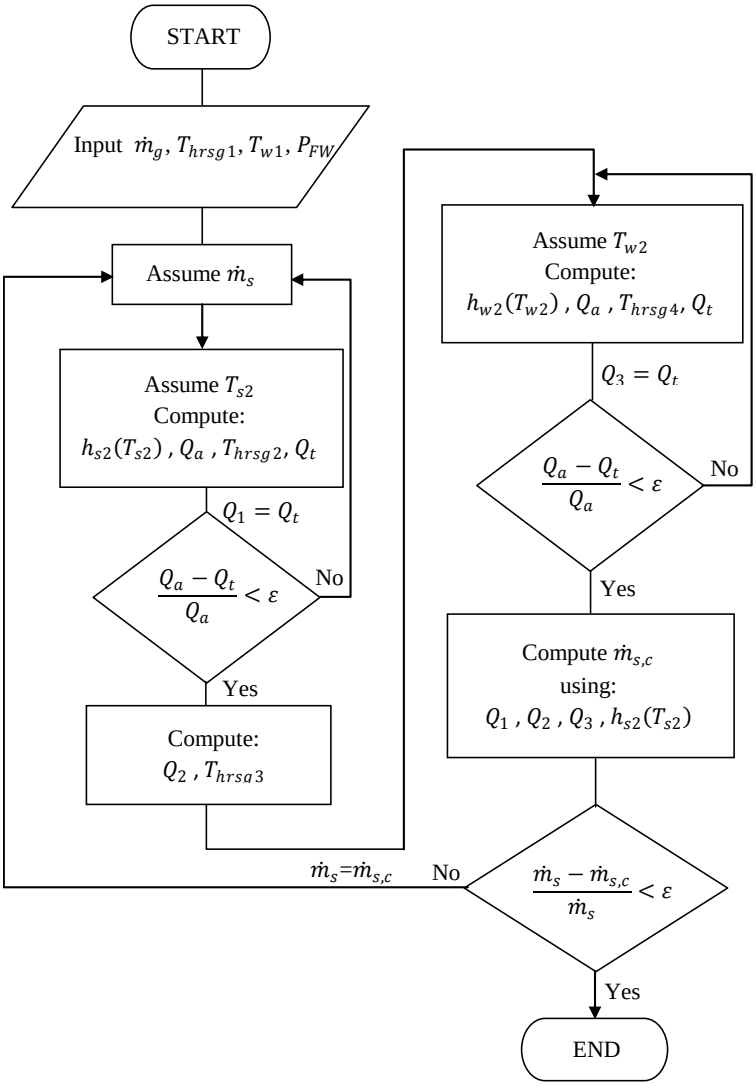

Figure 3.11. Evaluation of steam generation in HRSG

As first solar beam appears, the plants both work as an ISCC and the amount of steam generated in the heat exchangers network enhances the electricity production. The first value of steam mass flow $\dot{m}_s$ is assumed as displayed by the flowchart:

- Superheater level

Assume T_{s2} then find $h_{s2}(T_{s2})$ and calculate:

$$Q_a = \dot{m}_s(h_{s2} - h_{s1})$$

with: $$T_{hrsg2} = T_{hrsg1} - \frac{Q_a}{\dot{m}_g \overline{C_{pg}}}$$

calculate: $$Q_t = (UA)LMTD$$

with: $$LMTD = \frac{(T_{hrsg2} - T_{sat}) - (T_{hrsg1} - T_{s2})}{\ln \frac{(T_{hrsg2} - T_{sat})}{(T_{hrsg1} - T_{s2})}}$$

estimate: $$(UA) = (UA)_d \left(\frac{\dot{m}_g}{\dot{m}_{gd}}\right)^{0.65} \left(\frac{F_g}{F_{gd}}\right) \left(\frac{\dot{m}_s}{\dot{m}_{sd}}\right)^{0.15}$$

check $\frac{(Q_a - Q_t)}{Q_a} < 10^{-4}$ then the assumed duty Q_a and steam/gas temperatures $(\dot{T}_{s2}/T_{hrsg2})$ are correct then put $Q_t = Q_1$ and pass to the second step which is the evaporator level. Otherwise, the case $\frac{(Q_a - Q_t)}{Q_a} \geq 10^{-4}$ assume another value of steam temperature T_{s2}.

- Evaporator level

$$\ln \frac{(T_{hrsg2} - T_{sat})}{(T_{hrsg3} - T_{sat})} = \frac{UA}{\dot{m}_g \overline{C_{pg}}} \quad \text{and} \quad \ln \frac{(T_{hrsg2,d} - T_{sat})}{(T_{hrsg3,d} - T_{sat})} = K(\dot{m}_g)_d^{-0.4}$$

with: $$K = f\left(A/\overline{C_{pg}}\right)$$

then $$K = (\dot{m}_g)_d^{0.4} \ln \frac{(T_{hrsg2,d} - T_{sat})}{(T_{hrsg3,d} - T_{sat})}$$

calculate T_{hrsg3}, where: $$\ln \frac{(T_{hrsg2} - T_{sat})}{(T_{hrsg3} - T_{sat})} = K(\dot{m}_g)^{-0.4}$$

then: $$Q = \dot{m}_g \overline{C_{pg}} (T_{hrsg2} - T_{hrsg3})$$

and: $$Q_2 = Q + \frac{(Q_{PTC\ solar\ field})}{2}$$

where: $\frac{(Q_{PTC\ solar\ field})}{2}$ is the solar heat provided by one part of solar field carried by HTF and released to HRSG evaporator via SSG as a latent heat.

- Economized level

Assume T_{w2} then find $h_{w2}(T_{w2})$ and calculate:

$$Q_a = \dot{m}_s(h_{w2} - h_{w1})$$

with: $$T_{hrsg4} = T_{hrsg3} - \frac{Q_a}{\dot{m}_g \overline{C_{pg}}}$$

Calculate: $$Q_t = (UA)LMTD$$

with: $$(UA) = (UA)_d \left(\frac{\dot{m}_g}{\dot{m}_{gd}}\right)^{0.65} \left(\frac{F_g}{F_{gd}}\right)$$

$$LMTD = \frac{(T_{hrsg3} - T_{w2}) - (T_{hrsg4} - T_{w1})}{\ln \frac{(T_{hrsg3} - T_{w2})}{(T_{hrsg4} - T_{w1})}}$$

check: $\frac{(Q_a - Q_t)}{Q_a} < 10^{-4}$ then the assumed duty Q_a and steam/gas temperatures (T_{w2}/T_{hrsg4}) are correct then put $Q_t = Q_3$ and pass to the calculation of the steam mass flow $\dot{m}_{s,c}$. Otherwise, the case $\frac{(Q_a - Q_t)}{Q_a} \geq 10^{-4}$ assume another value of steam temperature T_{w2}.

Now we calculate the steam mass flow as follows:

$$\dot{m}_{s,c} = \frac{(Q_1 + Q_2 + Q_3)}{(h_{s2} - h_{w1})}$$

Check: $\frac{(\dot{m}_{s,c} - \dot{m}_s)}{\dot{m}_{s,c}} < 10^{-4}$ then the assumed value $\dot{m}_s$ was correct then end the calculation process. In case the assumed steam mass flow value $\dot{m}_s$ doesn't match $\dot{m}_{s,c}$, which is $\frac{(\dot{m}_{s,c} - \dot{m}_s)}{\dot{m}_{s,c}} \geq 10^{-4}$, the calculated steam mass flow rate $\dot{m}_{s,c}$ is assigned as an assumed value $\dot{m}_s = \dot{m}_{s,c}$ and starts from the first step which is the superheater and repeat the whole calculation procedure. T

We note that the quantity of steam mass flow evaluated $\dot{m}_s$ is doubled to find the total quantity of steam generated which includes the second quantity of steam generated from other HRSG and the second part of solar field.

The net power plant output is determined by calculating the instantaneous output of GT(s) and ST and that consumed by the feed pump:

$$W_{STnet} = \eta_m \eta_e (2\dot{m}_s)(h_{s,i} - h_{s,o}) \quad (3.43)$$

$$W_{ISCC} = 2W_{GTnet} + W_{STnet} - W_p \quad (3.44)$$

The power plant efficiency is calculated as the net power produced divided by power provided from the fuel:

$$\eta_{SCC} = \frac{W_{ISCC}}{\dot{m}_f Q_{cv}} \quad (3.45)$$

The incremental solar power production $(W_{sol,elec})$ and the solar-to-electric efficiency $(\eta_{sol,elec})$ are defined as:

$$W_{sol,elec} = W_{ISCC\ plant} - W_{CC} \quad (3.46)$$

$$Solar\ eletrci\ ratio = \frac{W_{sol,elec}}{W_{ISCC\ plant}} \tag{3.47}$$

3.4. Thermal performances simulation

The ISCC thermal plant integrates a PTC solar field into a conventional CC. The plant includes a solar field of 183120 m^2, two GT units of 47 MW each one, two HRSGs single pressure and an oversized steam turbine. The studied ISCC system is installed in Hassi R'mel one locality of Laghouat wilaya in Algeria due to the highest DNI of such location and it is performed under the conditions of the present locality.

Table 3.7. Design parameters [89, 91]

Parameters	value
Hassi R'mel data	
Latitude (degree)	33.8
Ambient pressure and temperature, mean wind speed (bar,°C, m/s)	1.013, 21, 6
PTC Solar field (LS-3 type)	
PTC aperture area (m^2)	545
C_L, N_L and C_c	6, 56, 82
Power block	
GT unit output (MW)	47
Exhaust gases temperature (°C)	544
Pinch point (°C)	11
Approach point (°C)	8
Superheated steam temperature (°C)	500
Heat loss factor and Blow down (%)	1
HRSG single pressure (P_{fw}) (bar)	93
Inlet feed water temperature (°C)	50
Mechanical and electrical efficiency (%)	98

3.5. Results and discussion

From sunrise to sunset the power plant operates as ISCC and at night works as CC. The on-site average day temperature during 21st of March is equal to 21°C [157] which corresponds to the design conditions. The simulation is carried out under the variation of DNI and ambient temperature during the day which is the off-design of the present numerical study. The solar field subprogram calculates the supplied solar energy to SSG which the output varies with the solar irradiation, as illustrated by Figures 3.12–3.18. Figure 3.12 illustrates the variation of the direct solar irradiation during the day, and shows that the DNI is higher at midday and expected to reach a maximum of 770 W/m^2. Figure 3.13 represents the solar thermal output during the day, which increases with solar irradiation from sunrise until sunset.

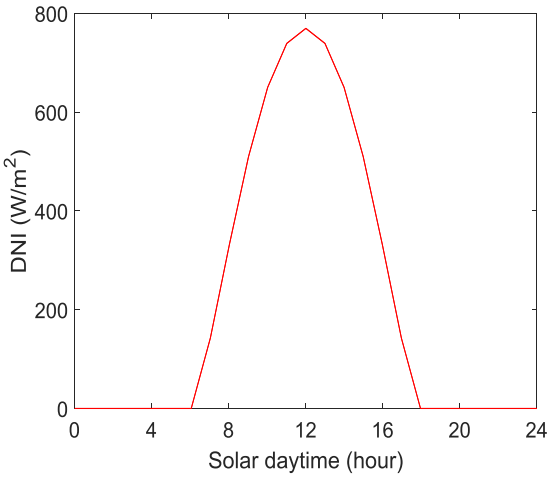

Figure 3.12. Direct Normal irradiation

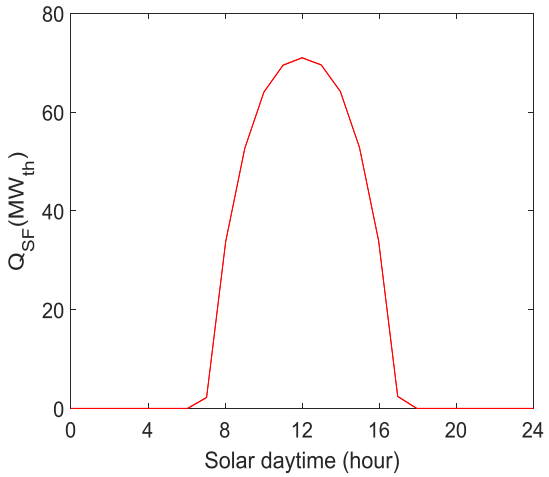

Figure 3.13. Solar Field thermal energy output

As shown by Fig.3.14 the additional steam mass flow generated by SSG fluctuates as a function of solar irradiation and may reach a value of 60 kg/s when DNI gets at its maximum. As a result, the total steam turbine output (Fig.3.15) is equal to 56.5 MW, which means an increase in electricity generation about 26.5 MW compared to about 30 MW at night. Fig.3.16 gives an idea about the power plant output during the 21st of March (design point) under Hassi R'mel climatic conditions. During night or cloudy periods ISCC operates as CC with one pressure level and produces about 125 MW, and according to Fig.3.17 thermal efficiency reaches 49 %. As the first irradiation appears, the net electricity production is increased to reach around 150.5 MW and reaches the highest efficiency of 59 % at midday. The estimated solar electricity ratio based on the difference in electrical output of ISCC mode and CC mode varies from sunrise to sunset according to the solar irradiation fluctuations, and its maximum reaches 15.5 % at midday, as revealed from Fig.3.18.

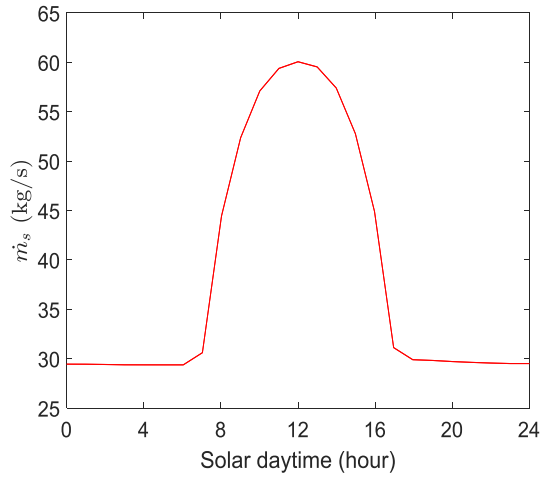

Figure 3.14. Steam generated rate

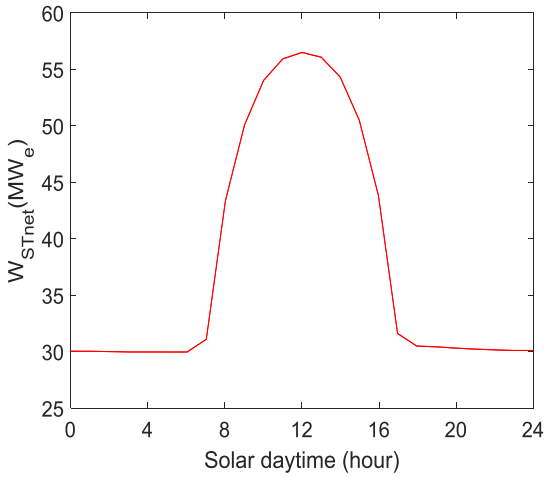

Figure 3.15. Net steam turbine output

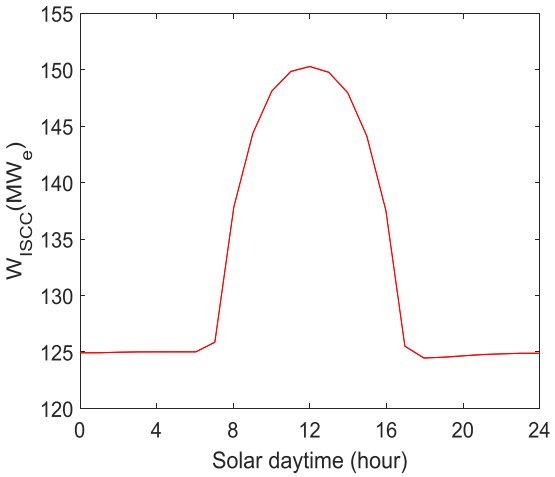

Figure 3.16. ISCC output

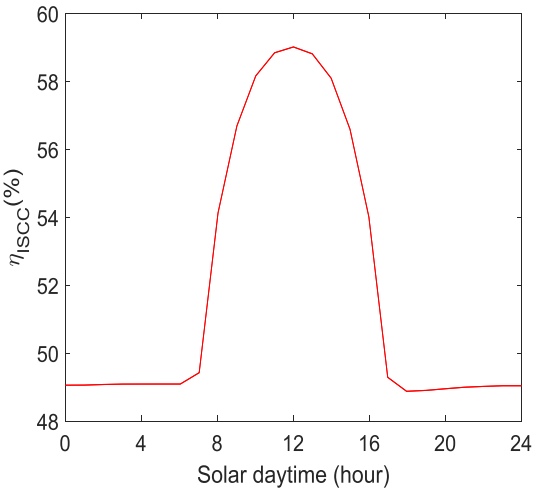

Figure 3.17. ISCC efficiency

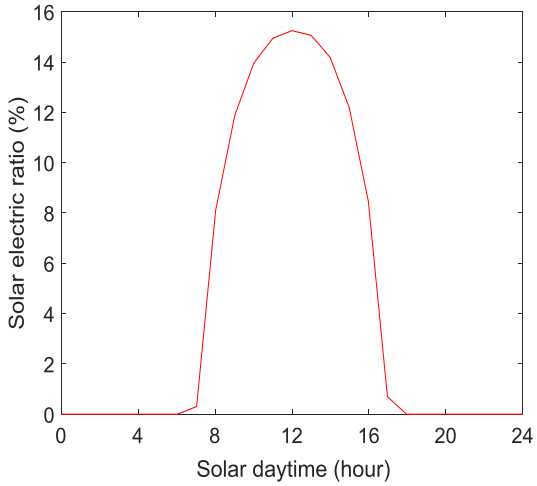

Figure 3.18. Solar electric ratio

3.6. Economic assessment

In electrical power generation, the distinct ways of generating electricity incur significantly different costs. Calculations of these costs at the point of connection to a load or to the electricity grid can be made. The cost is typically given per kilowatt-hour (kWh) or megawatt-hour (MWh). It includes the initial capital, discount rate, as well as the costs of continuous operation, fuel, and maintenance. This type of calculation assists policymakers, researchers and others to guide discussions and decision making. The levelised cost of electricity (LCOE) is a measure of a power source which attempts to compare different methods of electricity generation on a consistent basis. It is an economic assessment of the average total cost to build and operate a power-generating asset over its lifetime divided by the total energy output of the asset over that lifetime. The LCOE can also be regarded as the minimum cost at which electricity must be sold in order to break-even over the lifetime of the project.

The economic assessment of this ISCC Hassi R'mel's plant to evaluate the LCOE is based on the model used by Hosseini et al. [98]:

$$\mathrm{LCOE} = \frac{(\mathrm{CRF}.\mathrm{C} + \mathrm{O\&}M + PVF)}{\mathrm{Pel\_an}} \tag{3.48}$$

$$\mathrm{CRF} = \frac{\mathrm{R}}{(1 - (1 + \mathrm{R})^{-\mathrm{N}})} \tag{3.49}$$

C: Capital Cost

CRF: Cost recovery factor

O&M: Operation and Maintenance

PVF: Annual fuel cost

Pel_an: Annual electrical energy production

R: Discount rate

N: Expected life time of power plant (Year)

Table 3.8. Assumptions and Data [97, 98]

Assumptions and data	Value
Life expectancy of solar field (year)	30
Life expectancy of steam unit (year)	30
Life expectancy of gas unit (year)	15
Annual discount rate R (year)	10
Capacity factor	0.8
Annual discount rate R (year)	10
Capacity factor	0.8
Direct costs	
Specific cost of solar field $C_{sol,PTC}$($/kW)	1400
Specific cost of steam unit C_s($/kW)	635
Specific cost of gas unit C_g ($/kW)	235
Contingency (% of direct costs)	10
Indirect costs	
Engineering, procurement and construction (% of direct costs)	13
O&M cost factor of solar field k_{sol}(%)	1.5
O&M cost factor of steam unit of CC k_s(%)	2
O&M cost factor of gas unit k_g(%)	5
Q_{cv} (kJ/kg)	45806
Fuel price ($/m^3)	0.045
Emissions ($/kWh)	0.0073

The total investment cost for ISCC is the sum of GT, ST and solar unite cost. The operation and maintenance costs (O&M) include labour, spare parts, consumables and normal maintenance equipment requirements which can be estimated [98] as follows**:**

$$O\&M = k_{sol}C_{sol} + k_s C_s + k_g C_g \quad (3.50)$$

The economic lifetime of steam power plant and ISCC are expected to reach 30 years [99]. The GT life expectancy is about 15 years after which, the replacement cost has to be considered for both ISCC and CC [98, 101]. The conventional CC is taken as the reference power plant for the purpose of comparison. The economical assumptions and data to make this economic analysis are presented in Table 3.8. Thus, we examine three cases of this power plant which are the Gas turbines (GT), Combined cycle (CC) and the integrated solar combined cycle (ISCC), and the LCOE is used to compare these different cases at technical concept point which is given in the units of currency (US dollar) per kilowatt-hour ($/kWh).

Table 3.9 compares between the three power plants in terms of LCOE, fuel saving and emission, considering the CC as the reference power plant. Figure 3.19 and 3.20 show the calculated LCOE divided into three fragments: investment cost, O&M cost and fuel cost. The LCOE is greatly affected by the specific cost of power plant, especially for the solar parts, since their costs are very high compared to the fossil parts. According to Fig.3.19 when the environment cost is not taken into consideration CC power plant has the lowest LCOE followed by GT. In the case of ISCC, LCOE is 3 % higher than that of GT and 28 % higher than that of CC. If one considers the environmental effects, as shown by Fig.3.20, LCOE of ISCC becomes 0.0272 $/kWh which is about 6 % lower than for GT and 20 % higher than CC, but LCOE of CC is still the lowest.

Table 3.9. Estimated LCOE

Parameter	GT	CC	ISCC
DNI per year (kWh/m^2 yr)	---	---	1611.6
Annual electricity production (MWh)	658752	909228	972896.8
LCOE [a] ($/kWh)	0.0216	0.0174	0.0222
LCOE [b] ($/kWh	0.0289	0.0227	0.0272
Fuel saving in 30 years (Million $)	---	---	18.45
Avoided CO_2 emission in 30 years (Million Ton)	---	---	0.89

[a] Without considering environmental cost

[b] With considering environmental cost

Figures 3.21 and 3.22 show the specific fuel consumption (kg/MWh) and CO_2 emission (kg/MWh). ISCC has the lowest specific fuel consumption about 7 % which is lower than CC and 32 % lower than GT (Fig. 3.21). As a consequence ISCC saves about 18.45 million $ of fuel consumption through 30 years of its operation. Figure 3.22 permits concluding that CO_2 emission is proportional to fuel consumed by power plant which is extremely high in GT but less in CC power plant. Due to availability of solar energy during the day, ISCC produced the

lowest CO_2 emission, thus avoiding 0.89 million ton of CO_2 emission over 30 years of its operational period.

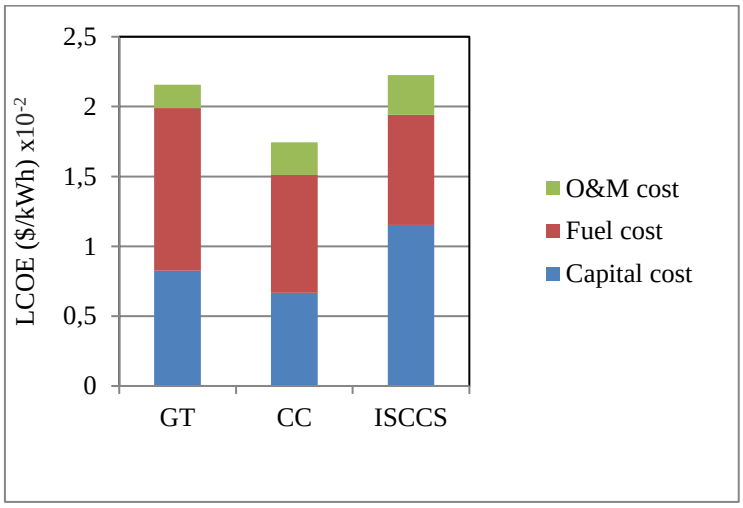

Figure 3.19. LCOE of different power plants, without environmental cost

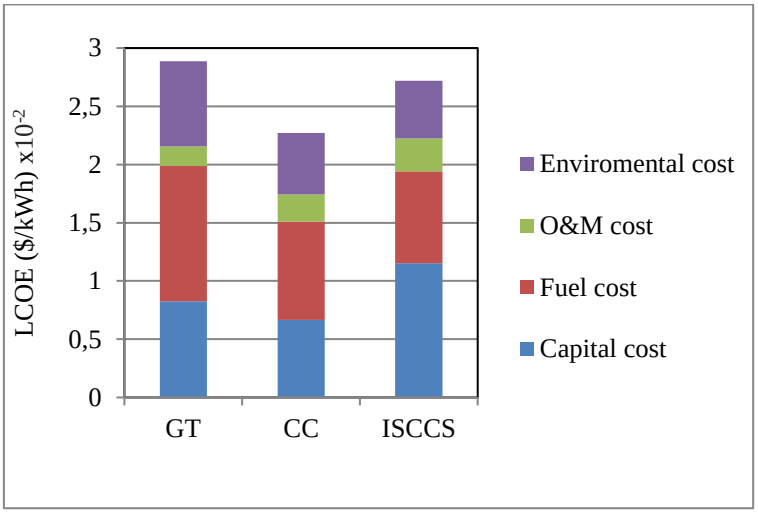

Figure 3.20. LCOE of different power plants by considering environmental cost

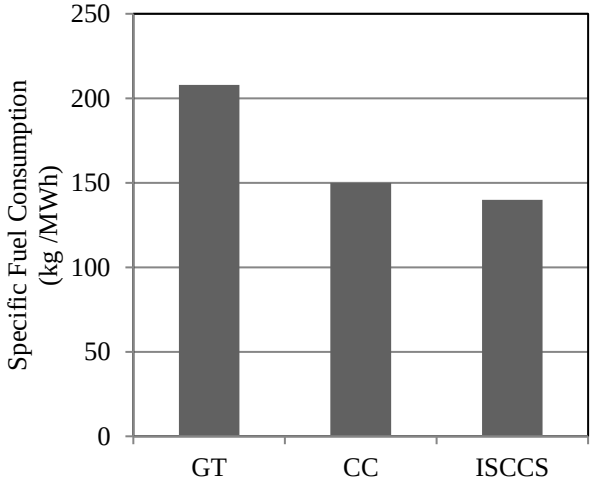

Figure 3.21. Natural gas specific consumption of different power plants

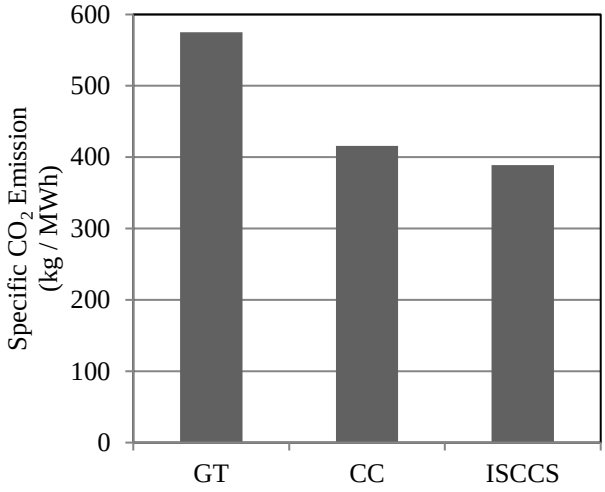

Figure 3.22. Specific CO_2 emission of different power plants

3.7. Conclusion

Thermodynamic and economic code to simulate the first ISCC thermal plant in Algeria was developed based on MATLAB programming. The simulation was carried out under the Hassi R'mel climate in the purpose to find out how much this technology is efficient from the thermodynamic point of view and demonstrate its feasibility and viability from economic aspect. Thus, the obtained results could be exploited for further solar power plants that should be implanted in the future. The ISCC study has shown that during daytime the solar energy can be converted for a net solar electricity ratio about 15.5 % and an overall thermal efficiency more than 59 % which is significantly higher than for CC. On the other hand, the economic assessment shows that when the environment cost effect is not considered LCOE of the ISCC plant is 0.0222 $/kWh which is about 27 % higher than for CC and it is 0.0272 $/kWh which is about 19 % higher than for CC when the environment cost is taken into account which make it very competitive. The annual solar contribution of ISCC results in fuel consumption about 140 kg/MWh which is 7 % lower than CC, thus saving about 18.45 million $ of fuel through 30 years of operation. Moreover, CO_2 emission is lowered by reducing 0.89 million ton rejected over 30 years.

The integration of fossil fuel–natural gas–with–solar energy for the replacement of latent heat by using SSG in parallel with HRSG is a very attractive option to make the transition from simple GT and CC plants to ISCC power plants. The results obtained from this study concur well the feasibility and benefits by integrating the solar technology, which is being considered as a part of the Algerian program to produce 22 000 MWe from the renewable energy to the horizon of 2030.

Chapter 4

Novel Hybridization of Solar Central Receiver System with Combined Cycle

4.1. Introduction

Nowadays the Central Receiver System (CRS) using the heliostat field reflectors to concentrate the solar radiation onto the top of a tower has demonstrated its technical feasibility and has become under commercialization [1]. Actually the most promising Solar Power Tower (SPT) technologies are those using the molten salt/saturated steam and the volumetric receiver, such as Gemasolar and Planta Solar 10 (PS10) using molten salt and saturated steam, respectively. In SPT equipped with a volumetric receiver the solar radiation is absorbed deep inside a volume of highly porous structure. The selection of either open or closed volumetric receiver considers some advantages of air as it has no risk of freezing [57] added to capability of reaching a high temperature 850-1000 °C [1].

In the concept of ISCC, the solar heat is introduced in the bottoming Rankine cycle; hence a Solar Steam Generator (SSG) is added, offering several advantages over the solar-only electric generation system or Rankine cycle [130]. Okoroigwe et al. [2] reviewed CCs coupled with SPT and compared with those using Parabolic Trough Collector (PTC) technology, and concluded that the former is still immature. According to the literature, very limited research was dedicated to the development of SPT coupled with CC. Most of ISCC power plants are still those using PTC technology, whereas SPT plants with Jülich concept are running in a solar-only plant [122]. The aim of this section is to study a new configuration of solar hybridization of ISCC systems using an open volumetric air receiver, which is an integration of SPT system into a conventional CC. In the best knowledge of the authors this configuration was not studied before. Consequently, the proposed ISCC integrating a SPT system is investigated from the point of view of thermal performances and economic issue.

4.2. Thermal and economic investigations of a new integration of a Solar Central Receiver System with Combined Cycle

Besides the parabolic trough collectors (PTCs) technology the mature and proven central receiver system power plant (CRS) using heliostat field reflectors has demonstrated its technical feasibility and commercialized. The selection of a SPT using a volumetric air receiver is based on some advantages of the air as it is free, since there are no risk of freezing and may reach higher temperatures of 850-1000°C due to the high concentration ratio [1, 57]. A new configuration of an ISCC is proposed which integrates a solar tower with an open volumetric receiver into a CC, thus thermal performances investigation with considering the economic issue of such proposed solar thermal plant is carried out in the present chapter.

4.2.1. System Configuration

The solar field consists of numerous heliostats reflecting solar radiation and concentrating it onto the top of the solar tower similar to PS10 thermal plant [58], but has a modified volumetric receiver integrated with the power block to constitute the complete ISCC system. When the solar radiation is available the open volumetric air receiver allows transferring the concentrated solar energy to cleaned flue gases (natural gas is the cleanest-burning fuel), and thus operates as a supplementary firing (fired mode) in HRSG. As exit gases temperature from GT is at 544°C and the temperature difference across the receiver is not high, this allows reaching a high temperature about 850°C. The exhaust gases from HRSG are cooled down more than in unfired mode and the energy recovered is higher and HRSG operates more efficiently. Compared with a solarized GT where major modifications are required to resist at pressure more than 15 bar, this configuration with an open volumetric air receiver has the advantage of simplicity. Exhaust gases from GT are at low pressure and the temperature difference across the receiver is not too high, inducing less stress on the receiver. Furthermore, there is no need for another SSG and the use of a single-pressure level makes it simpler and less expensive compared with the multi-pressure levels HRSG [155], and since this system operates as ISCC system during days and reverts to ordinary CC during nights/ cloudy periods no TES has to be considered. The thermal performances of this hybridized system are investigated under the geographical site of Hassi R'mel (Algeria) for the climate conditions of 21st of March and for the maximum of DNI. With the variation of DNI during the day the temperature of flue gases of constant mass flow rate varies through the receiver, which in turn induces a variation of gases temperature entering HRSG, leading to off-design operation (fired mode). HRSG is considered as the main subsystem where all the thermal

energy is transferred to generate the superheated steam. At design operation (unfired mode) the selection of the pinch point and approach point for the evaporator is required to predict HRSG performance. The heat loss factor and the blow down for HRSG are considered in the calculation, but the pressure loss of steam is neglected. In the other side, the pressure drop through the flue gas cleaner and HRSG are taken into account but neglected through the receiver.

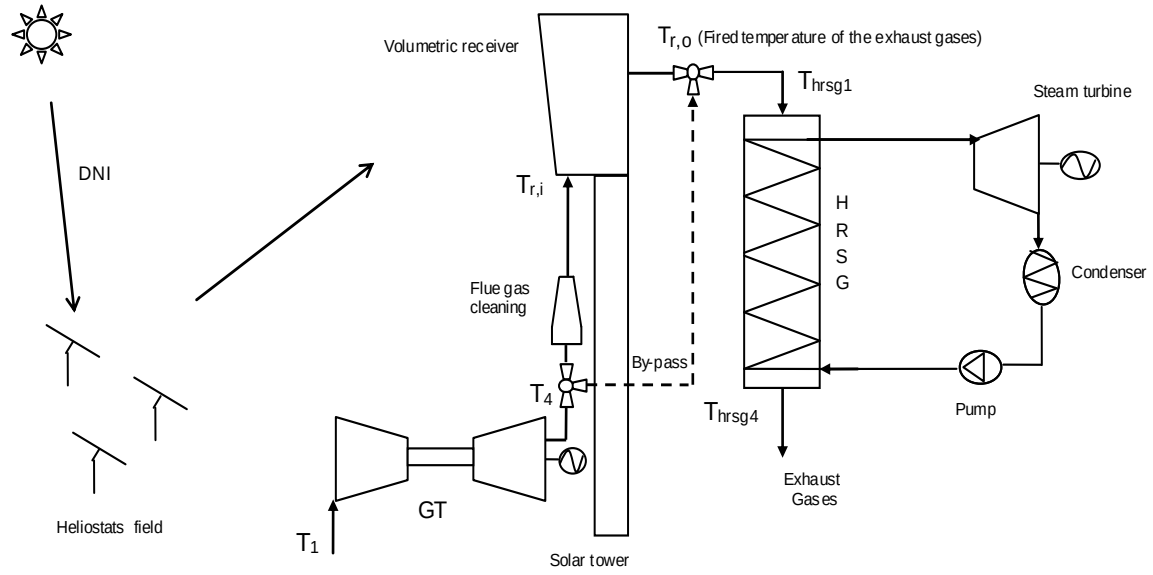

Figure 4.1. Integrated solar tower to an CC power plant (ISCC)

4.2.2. Thermodynamic Modelling

This configuration of ISCC consists, in addition to the Brayton and Rankine power blocks, of a solar field and an open volumetric air receiver where the concentrated solar energy is transferred to flue gases before entering the single pressure level HRSG. All the developed thermodynamic models are implemented under MATLAB.

4.2.2.1. Solar field

Data of solar radiation are critical in selection and sizing of CSP equipments and prediction of their performance. These data obtained from the combination of ground measurements and satellite data [158] are not necessary available for all the countries. To overcome this difficulty the radiation models for direct normal irradiation (DNI) are an alternative recourse, which are simple models requiring less than three inputs (Hottel, Liu and Jordan (HLJ) [159], Meinel [160], Kumar [161] and ASHRAE [162]) while more inputs are used for the complex models (Davies and Hay model [163] and Iqbal [164] etc.) as detailed in Appendix.

It is of great importance to get the most efficient heliostat field layout since has an impact on SPT investment and a source of energy losses [1]. Some developed codes based on Monte

Carlo ray tracing [112], Genetic Algorithm [110] and software such as HFLCAL [116] and HFLD [123] have been used to perform the optical heliostat field efficiency with an attention paid to minimize the losses due to shading and blocking [112]. The expected optical efficiencies for the heliostat field are in the range of 0.58-0.76 [115]. The solar field consists of a number of heliostats tracking the sun in two axes to reflect the solar radiation onto the receiver. The optical losses due to the cosine effect, atmospheric attenuation, heliostat reflectivity added to shadowing, blocking and spillage losses are shown to affect the overall optical heliostat field efficiency [112] estimated as follows:

$$\eta_{opt,helio} = \eta_{cos}\eta_{atm}\eta_{ref}\eta_{sb}\eta_{spill} \tag{4.1}$$

- *Cosine losses*

In order to guarantee an accurate tracking of the sun path during a day, each heliostat has to change its orientation according to incident angle. The cosine efficiency is calculated as the dot product of the incident sun ray direction and the normal of the mirror surface [165].

$$\eta_{\cos} = \vec{\imath} \times \vec{\mathrm{n}} \tag{4.2}$$

- *Atmospheric attenuation*

During its path from mirror to the receiver, reflected rays are affected by the atmospheric attenuation. Losses due to the atmospheric attenuation are function of the distance between heliostat and the receiver located on the top of the tower. Also, it depends on some weather conditions i.e. the visibility. It can be calculated as [165]:

$$\eta_{\mathrm{atm}} = \begin{cases} 0.99321 - 0.000176\,\mathrm{S}_0 + 1.97\,10^{-8}\mathrm{S}_0^2 \;;\; \mathrm{S}_0 \le 1000\ \mathrm{m} \\ \exp(-0.0001106\,\mathrm{S}_0) \qquad\qquad\qquad\quad ;\; \mathrm{S}_0 \ge 1000\ \mathrm{m} \end{cases} \tag{4.3}$$

- Mirror reflectivity

It is the quality of reflective surface; it depends on degradation and cleanliness. In this study it is assumed to be constant equal to 0.88 [165].

- Spillage loss

A portion of reflected radiation losses its path and cannot hit the receiver. This is caused by tracking accuracy and mirror quality. This phenomenon is called Spillage [165].

$$\eta_{\mathrm{spill}} = \frac{1}{2\pi\,\sigma_{\mathrm{tot}}^2}\int(\mathrm{x})\int(\mathrm{y})\exp\left(\frac{-\mathrm{x}^2+\mathrm{y}^2}{2\,\sigma_{\mathrm{tot}}^2}\right)\mathrm{dxdy} \tag{4.4}$$

$$\sigma_{\mathrm{tot}} = (\sigma_{\mathrm{solar}}^2 + \sigma_{\mathrm{mirror}}^2 + (2\,\sigma_{\mathrm{track}})^2)^{0.5} \tag{4.5}$$

- Blocking/Shading loss

Blocking means that the heliostat located behind its neighbour cannot reflect its entire surface to the receiver, a portion of the reflected rays is blocked by the back side of the front heliostat. Shading is similar to the blocking, but it affects incident rays, heliostat placed in front of its

neighbour shads the heliostat behind. A detailed description of the shadowing and blocking method calculation is presented on the next section [165].

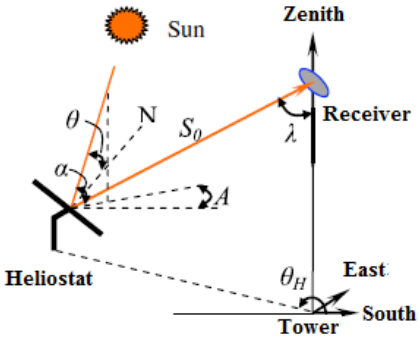

Figure 4.2. Position and angles of the heliostat relative to the receiver [165]

As this SPT hybridization operates with an open volumetric air receiver, and since the task in this paper is not to optimize the solar field, the same optimized PS10 heliostat field [166] is considered.

Table 4.1. Heliostat field data of PS10 [166].

Parameter	value
Heliostat number	624
Heliostat surface	12.84 x 9.45(m^2)
η_{cos}	0.8283
η_{atm}	0.9498
η_{ref}	0.8800
η_{sb}	0.9255
η_{spill}	0.9926

4.2.2.2. Solar receiver

The receiver absorbs the maximum of solar energy while keeping the convection and radiation losses at minimum. The cavity receiver used in PS10 to elevate the temperature of molten salt is substituted with an open volumetric air receiver. The concentrated solar radiation is absorbed deep inside a volume made of a highly porous structure and presents the so-called volumetric effect where the front surface temperature is lower than the outlet air temperature [113]. Compared with a solarized GT where major modifications are required to resist at pressure more than 15 bar, this configuration with an open volumetric air receiver has the advantage of simplicity because of the exhaust gases from GT are at low pressure, thus less stress on the receiver.

The receiver losses are by reflection, convection and radiation.

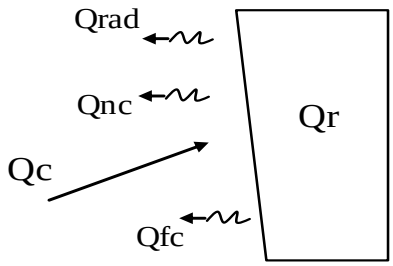

Figure 4.3. Volumetric receiver energy balance

From energy balance the power transmitted (Q_r) by the receiver to the working fluid [167].

$$Q_r = \alpha Q_c - Q_{loss} \tag{4.6}$$

Where Q_c is the solar energy reflected by the heliostats and concentrated on the receiver [165].

$$Q_c = \eta_{opt,helio} N\, S_{helio}\, DNI \tag{4.7}$$

DNI is modelled through HLJ model [59] which has been applied to assess the clear sky solar radiation for numerous locations throughout the world as well as in Saharan regions.

Q_{loss} is the total losses by natural convection, forced convection and radiation [167].

$$Q_{loss} = Q_{nc} + Q_{fc} + Q_{rad} \tag{4.8}$$

The thermal energy lost by natural convection from the receiver is given by.

$$Q_{nc} = h_{nc} S_r (T_r - T_a) \tag{4.9}$$

With

$$h_{nc} = 0.81\ (T_r - T_a)^{0.426} \tag{4.10}$$

The temperature of receiver is given by [1]:

$$T_r = \sqrt[4]{\frac{\alpha C_c \eta_{opt} DNI}{\sigma\ \varepsilon} + {T_a}^4} \tag{4.11}$$

The thermal losses due to forced convection are estimated by [167]:

$$Q_{fc} = h_{fc} S_r (T_r - T_a) \tag{4.12}$$

$$Nu = \frac{h_{fc}\, H}{k_{air}} = 0.0287 Re^{0.8} Pr^{\frac{1}{3}} \tag{4.13}$$

The radiative heat loss is estimated by [168]:

$$Q_{rad} = \sigma\ \varepsilon\ S_r \left({T_r}^4 - {T_a}^4\right) \tag{4.14}$$

The total energy transferred to flue gases in the receiver leads to an increase in outlet temperature.

$$Q_r = \dot{m}_g \overline{C_{pg}} \left(T_{r,o} - T_{r,i}\right) \tag{4.15}$$

The specific heat of flue gases is function of temperature; hence the outlet temperature of flue gases is obtained iteratively.

4.2.2.3. Gas turbine

GT thermodynamic model is detailed in chapter 3. The selected GT size is based on the quantity of exhaust gases which could be heated up by solar energy available in the receiver to reach the maximum temperature about 850 °C at solar noon [113]. In contrast to the solarized gas turbine where the solar heat is introduced into an open or closed Brayton cycle this hybridization does not require significant modifications in the gas power block.

The power of GT integrated in the system corresponds to 30 MW and the exhaust gas flow rate is equal to 80 kg/s. Table 4.2 presents the existing GTs in the same power range which could match with this ISCC power plant.

Table 4.2. GTs in the range of 30 MW

GT type	Output (MW)	Exhaust mass flow (kg/s)	Exhaust gases temperature (°C)
Siemens/SGT-700	32.8	95	533
Siemens/SGT-A30 RB	29.9	95	503
GE/LM2500+	30.2	85	518
Kawasaki/L30A	30.12	86.5	470

4.2.2.4. Rankine cycle

The steam cycle consists of HRSG with a single pressure operating in fired mode, an oversized steam turbine and a cooling system. The steam pressure and pinch point have a crucial role, and the exit gas temperature from the economizer of HRSG is not arbitrarily assumed [155]. Performance analysis of HRSG is achieved by determining the gas–steam temperature profiles, duty of each component, steam generation and exit gas temperature [156]. The steam cycle in unfired mode (design mode) in the absence of solar radiation where the ISCC plant works as a CC, the same procedure is adopted to evaluate the thermodynamic parameters as in chapter 3.

- *Off-design operation*

Off-design analysis illustrates the effect of outlet temperature from the receiver on the power plant performance. Once the design mode is established, to predict HRSG performance under different exhaust gas temperatures several guessed values and iterations are required to arrive at the final heat balance, steam generation and duty. Additional steam generated while the solar radiation is available leads to decreasing the outlet temperature of gases from this single

pressure HRSG and thus more energy is recovered to increase the overall performance of the power plant.

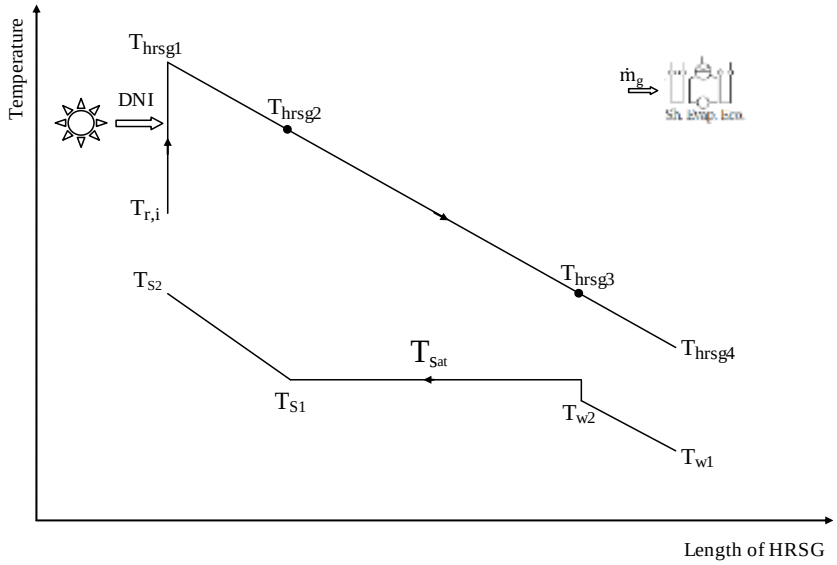

Figure 4.4. Fired mode gas-steam temperature profiles

The value of UA at off-design is obtained by using the correction factors for gas and steam flows [155]:

$$UA = (UA)_d \left(\frac{\dot{m}_g}{\dot{m}_{g,d}}\right)^{0.65} \left(\frac{F_g}{F_{g,d}}\right) \left(\frac{\dot{m}_s}{\dot{m}_{s,d}}\right)^{0.15} \tag{4.16}$$

The steam flow $\dot{m}_s$ in off-design is assumed and iterations are required until convergence. From the relation between design and off-design values of (UA) the duty in off-design $Q = (UA)\ F.LMTD$ is obtained and subsequently the generated steam.

Thermodynamic steps followed to estimate the generated steam mass flow in off-design are as detailed above in chapter 3.

The thermal energy transferred from hot gases to steam is given by:

$$Q_{hrsg} = \dot{m}_g \bar{C}_{pg} (T_{hrsg1} - T_{hrsg4}) \tag{4.17}$$

The efficiency of HRSG is defined as the ratio between the thermal energy transferred from exhaust gases to water/steam and the sum of exhaust gases enthalpy and the supplementary energy in the fired mode [155]:

$$\eta_{hrsg} = \frac{\dot{m}_s (h_{s2} - h_{w1})}{(\dot{m}_g C_{pg} T_{hrsg1,d} + Q_r)} \tag{4.18}$$

With T_{hrsg1} is the inlet temperature of HRSG and Q_r is the solar thermal energy gained by flue gases in the receiver.

The solar thermal energy transferred to steam:

$$Q_{sol,tr} = \dot{m}_s(h_{s2} - h_{w1}) - \dot{m}_{s,d}(h_{s2,d} - h_{w1}) \quad (4.19)$$

The efficiency of solar energy gained by exhaust gases and transferred to steam in HRSG:

$$\eta_{sol,tr} = \frac{Q_{sol,tr}}{Q_r} \quad (4.20)$$

The net power plant output (W_{ISCC}) is determined by calculating the outputs from GT and steam turbine and input to feed pump:

$$W_{ISCC} = W_{GTnet} + W_{ST} - W_p \quad (4.21)$$

With the steam power given by

$$W_{ST} = \eta_m \eta_{el}(h_{s,i} - h_{s,o}) \quad (4.22)$$

The power plant efficiency is calculated as the net power produced divided by that provided by the fuel:

$$\eta_{ISCC} = \frac{W_{ISCC}}{\dot{m}_f Q_{cv}} \quad (4.23)$$

The solar fraction (SF) is defined as the amount of solar thermal energy divided by that input.

$$SF = \frac{Q_r}{Q_r + \dot{m}_f Q_{cv}} \quad (4.24)$$

The incremental solar power production $(W_{sol,el})$ and solar-to-electric efficiency $(\eta_{sol,el})$ are defined as:

$$W_{sol,el} = W_{ISCC} - W_{CC} \quad (4.25)$$

$$\eta_{sol,el} = \frac{W_{sol,el}}{DNI\ A_{solar\ field}} \quad (4.26)$$

The solar electric ratio (Sol, el, rat) is defined as the amount of electricity generated from solar energy $W_{sol,el}$ divided by the output of power plant W_{ISCC}:

$$Sol, el, rat = \frac{W_{sol,el}}{W_{ISCC}} \quad (4.27)$$

The Rankine cycle efficiency $(\eta_{Rankine\ cycle})$ of the solar electric conversion is given by:

$$\eta_{Rankine\ cycle} = \frac{W_{sol,el}}{Q_r} \quad (4.28)$$

4.3. Case Study

This novel ISCC hybridization includes: solar field of 624 heliostats, open volumetric air receiver, GT unit of 30 MW, single pressure HRSG and oversized steam turbine. GT selection is based on the quantity of exhaust gases which could be heated up by solar energy available in the receiver to reach the maximum temperature about 850 °C at solar noon [113]. The design point (Table 4.3) corresponds to unfired mode when exhaust gases enter directly

HRSG, and the obtained performances are summarized in Table 4.4. The proposed integration of central receiver with conventional CC is performed for the site of Hassi R'mel site where the highest DNI is available [91], while adopting the same solar field layout as PS10 [166].

Table 4.3. Parameters at design-point

Parameters	Value
Hassi R'mel data	
Latitude (degree)	33.8
Ambient temperature and pressure (°C, bar) of 21st March	21, 1.013
Solar field	
Heliostat surface (m^2)	12.84x9.45
Heliostat number	624
Optical efficiency (%)	63.59
Receiver surface area (m^2)	80
Power block	
GT output (MW)	30
Exhaust gas temperature (°C)	544
Pinch point (ΔT_{pp}) (°C)	11
Approach point (ΔT_{ap}) (°C)	8
Superheated steam temperature (T_{s2}) (°C)	500
Heat loss factor (%)	1
Blow down (%)	1
HRSG single pressure (P_{fw}) (bar)	93
Inlet feed water temperature (T_{w1}) (°C)	50
Mechanical and electrical efficiency (%)	98

Table 4.4. Performance of HRSG in unfired mode

Surface	Gas temperature in /out (°C)	Wat. /Stm. temperature in /out (°C)	Duty (MW)	Pressure (bar)	Mass flow rate (kg/s)	Pinch Point (°C)	Approach point (°C)	UA (kW/°C)
Superheater	544 - 476	305.7 - 500	6.34	93	9.82	-	-	67.57
Evaporator	476 - 316	297.7 - 305.7	14.64	93	9.82	11	8	251.12
Economizer	316 - 200	50 - 297.7	10.30	93	9.82	-	-	161.98

Fig.4.5 shows the concentrated solar radiation reaches a maximum about 463 kW/m^2 which corresponds to the maximum of DNI of 769 W/m^2 obtained at solar noon of the 21st of March. The local solar noon is the time when the sun crosses the meridian which usually does not coincide with the 12:00 o'clock time. The hour angle is 0° at solar noon when the sun is at its highest point in the sky during a given day [159]. If the local solar time is used instead of the clock time, both the longitude correction and the equation of time correction can be ignored.

All the hours of timing used in the present work are assumed to be given in solar time (ST) according to reference [169].

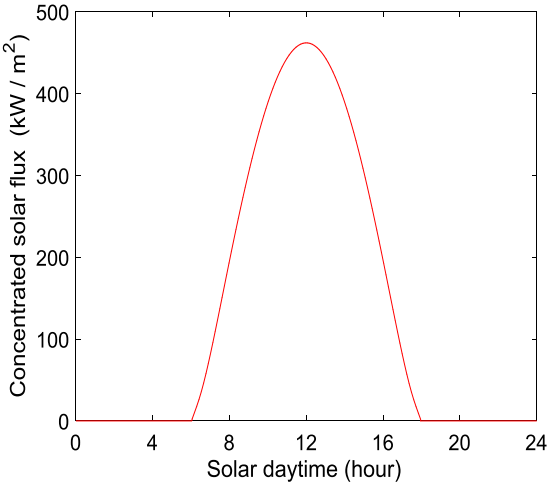

Figure 4.5. Concentrated solar radiation

4.4. Results and Discussion

Fig.4.6(a-b) shows the gas-steam temperature profiles for unfired and fired mode operations. The outlet temperature of the receiver is the same as that at inlet of HRSG. As shown in Fig.4.6(a) the temperatures of gases entering and exiting HRSG are 544°C and 200°C, respectively. Fig.4.6(b) reveals that when DNI reaches its peak value at solar noon the temperature of exhaust gases from HRSG cools down to reach a low value of 157 °C, hence more output and superheated steam are produced as the exhaust gases are heated up through the receiver to reach a temperature of 850 °C. Accordingly the economizer acts as a large heat sink owing to the large quantity of steam generated.

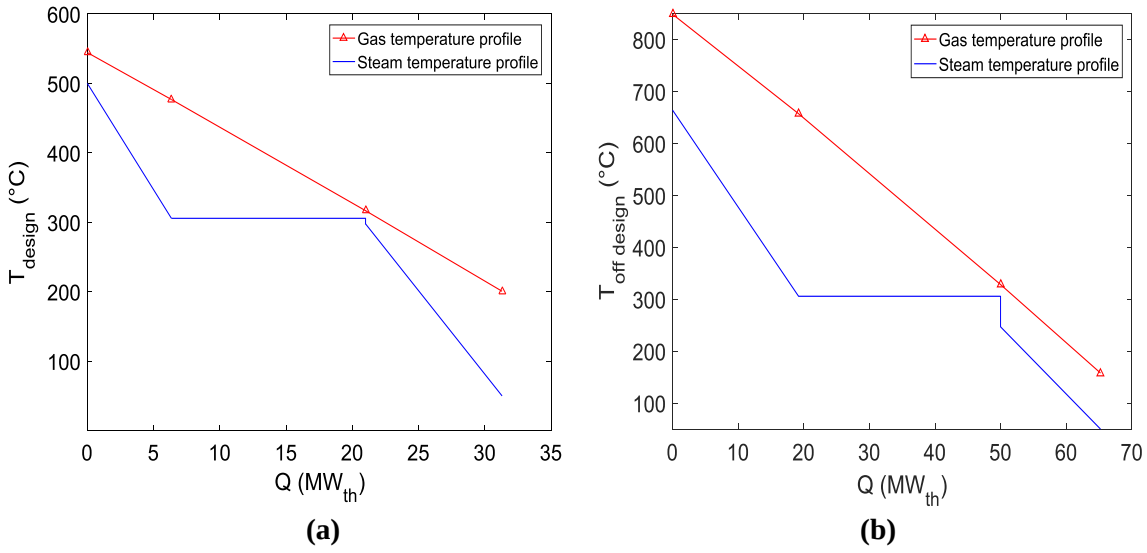

Figure 4.6. HRSG gas-steam temperature profiles: a) unfired mode; b) fired mode

Fig.4.7 displays the impact of fired mode on the outlet temperature from HRSG during the day depending on the solar time (ST). This phenomenon could be explained by an additional quantity of steam generated which cools down the exhaust gases and more energy is transferred to steam production. Fig.4.8 shows that about 30 MW_{th} of solar energy available in the open volumetric air receiver is transferred to gases. The energy recovered in HRSG exceeds 33 $MW_{th,}$ since the supplementary firing enhances the efficiency of HRSG, as depicted in Fig.4.9. This latter also shows that the solar energy is converted at an efficiency more than 100 % as the solar energy transferred to exhaust gases is around 30 MW_{th} and that to water is 33 MW_{th}, with 3 MW_{th} gained from the fired mode as the exhaust gases are cooled down from 200 °C to 157 °C. The efficiency of HRSG in the fired mode reaches about 79 % which is 18 % higher than in unfired mode. As also seen from Fig.4.10 the solar energy transferred to water/steam leads to more steam production, exceeding 18 kg/s and an output of 22.8 MW_e. Fig.4.11 shows that the steam turbine output in fired mode is higher by 12.83 MW_e than that in unfired mode of 10.3 MW_e .

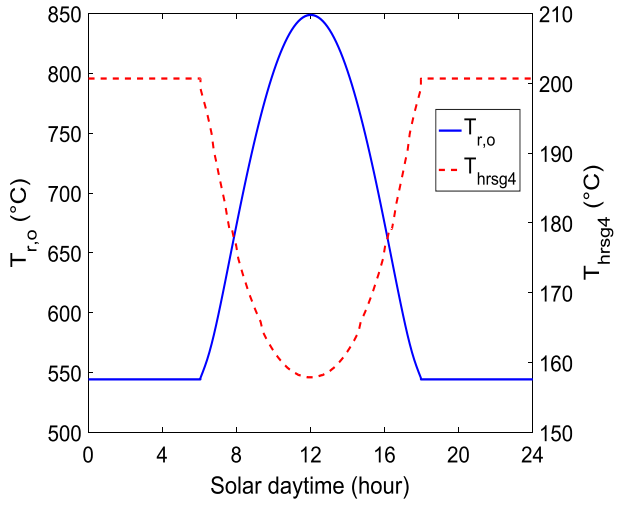

Figure 4.7. Inlet and outlet temperatures of HRSG

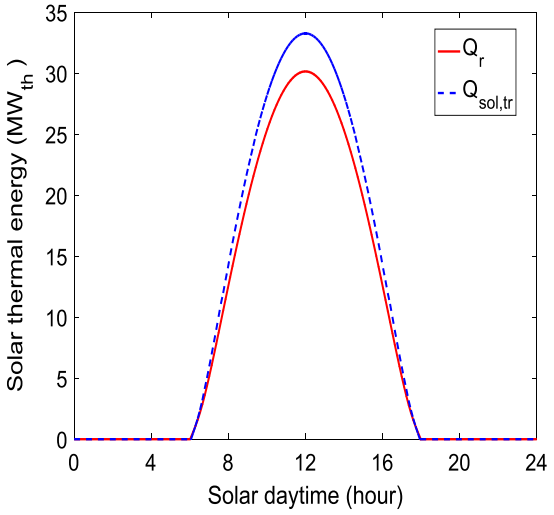

Figure 4.8. Solar thermal heat transferred to HRSG

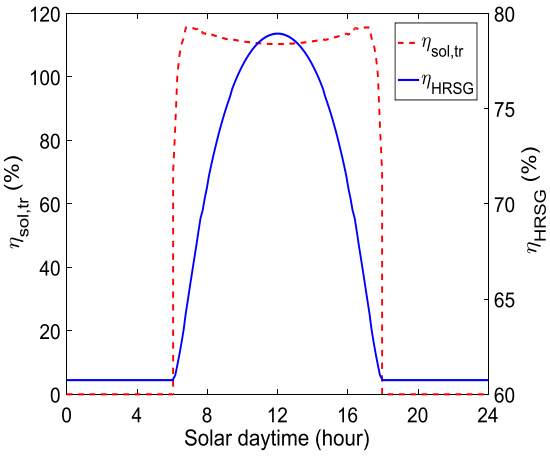

Figure 4.9. Efficiency of the solar thermal heat transfer

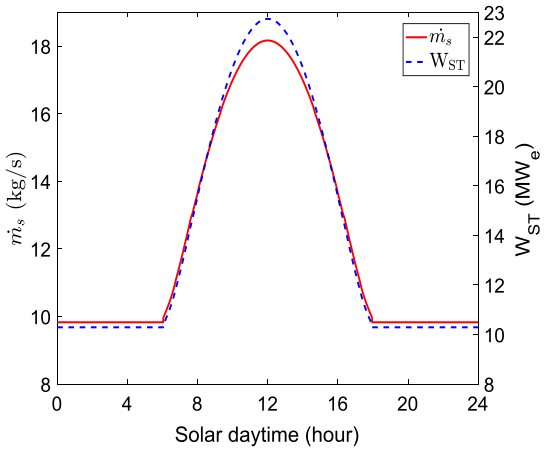

Figure 4.10. Steam turbine mass flow rate and output

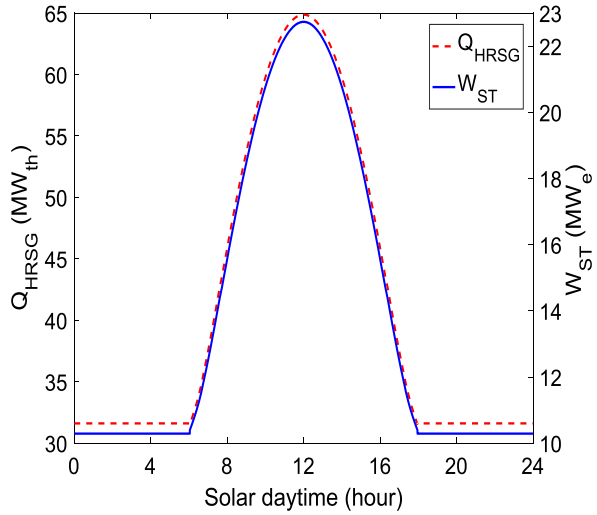

Figure 4.11. HRSG thermal heat and steam turbine output

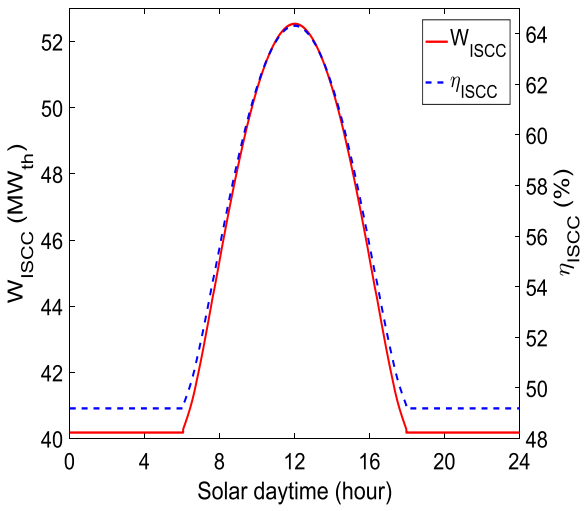

Figure 4.12. Output and efficiency of ISCC plant

Fig.4.12 presents the net electricity production and thermal efficiency of ISCC, revealing a high electricity production about 52.6 MW_e at solar noon compared with 40 MW_e delivered by CC alone, while the overall efficiency reaches a value of 64.41 %. The solar thermal conversion to electricity and solar-electric-ratio are presented in Fig.4.13. By adopting the same solar field as PS10 the conversion of solar energy into electricity may reach a maximum of 12.43 MW_e at solar noon and the solar electricity ratio a value of 23.5 %.

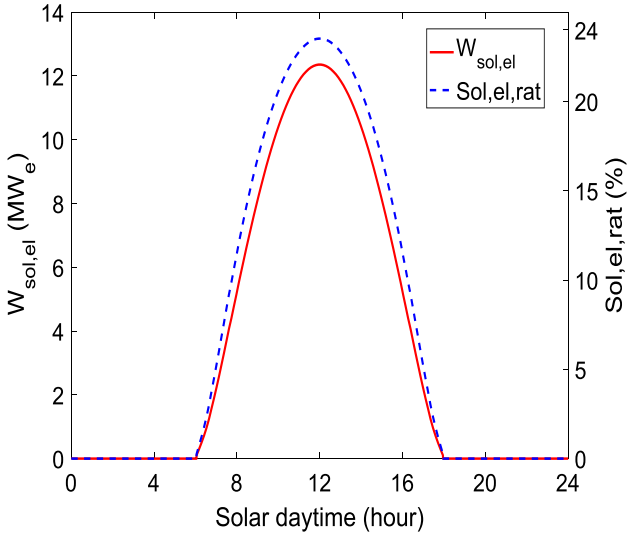

Figure 4.13. Solar electricity conversion and solar electric ratio

4.5. Comparisons of Present Configuration with PS10 and ST-ISCC

The present configuration of ISCC is compared with Abengoa PS10 in Seville (Spain) [170] under the same heliostats solar field. Table 4.5 shows that this new configuration has a good conversion of solar thermal energy with more electricity produced compared with the solar tower molten salt PS10 using a cavity receiver. Indeed, with 28.6 MW_{th} of solar energy

transferred to HTF there is about 11.7 MW_e of solar electricity produced, which is higher than PS10 where 35.8 MW_{th} is transferred to HTF in the cavity receiver to produce 11 MW_e of solar electricity. As a result, higher efficiency of solar energy conversion reaches up to 40.9 % against 30.7 % of PS10, since the open volumetric air receiver plays the role of a supplementary firing, in addition to improvement of HRSG efficiency and solar energy conversion.

Table 4.5. Comparison with PS10 performances

Parameters	Present configuration	PS10 [171]
Solar thermal input (MW_{th})	28.6	35.8
Solar electricity (MW_e)	11.7	11
Efficiency of solar energy conversion (%)	40.9	30.7

The second case consisted in comparing the configuration studied by Franchini et al. [93] of an integrated (ST-ISCC), consisting of the same GT Siemens SGT-800 and HRSG of dual pressure integrated with SPT via a cavity receiver. The solar thermal energy is transferred to the bottoming cycle by means of SSG using synthetic oil (Therminol VP-1) as HTF. Table 4.6 gives the data for the design performance of ST-ISCC where additional steam generated by solar energy is achieved by SSG in parallel to HRSG through HTF Therminol VP-1.

Table 4.6. ST-ISCC plant validation parameters [93]

Parameters	Value
CC	
Pressure ratio	19.9
GT power output (MW)	46.4
GT efficiency (%)	37
GT exhaust gas mass flow (kg/s)	131.5
GT exhaust temperature (°C)	548
HP & LP pressure (bar)	69 & 7.7
HP & LP superheater temperature (°C)	522 & 218
Condenser pressure (bar)	0.06
HP & LP pinch point (°C)	9 , 8
Approach point (°C)	26
HP & LP turbine isentropic efficiency (%)	83 & 87.5
Solar field	
Heliostat surface (m^2)	120
Heliostat number	820
Receiver optical efficiency (%)	90
ST-ISCC	
SSG solar thermal power (MW_{th})	66.3
ST-ISCC net power output (MW_e)	89.3

This latter as compared with the proposed configuration of open volumetric air receiver, which has no SSG, operating directly as a supplementary firing generates more steam and improves the overall performance. Moreover, the comparison of solar energy conversion between this proposed hybridization and that of reference [93], by referring to sunny day of July month, shows a good agreement.

The DNI of Seville (Spain) solar thermal plant is estimated based on HLJ model [159]. Fig.4.14 shows that DNI reaches the highest value of 888 W/m^2 which is lower compared with that of 947 W/m^2 of reference [93]. This deviation of 6 % is due to the model uncertainty within 10 % of measurement tolerance. Fig.4.15 compares between the daily profiles of DNI, intercepted solar energy (Q_c), net thermal power (Q_r) transferred to HTF of the present study and reference [93], revealing less (Q_c) intercepted and (Q_r) transferred in the receiver. As displayed by Fig.4.16, the solar fraction which contributes in the net power output of ISCC may reach a value of 0.27 which is 10 % lesser than that of reference [93]. Moreover, Fig.4.17 shows that the electric solar power production may reach a high value of 18.65 MWe which is 2 % higher than reference [93], and the hourly solar-to-electric efficiency $\eta_{sol,elec}$ (Fig.4.18) is slightly higher than that of reference [93]. As one may conclude that this novel hybridization via a volumetric receiver seems converting the solar energy into electricity more efficiently, as this latter works as a supplementary firing without additional SSG.

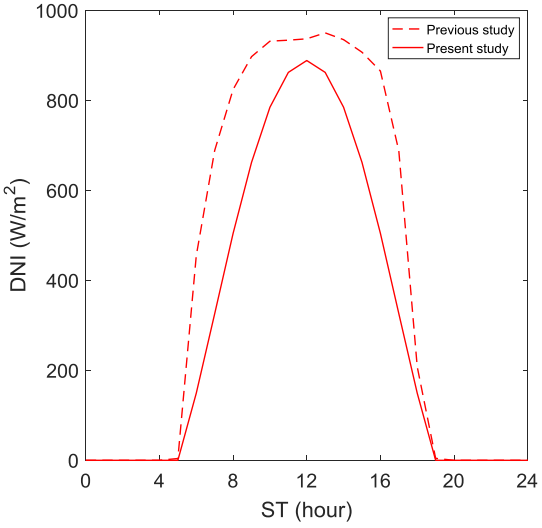

Figure 4.14. DNI

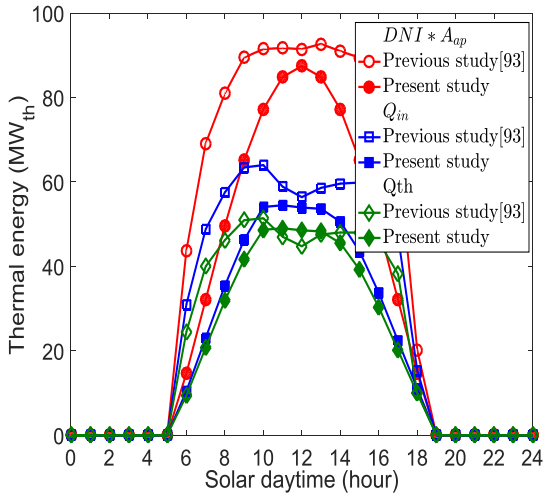

Figure 4.15. Intercepted radiation and net thermal power

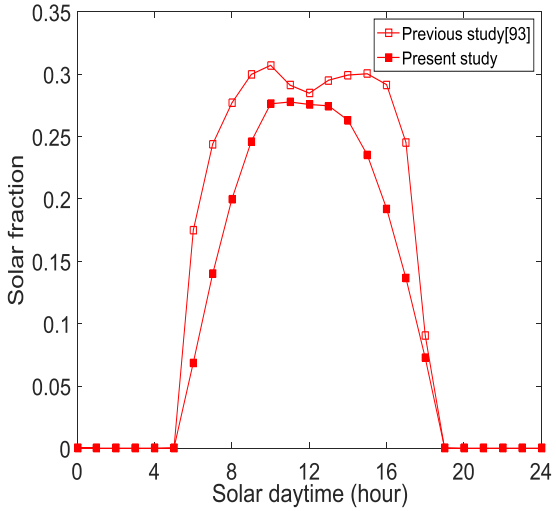

Figure 4.16. Hourly solar fraction

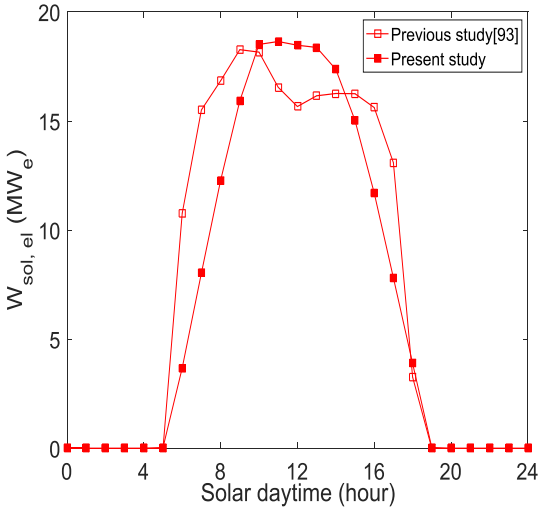

Figure 4.17. Hourly solar power production

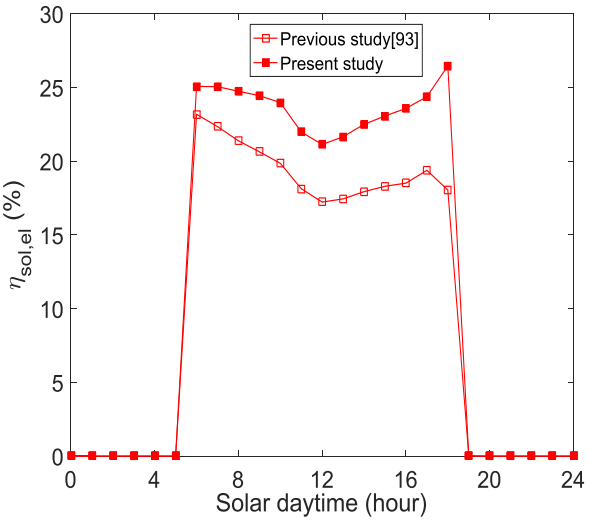

Figure 4.18. Hourly solar-to-electric efficiency

4.6. Economic Assessment

This novel hybridization seems performing well in terms of solar electricity conversion and plant efficiency. However the economic feasibility and viability of the solution have to be assessed in term of LCOE. Also comparisons are made between GT, CC and ISCC, where the conventional CC is taken as a reference plant. The same economic model as presented in chapter 3 to assess the LCOE is adopted [98].

The total investment cost of a new integration of solar tower with CC is the sum of GT, steam turbine and solar unit costs. The economical assumptions and data are presented in Table 4.7. The comparisons between LCOE values are given in Table 4.8 including the fuel saving and CO_2 emission. Fig.4.19 (a-b) presents the estimated LCOE for GT, CC and ISCC. LCOE is subdivided into three parts: investment cost, fuel cost and O&M cost, and is latter is greatly

affected by the specific cost of power plant especially the solar power components since its cost is comparatively very high. When environment cost is not considered, CC has the lowest LCOE followed by GT, and in that case LCOE of ISCC is about 18 % higher than that of GT and 37 % higher than that of CC. If one is concerned with the environmental issue LCOE becomes 0.0335 $/kWh which is about 10 % and 30 % higher than that of GT and CC, respectively, but LCOE of CC is still the lowest value.

Table 4.7. Economic assumption and data

Assumptions and data	Value
Life expectancy of solar field (year) [172]	30
Life expectancy of steam unit (year) [93]	30
Life expectancy of gas unit (year) [93]	15
Annual discount rate R (year) [93]	10
Capacity factor	0.8
Direct costs	
Specific cost of solar field $C_{sol,Helio}$ ($/kW) [123]	818
Specific cost for tower with receiver $C_{sol,Tow}$ ($/kW) [123]	286
Specific cost of steam unit C_s ($/kW) [173]	1052
Specific cost of gas unit C_g ($/kW) [173]	314
Contingency (% of direct costs)	7
Indirect costs	
Engineering, procurement and construction (% of direct costs) [172]	11
O&M cost factor of solar field k_{sol} (%) [98]	1.5
O&M cost factor of steam unit of CC k_s (%)[98]	2
O&M cost factor of gas unit k_g (%)[98]	5
Q_{cv}= Lower Heating Value of natural gas (kJ/kg) [98]	46595.3
Fuel price ($/MMBTU) based on average 2018 [174]	3.16
Emissions ($/ton) [98]	9.9

Table 4.8. LCOE for different power plants

Parameter	GT	CC	ISCC
DNI_an (KWh/m^2 yr)	-	-	2014.5
Annual electricity production (MWh)	210240	276816	302360
LCOE[a] ($/kWh)	0.0250	0.0219	0.0301
LCOE [b]($/kWh)	0.0307	0.0262	0.0341
Fuel saving in 30 years Million $)	---	---	7.07
Avoided CO_2 emission in 30 years (Million ton)	---	---	0.33

[a] Without environmental cost.

[b] With environmental cost.

Fig.4.20 and Fig.4.21 present the specific fuel consumption (SFC) in (kg/MWh) and the emission of CO_2 (kg/MWh), which has been evaluated from the fuel consumption assuming

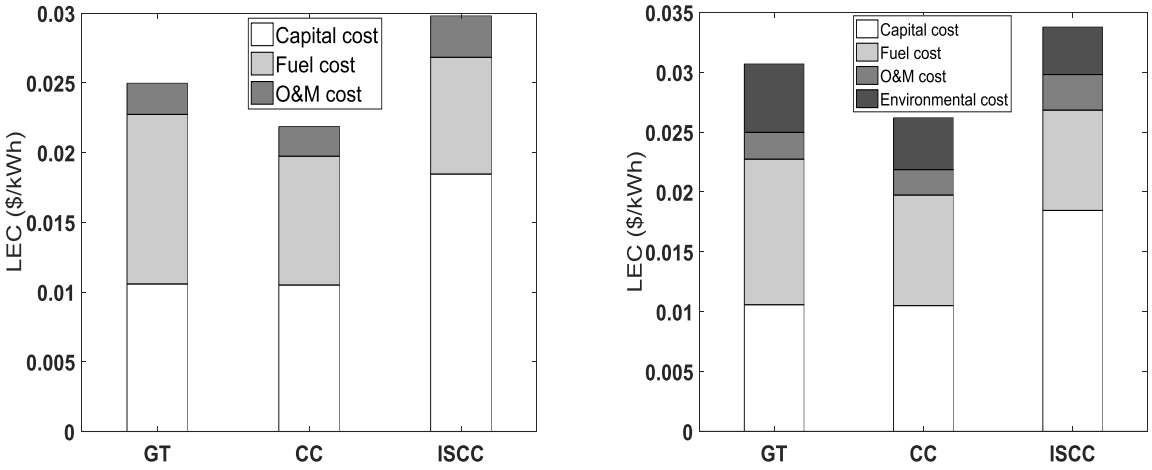

Figure 4.19. LCOE of different power plants: a) Without environmental cost; b) With environmental cost.

an emission factor of 249 kg/MWh_{fuel}. CO_2 is the main part of atmospheric pollution and responsible of the greenhouse effect, and thus leads to considering environmental cost [98]. According to Fig.4.20, ISCC has the lowest SFC which is about 7 % lower than that of CC and 44 % lower than GT. Subsequently, ISCC may save about 7.07 million $ of fuel through 30 years of operational service. According to Fig.4.21, CO_2 emission is proportional to the fuel consumed, which is extremely high for GT and low for CC, while ISCC has the lowest CO_2 production, and hence avoiding emission of 0.33 million ton over 30 years of operational service. With this novel hybridization even though LCOE is higher due to excessive capital cost of the solar part, ISCC becomes economically competitive vis-à-vis GT and CC when the environmental issue is considered in addition to its simplicity in installation.

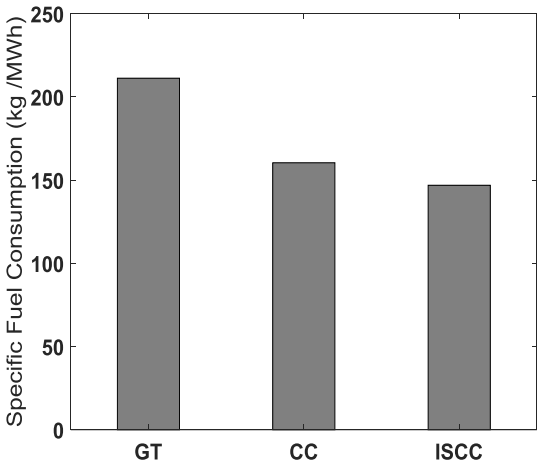

Figure 4.20. Specific fuel consumption

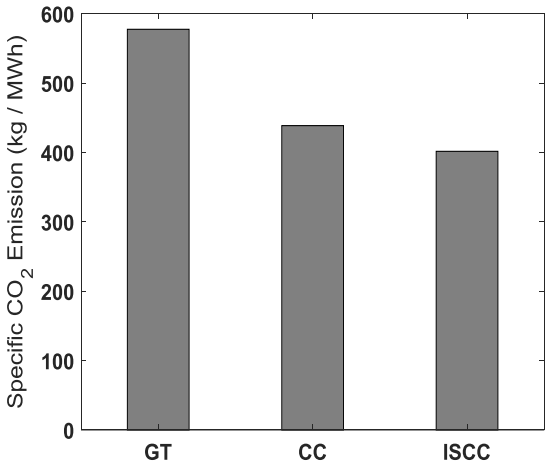

Figure 4.21. Specific emission of CO_2

4.7. Optimization

In solar systems various stochastic optimization techniques such as Genetic Algorithm (GA), Artificial Neural Networks (ANN), Particle Swarm Optimization (PSO) and Simulated Annealing (SA) etc. are implemented to set the optimal design and parameters to improve the thermal efficiency and reduce the total cost [175]. GA algorithms as one of most popular optimization techniques are useful to solve real-world problems of large non-linearity where the search for the optimum is not restricted by the local optima [176]. Over the past decade GA has been extensively used in solar thermal systems [177]. In multi-objective optimization problems formulated as $min\big(f_1(x),\ f_2(x), \dots, f_k(x)\big)$, a feasible solution $x^1 \in X$ is said to (Pareto) dominate another solution $x^2 \in X$, if $f_i(x^1) < f_i(x^2)$ for $i \in \{1,2, \dots, k\}$ and $f_j(x^1) < f_j(x^2)$ for at least one index $j \in \{1,2, \dots, k\}$. A solution $x^1 \in X$ is called non-dominated or Pareto optimal if none of the objectives can be improved without degrading one or more of other objective values [178]. The number of optimal parameters and the manner in which their values are interpreted have an effect on the speed of convergence of the optimization routine; hence the parameters having a large impact on performance should be preferentially selected [117]. In the present study, the Rankine cycle is the crucial part and has a direct impact on ISCC performance since HRSG is the main subsystem to generate steam. Before performing optimization it is necessary to select the set of decision variables which have a direct impact on the performance. The decision variables as depicted in Table 4.9 are: steam pressure, pinch point and approach point for the Rankine cycle and GT power parameters. Besides, there are some technological limitations (constraints), shown in Table 4.9, which include limitations of steam pressure and temperature and steam quality. The limitations of steam operating pressure and temperature are related to the economic and material issues. The steam pressure has to be selected no more than 10 MPa, below the supercritical pressure around 25 MPa and the temperature should not exceed 600°C. The steam temperature and pressure are shown to affect the quality of steam at turbine exit which should not be lower than 0.85 - 0.88. By referring to the surrounding heliostat field the north side field is not suitable for the large scale thermal power plants [179]; therefore the GT size margin as selected in the current optimization will not be large in order to get a feasible thermal plant scale in the case of the north side heliostat field. The solar field area is function of the flue gases, depending on the GT power parameters, which should be designed to obtain an outlet temperature of 850 °C from the receiver corresponding to the highest DNI and the

same optical heliostat field efficiency as PS10 [166]. Also, the assumed value of the concentration ratio is in the range of 940 - 950 [1].

Table 4.9. Decision variables and constraints

Decision variables	Lower limit	Upper limit
GT power (MW)	25	50
Pressure steam (P_{fw}) (bar)	70	100
Pinch point (ΔT_{pp}) (°C)	5	10
Approach point (ΔT_{ap}) (°C)	10	20
Constraints		
Steam pressure (P_{fw}) (bar)	$\leq$ 100	
Steam temperature (T_{s2}) (°C)	$\leq$ 600	
Steam quality (x)	$\geq$ 0.85	

To determine the optimal parameters of present ISCC power plant, including the power of GT, solar field, steam pressure, pinch point and approach point, a multi-objective optimization population-based GA "gamultiobj" is used under MATLAB Global Optimization Toolbox [180], coupled with the main program implementing the thermo-economic models of the different power blocks. An initial population size of 50 runs is adopted for the three scenarios as below. The evolution of population during optimization process leads the final generations to form the well-defined Pareto-fronts.

Scenario 1: The design objectives are to maximize the thermal plant power W_{ISCC} and efficiency η_{ISCC} by considering the decision variables and constraints shown in Table 4.9. The convention of used optimization Toolbox is for a minimization problem, thus a maximization problem can be treated by minimizing the negating value of the objective function. This bi-objective design problem is formulated as follows:

$$min\{-W_{ISCC}, -\eta_{ISCC}\} \tag{4.29}$$

subject to

$$\begin{cases} P_{fw} - 100 \leq 0 \\ T_{s2} - 600 \leq 0 \\ 0.85 - x \leq 0 \end{cases}$$

After 102 generations the well-defined Pareto front is reached, showing (Fig.4.22 (a)) that the Pareto-optimal points are very close. The final optimum is selected as the extreme point (in red) at insignificant drop in efficiency. The trade-off of the maximum possible power generation for a maximum efficiency corresponds to 87.526 MW and for the thermal efficiency of 64.266 %.

Scenario 2: The design objectives are maximizing the thermal plant efficiency η_{ISCC} while minimizing LCOE by considering the decision variables and constraints shown in Table 4.9. This bi-objective design problem is formulated as follows:

$$min\{-\eta_{ISCC}, LCOE\} \tag{4.30}$$

subject to

$$\begin{cases} P_{fw} - 100 \leq 0 \\ T_{s2} - 600 \leq 0 \\ 0.85 - x \leq 0 \end{cases}$$

After 162 generations the well-defined Pareto-optimal points are depicted in Fig.4.22 (b), showing optimal points very close. The selected good trade-off point occurs for an efficiency of 64.207 % and LCOE of 0.02634 $/kWh.

Scenario 3: The design objectives are to maximize the thermal plant efficiency η_{ISCC} while minimizing $LCOE$ and taking into account the environment cost. After 182 generations the Pareto front (Fig.4.22 (c)) shows that LCOE increases while the thermal plant efficiency improves. Comparison between the two extreme points, i.e. lowest LCOE for the right extreme point and highest efficiency for the left extreme point allows selecting the best point defined for an efficiency of 64.205 % and LCOE equal to 0.02883 ($/kWh) which is close to the lowest value of LCOE.

The trade-off results for each selected Pareto-optimal points corresponding to the three scenarios are compared in Table 4.10, which also is shows the optimal solar field area and receiver area.

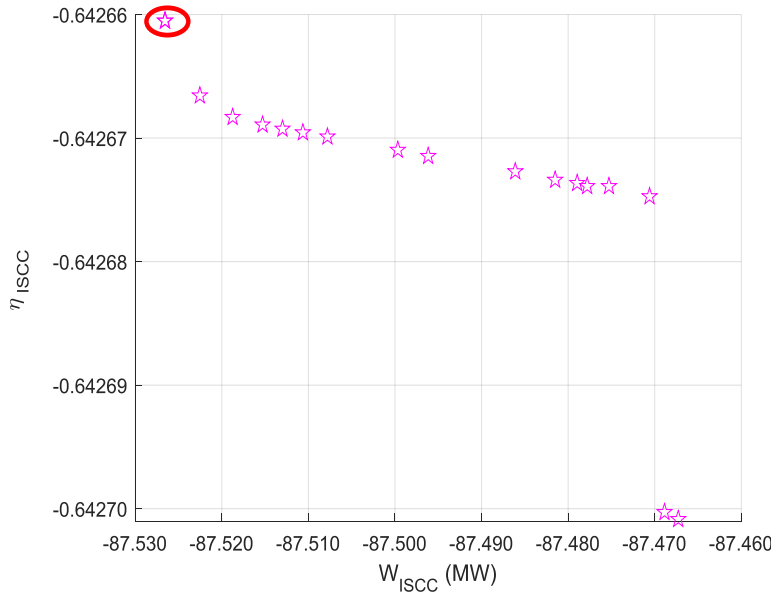

(a)

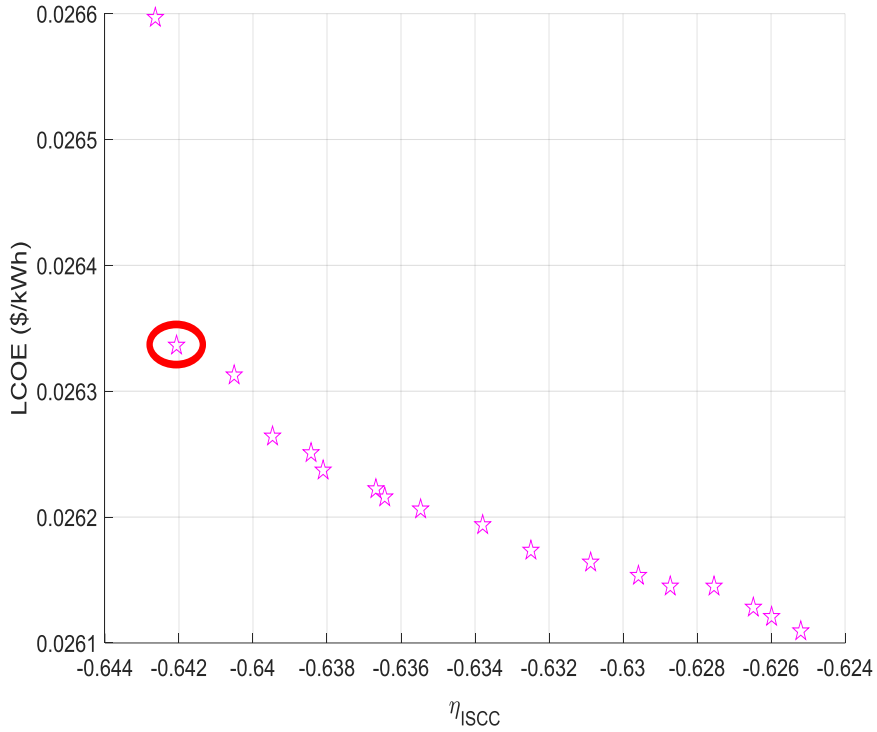

(b)

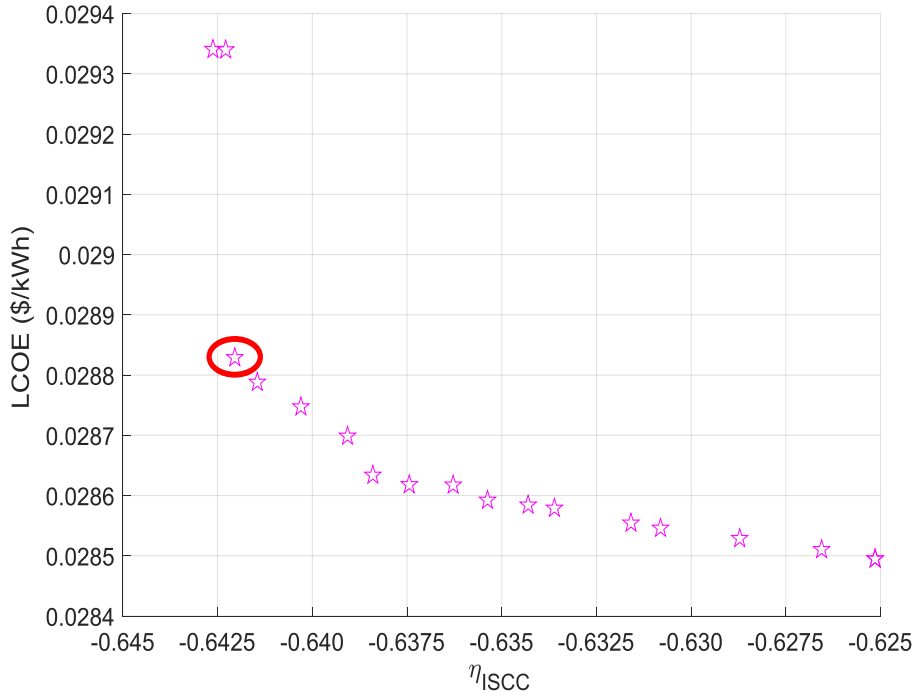

(c)

Figure 4.22. Pareto fronts: a) 1st case**;** b) 2nd case; c) 3rd case

Table 4.10. Optimum parameters and performances

Scenario	ISCC Power (MW)	ISCC Efficiency (%)	LCOE ($/kWh)	GT (MW)	Steam pressure (MPa)	Pinch point (°C)	Approach point (°C)	Solar field area (m^2)	Receiver area (m^2)
1	87.526	64.266	-	49.998	9.994	5.004	10.047	126000.455	133.503
2	-	64.207	0.02634	49.704	9.838	5.179	10.049	125259.709	132.718
3	-	64.205	0.02883	49.055	9.990	5.049	10.882	123624.344	130.985

The three optimized scenarios added to that corresponding to Hassi R'mel's case are compared for the solar to electricity efficiency, Rankine performance, solar fraction and global ISCC efficiency, from sunrise to sunset. When referring to Hassi R'mel's site Fig.4.23 shows that the efficiency of solar conversion to electricity is lower in contrast to the three optimized scenarios which exhibit higher values. The Rankine cycle efficiency (Fig.4.24) reveals a lower value for Hassi R'mel's site compared with the three scenarios having almost the same efficiency. Also, the global efficiency of ISCC (Fig.4.25) for the three scenarios are close while that of Hassi R'mel case is below, and similarly for the solar fraction depicted in Fig.4.26.

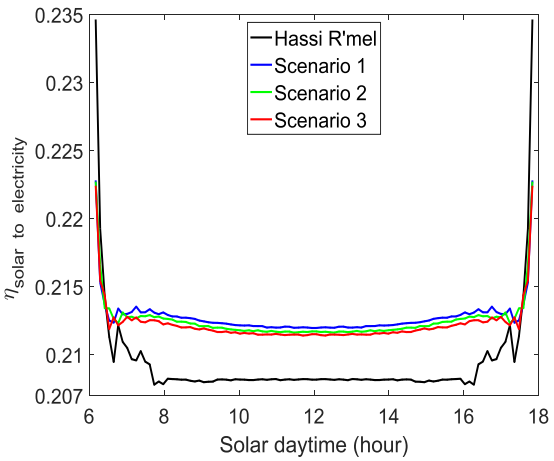

Figure 4.23. Solar-to-electric conversion

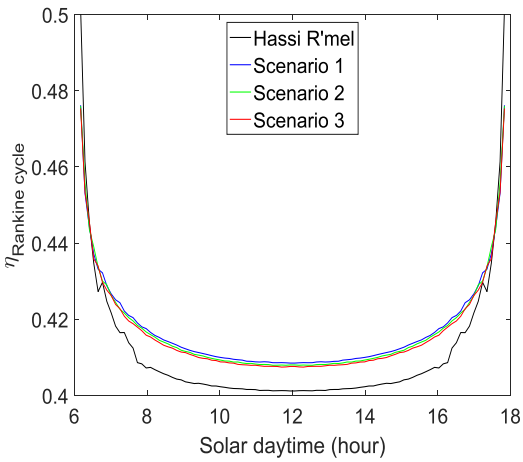

Figure 4.24. Rankine cycle efficiency

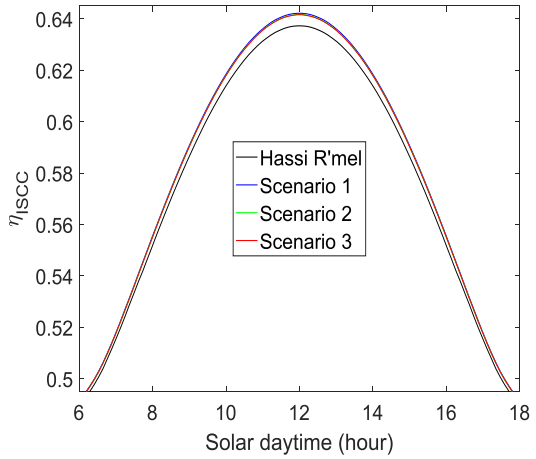

Figure 4.25. ISCC efficiency

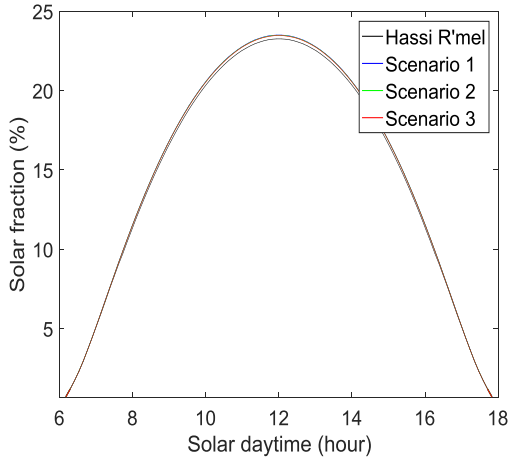

Figure 4.26. Solar fraction

Table 4.11 compares between the mean values of performances during one day of 21st March, revealing that the different efficiencies namely solar to electric, Rankine cycle and ISCC are slightly higher than that of Hassi R'mel case. Table 4.12 reveals that the values of LCOE between the three optimized scenarios are lower than that of Hassi R'mel case. By considering the environment, LCOE is about 12 % more for the three optimized scenarios but lesser than that of Hassi Rmel case which is about 16.5 %. As a conclusion, the economic issue has a significant impact on the ISCC integration and the values of LCOE without and with consideration of environmental cost are prospective.

Table 4.11. Comparison between mean values of performances during one day

Scenario	$\eta_{Sol,elec}$	$\eta_{Rankine\ cycle}$	η_{ISCC}	*Solar Fraction*
1st case	0.2126	0.4134	0.5820	15.59
2nd case	0.2123	0.4128	0.5816	15.58
3rd case	0.2120	0.4122	0.5815	15.56
Hassi R'mel case	0.2080	0.4045	0.5779	15.36

Table 4.12. LCOE for different cases

Scenario	LCOE[a] ($/kWh)	LCOE[b] ($/kWh)
1st case	0.026380	0.028766
2nd case	0.026367	0.028767
3rd case	0.026423	0.028854
Hassi R'mel case	0.029560	0.033536

4.8. Conclusion

In the present section, we have presented a new configuration of an ISCC integrating a SPT system with a volumetric receiver. Thereby, complete thermodynamic and economic models are developed and simulated using a MATLAB code and completed with optimization to find out the optimal layout. The study explained how the solar heat in the proposed configuration of ISCC impacts the performances of the plant and showed how much the solar-to-electricity is converted. This novel hybridization, the volumetric receiver plays the role of supplementary firing which led to enhance the global performances of ISCC plant. In the fired mode the efficiency of HRSG is increased to 79 % and therefore a higher solar to electricity conversion. With the same heliostats field of PS10 the overall thermal efficiency may reach up to 64.40 % and the solar energy conversion ratio to 23.5 % while the produced electricity is about 52.6 MW. These indisputable improvements in performance during sunny periods are beneficial to the grid flexibility. Besides, the economic analysis showed that LCOE is about 0.0335 $/kWh which could be further reduced by 16 % through an optimization to reach

about 0.0287$/kWh and becomes competitive with environmental issue considered. In addition, there are fuel saving about 7.07 Million $ and pollutant reduction to 0.33 Million ton during 30 years of operation. All these outcomes allow concluding that this novel hybridization of CRS could be a promising option as it is technically and economically viable over the operating lifetime.

As a consequence, the present investigation of the proposed ISCC adopting a SPT system showed a good agreement as it was compared to the previous works in terms of thermal performance and solar-to-electricity efficiency. We realize that this proposed system could be among the promising ISCC existed till the present day mainly those ones using PTC. Hence, a comparative study between the new ISCC configuration integrating CRS and the first ISCC plant in Algeria is carried out in the next step to determine the most efficient system.

Chapter 5

Comparison Study of Two Integrated Solar Combined Cycle Power Plants

5.1. Introduction

Nowadays, the integration of solar energy into a combined cycle (CC) using concentrated solar power (CSP) technology to constitute the so-called Integrated Solar Combined Cycle (ISCC) is being more attractive than stand-alone CSP plants. At present, the most operating ISCC power plants are those using Parabolic Trough Collector (PTC) and Solar Power Tower (SPT) technologies. Thus, several layouts have existed which some are commercialized or underdeveloped throughout the world [1, 2, 181]. In the concept of ISCC adopting PTC technology (ISCC-PTC) the solar heat from the solar field generally is injected into the bottoming cycle (steam cycle) parallel to the HRSG via an intermediate solar steam generator (SSG) and it is injected into the topping cycle (Brayton cycle) in case the ISCC is running with SPT technology (ISCC-SPT) like in the solarized gas turbine.

The present chapter is a comparison of the instantaneous and annual thermal performances of the two ISCC configurations studied above in chapter 3 and 4, one which adopts the PTC technology (ISCC-PTC) and the second which is driven by the SPT system (ISCC-SPT). The first ISCC-PTC configuration is with Hassi R'mel's ISCC design where solar thermal energy is introduced as a latent heat in parallel to the evaporator of the HRSG single pressure via the SSG. The performances of such configuration are already investigated and carried out in the references above [90, 91, 102, 103]. The second ISCC-SPT one is based on the SPT technology which is a new proposed configuration since there is very limited research was dedicated to the development of SPT coupled to the CC according to the literature and to the reference [2]. This configuration consists of integrating solar heat to heat up the exhaust gases from the gas turbine (GT) before entering the HRSG via the volumetric receiver. Hence, the receiver plays the role of supplementary firing which is an excellent way for generating additional steam in HRSG with single pressure and improving its efficiency. The obtained results from the simulation of these two ISCC systems are compared to each other to find out

the most efficient system based on the solar conversion to electricity (solar-to-electric efficiency) with considering the maturity level for each one. Furthermore, the economic assessment of the cost of electricity production expressed by the Levelized cost of energy (LCOE) is taking into account in the present comparison.

5.2. ISCC system layouts

ISCC system consists of Brayton and Rankine power blocs, and a solar system. Firstly, the ISCC-PTC is with Hassi R'mel's ISCC concept that integrates a PTC field with a CC which is proposed and designed by Abener and Abengoa Solar [89]. It consists of one PTC solar field, a steam power bloc, a SSG and a single GT as shown in the Fig.3.5. Secondly, the ISCC-SPT is a new proposed configuration that integrates SPT technology into a CC where solar thermal energy is used as sensible heat. The plant is composed of heliostat solar field, a solar tower with volumetric receiver, a GT and steam power bloc. The flue gases from the GT before entering a heat recovery steam generator are heated up until the fired temperature by the solar heat in a volumetric receiver. The latter plays the role of a supplementary firing since it is considered an excellent way to generate additional steam efficiently in the HRSG as shown by Fig.4.8. Thus, the solar hear is used as sensible heat to raise the flue gases temperature.

5.3. Simulation of the ISCC-PTC and ISCC-SPT thermal plants

The two ISCC systems to be considered in the present investigation integrate a conventional CC and a solar system which one is with the PTC solar field and the other one is with SPT solar system. Both consist of a solar field area of 117720 m^2, a GT unit of 47 MW, a HRSG single pressure, and an oversized ST. The chosen solar field size area is based on flue gases mass flow from the selected GT that could be heated up by solar energy available in the volumetric receiver of SPT system to reach the fired temperature of about 850 °C. This temperature value is based on the highest DNI, mean ambient temperature and wind speed values for the day of the 21st of March. We note that Hassi R'mel ISCC's configuration has the flexibility to operate with one GT unit of 47 MW and one PTC solar field side. Consequently, the selected GT size in the current simulation is suitable to get a feasible SPT scale system using a volumetric receiver with the north side heliostat field. In contrast to SPT systems using a surrounding field which are suitable for large scale [179]. Simulation of these two ISCC plants is performed under Hassi R'mel location due to the highest DNI where the first ISCC system in Algeria was installed.

Table 5.1. Design parameters

Parameters	value
Hassi R'mel data	
Latitude (degree)	33.8
Ambient pressure and temperature, mean wind speed (bar,°C, m/s)	1.013, 21, 6
PTC Solar field (LS-3 type)	
PTC aperture area (m^2)	545
C_L, N_L and C_c	6, 36, 80
Heliostats Solar field	
Heliostat surface unit (m^2)	12.84x9.45
Heliostats number, and C_c	970, 940
Power block	
GT output (MW)	47
Exhaust gases temperature (°C)	544
Pinch point (°C)	11
Approach point (°C)	8
Superheated steam temperature (°C)	500
Heat loss factor and Blow down (%)	1
HRSG single pressure (P_{fw}) (bar)	93
Inlet feed water temperature (°C)	50
Mechanical and electrical efficiency (%)	98

5.4. Results and discussion

Two configurations of ISCC systems based on two different CSP technologies have been investigated and simulated in this study. The obtained results are compared between these two integrated solar systems in terms of thermal performances and economic issue with more attention is paid to solar-to-electric conversion. Therefore, the same solar field area of about 117720 m^2 was assumed for performance simulation. Firstly, the modeling is focused on three selected sunny days which are: 21st of March, 21st of June, and 21st of December to simulate the instantaneous thermal performances. Secondly, annual thermal performances are simulated to find out the most efficient solution of solar integration mainly in terms of solar-to-electric conversion between these two ISCC layouts. We note that the earth's position of 21st of September toward the sun is almost the same as that of 21st of March (Eqs. from Apendix), thus their DNIs both are almost equivalent and we report only that from March. All the simulation results are reported in solar time.

5.4.1. Selected days simulation results

The simulation is carried out under meteorological conditions of Hassi R'mel location in terms of ambient temperature (Ta) and direct normal irradiation (DNI) profiles as reported in Fig. 5.1 and Fig. 5.2 for the three selected days under a mean value of wind speed (V_w).

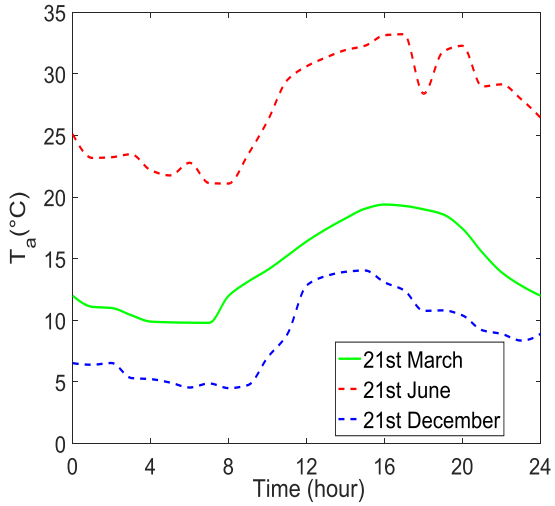

Figure 5.1. Ambient temperature profiles

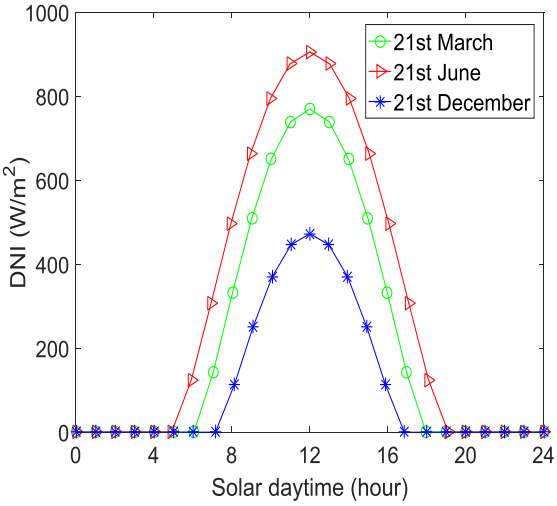

Figure 5.2. DNI profiles

Fig. 5.3 to Fig. 5.5 show thermal performances of the PTC and SPT solar systems. The analysis reveals that more solar thermal energy is collected or reflected by PTC collectors toward the receiver in the summer day than that reflected by heliostats of the SPT system, but the latter has the highest values for winter and spring days as shown by Fig. 5.3. The useful solar thermal energy (Fig. 5.4) transferred into the PTC receiver reaches the highest value for a summer day at solar noon but for spring day it has the same value as that of the SPT system and the lowest value in winter. This is explained by Fig. 5.5 where the global optical efficiency for the PTC system exhibits the highest value about 67 % at solar noon for the summer day which allows transferring more thermal energy to HTF while in the spring day both solar systems exhibit the same optical efficiency value of about 52 %. Also, we notice from Fig. 5.5 that the optical efficiency of SPT system is constant for the selected days and the useful solar thermal energy gained by its receiver has the highest value on the winter day. This is due to its optical efficiency which is higher than that shown by PTC (Fig. 5.5).

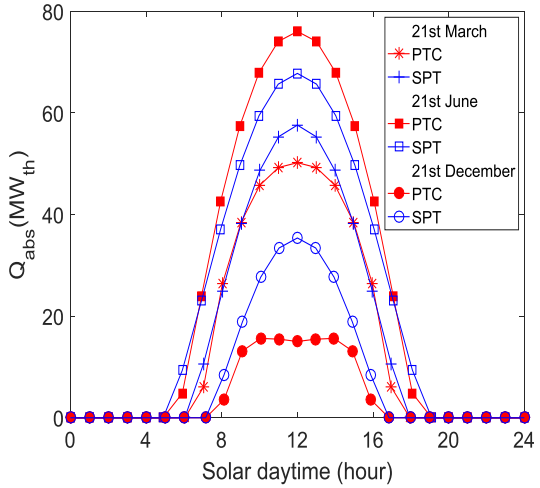

Figure 5.3. Reflected solar thermal energy

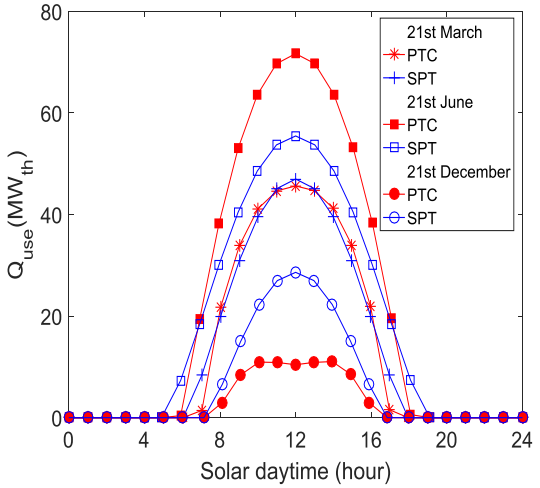

Figure 5.4. Transferred solar thermal to HTF

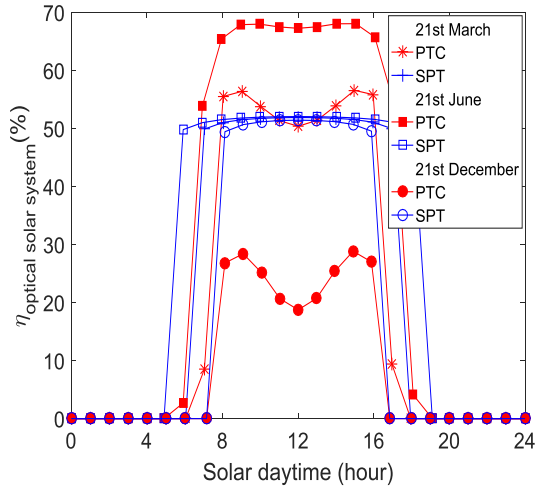

Figure 5.5. Optical efficiency of the solar system

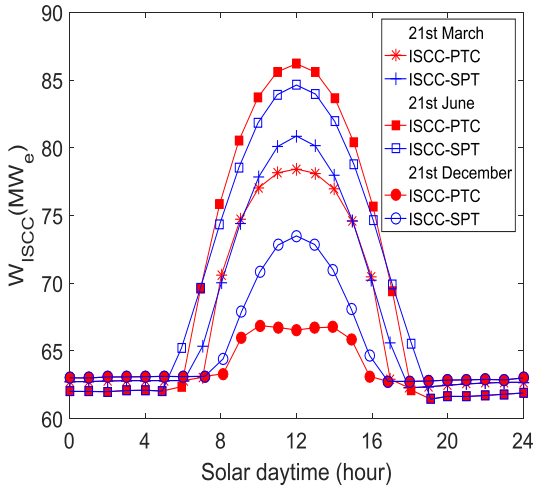

Figure 5.6. ISCC output

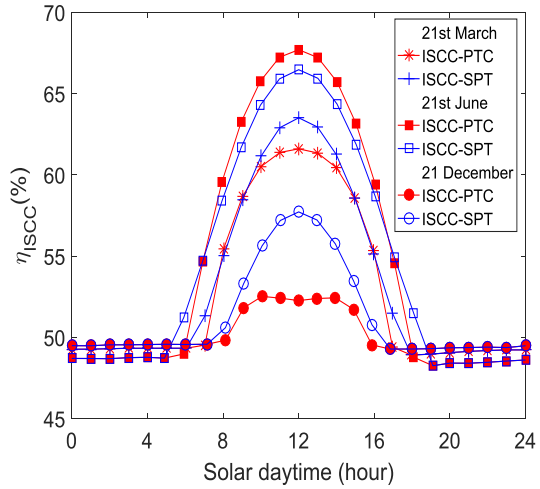

Figure 5.7. ISCC efficiency

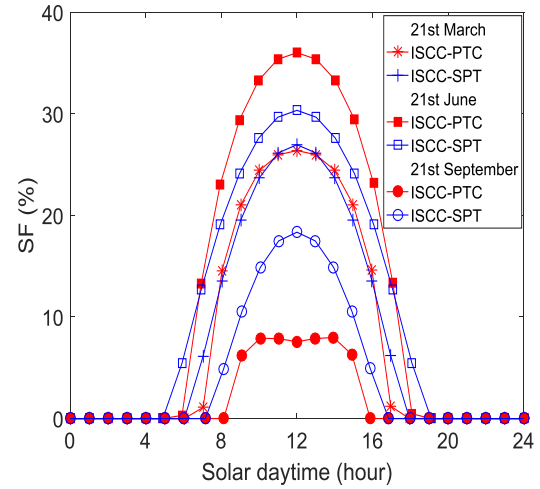

Figure 5.8. Solar fraction

Fig. 5.6 shows that both ISCC systems produce more electricity in the summer period and reach an interesting performances efficiency as well according to Fig. 5.7. In this day, ISCC-PTC exhibits the highest values which are of about 86.2 MW and 67% when the DNI is at its

maximum, higher than those achieved by ISCC-SPT system (84.6 MW and 66.5% respectively). On the contrary to winter and spring days, the ISCC-SPT shows the highest performances for both selected days higher than those from ISCC-PTC. As it is seen from Fig. 5.8 for spring day, with the same solar thermal energy expressed by a solar fraction (SF), ISCC-SPT layout shows more power and more overall efficiency than those of ISCC-PTC (Fig. 5.6 and Fig. 5.7). This is interpreted as the former system converts solar thermal energy better than the latter one. We note in Fig. 5.6 and Fig. 5.7 that there is a deviation in CC performance profiles during night time for the selected days; this is due to the ambient temperature variation during the day as it has a serious impact on the GT performance, they are high for cold weather and drop down for hot ambient temperatures [85].

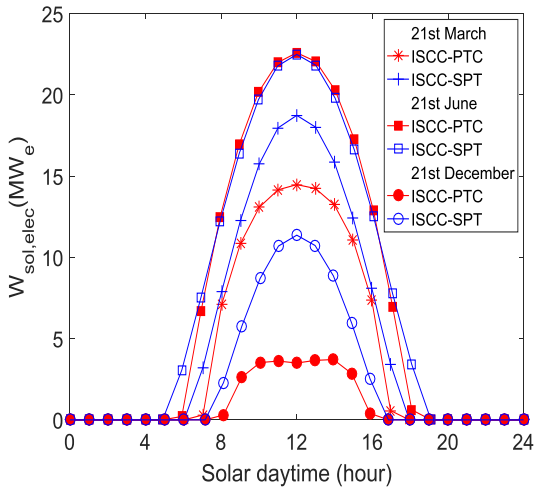

Figure 5.9. Solar-to-electric power conversion

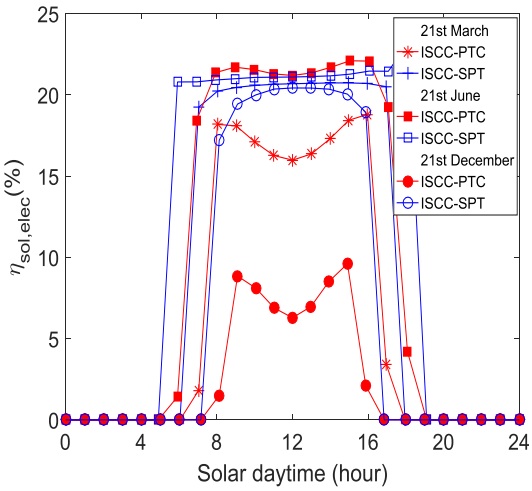

Figure 5.10. Solar-to-electric efficiency

As seen above from the results, the ISCC configuration using SPT has the best performances of converting solar to electricity; Fig. 5.9 to Fig. 5.11 show as well a noticeable enhancement in solar-to-electric conversion for such plant. However ISCC-PTC has the best optical values on the summer day since the PTC system allows the highest solar share compared to the SPT system, with the same solar field area ISCC-SPT converts solar energy into electricity efficiently much higher that of ISCC-PTC (Fig. 5.9 and Fig. 5.10). As it is seen from Fig. 5.10, the plant with SPT has the highest solar-to-electric efficiency with a constant value for the three selected days which is about 21% much higher than that from ISCC-PTC. The latter exhibits lower values for the selected days, except for same where it exhibits the same value as the plant with SPT.

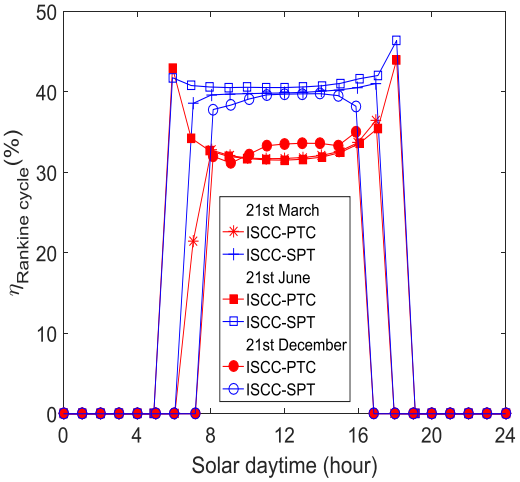

Figure 5.11. Steam cycle efficiency of solar-to-electric conversion

In solar thermal power plants, solar-to-electric conversion is a key parameter to assess the solar integration technique in terms of thermal performances and electricity production. In the present work, the Rankine cycle is an important subsystem in which all thermal energy includes that one from solar is transferred to the working fluid (steam). The ISCC-PTC integrates solar heat as a latent heat in parallel to HRSG evaporator and ISCC-SPT integrates it as a fired mode for the HRSG while optical efficiencies of their solar systems are not the same due to their different technologies and designs. Therefore, Fig. 5.11 explains more which ISCC configuration is more efficient in terms of solar thermal energy conversion into electricity in Rankine power block as defined by Eq. (4.26). It is seen that the ISCC-SPT configuration has the highest Rankine cycle efficiency with a constant value of about 40% during all the season days against 33 % of that ISCC-PTC.

We conclude through this investigation of two different techniques of solar integration in a conventional CC as one is used as latent heat in Rankine block and the other one is used as supplementary firing, are an interesting solutions to generate or to convert solar radiation into electricity. However ISCC-PTC layout can reach the highest output and efficiency values for the summer day, the proposed ISCC-SPT configuration converts solar into electricity more efficiently during all the season days as the solar integration makes the HRSG operate in fired mode.

5.4.2. Annual performances

Assessments of annual performances for the two investigated ISCC thermal plants are simulated throughout one year under an assumed full load operation of 8760 hours per year while their solar systems both operate only in daylight hours. Monthly average *DNI* $A_{solar\ field}$,

reflected or absorbed solar energy (E_{abs}) and useful thermal energy (E_{use}) are reported in Fig. 5.12 and Fig. 5.13 for PTC and SPT systems respectively based on an average daily basis for each month.

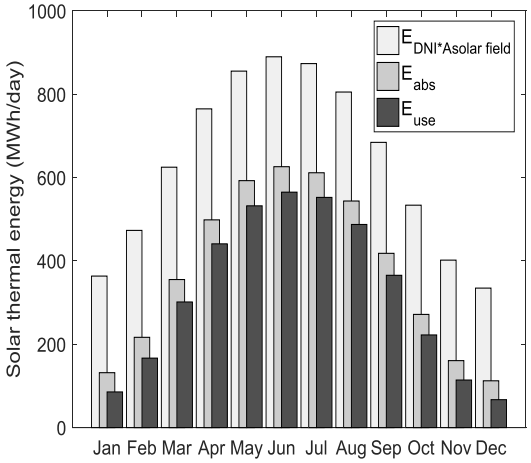

Figure 5.12. Monthly solar thermal for PTC system

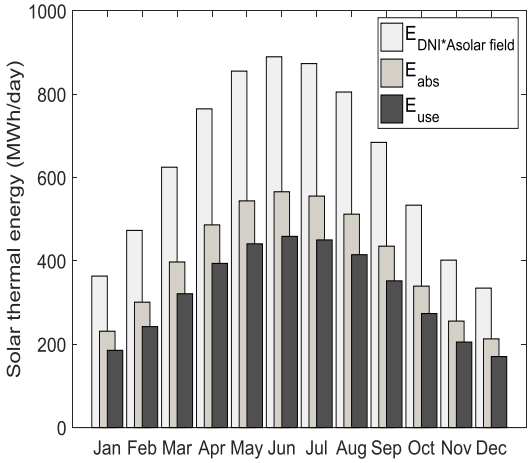

Figure 5.13. Monthly solar thermal for SPT system

Through Fig. 5.12 and Fig. 5.13, the PTC system exhibits high values of E_{abs} and E_{use} (Fig. 5.12) compared to those from the SPT system (Fig. 5.13) in the warm period (summer). Thus, the instantaneous thermal efficiency of PTC exceeds the value of 65% (Fig. 5.5) and this is due to lower cosine losses, but it drops dramatically in winter as its optical efficiency is low (Fig. 5.5). In contrast, E_{abs} reflected by heliostats and E_{use} transferred into the volumetric receiver for the SPT system are much more stable throughout the year. Thanks to better and constant optical efficiency exhibited by SPT during the cold period (mainly in the winter) as shown by Fig. 5.5 because the solar zenith angle is higher.

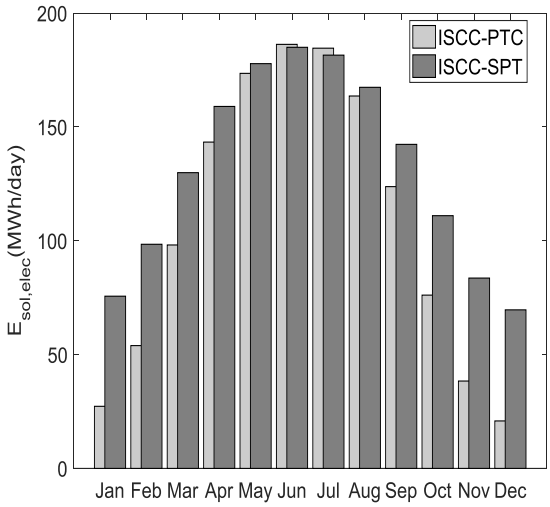

Figure 5.14. Monthly solar electricity production

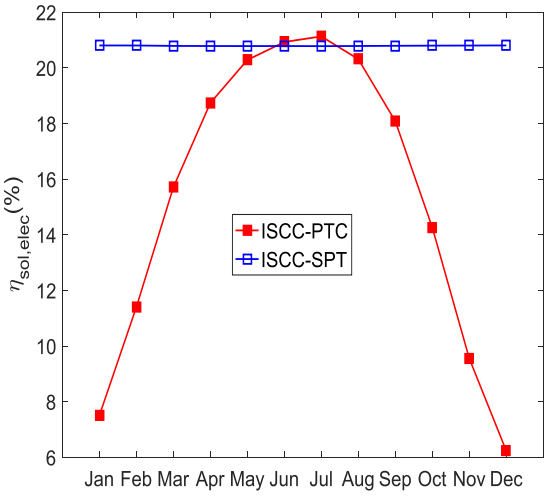

Figure 5.15. Monthly solar-to-electric efficiency

In this study, it is important to investigate these two studied ISCC systems from the solar-to-electric conversion point of view since it is the key parameter that gives an idea about how much these two thermal plants are efficient. Therefore, Fig. 5.14 and Fig. 5.15 display the amount of electricity produced from solar radiation and the solar-to-electric efficiency respectively (based on an average daily basis for each month). With the same solar field area, the solar electricity generated by the ISCC-SPT layout is more important than that produced from the ISCC-PTC layout all along the year except for June and July months where it is slightly lower (Fig. 5.14). Also, Fig. 5.15 displays that ISCC-SPT exhibits a high value of solar-to-electric efficiency of about 20.8% which is constant during the year, much better than that exhibited from the ISCC-PTC except for June and July where it is slightly lower. This is explained as ISCC-SPT converts solar energy into electricity with high thermodynamic efficiency, even though ISCC-PTC system gained more useful solar heat during warm periods as seen in Fig. 5.12 above. It is seen also, that ISCC-PTC exhibits unsteady efficiency value all over the year while it drops dramatically during cold periods (Fig. 5.15). To find the most efficient ISCC system that is showing the best performances among the two studied plant layouts; thus annual energy balance includes available solar energy irradiation ($DNI\ A_{solar\ field}$), the reflected solar energy ($E_{sol,ther,abs}$), the useful solar thermal energy ($E_{sol,ther,use}$) and the solar electrical energy ($E_{sol,elec,an}$) have been computed and reported in Table 9 with annual average efficiency ($\eta_{sol,elec}$) and a solar fraction (SF).

Table 5.2. Annual energy yield

Annual parameters	ISCC-PTC	ISCC-SPT
$DNI\ A_{solar\ field}\ (GWh)$	228.20	228.20
$E_{sol,ther,abs}\ (GWh)$	136.19	145.13
$E_{sol,ther,use}\ (GWh)$	117.03	117.31
$E_{sol,elec,an}\ (GWh)$	38.69	47.44
$\eta_{sol,elec}(\%)$	15.4	20.8
$SF\ (\%)$	9.35	9.55
$\eta_{ISCC}(\%)$	56.23	57.19
$E_{ISCC}\ (GWh)$	581.61	585.90

Through this annual energies analysis (Table 5.2) of ISCC-PTC and ISCC-SPT systems, despite SPT reflects more solar energy $E_{sol,ther,abs}$ toward the volumetric receiver than PTC (145.13 GWh against 136.19 GWh) both systems convert solar radiation into useful thermal heat equally ($E_{sol,ther,use}=117\ GWh$). It is seen also with the same quantity of solar heat available inside of both receivers corresponding to the same SF, more electricity ($E_{sol,elec,an}$) is

generated by the ISCC-SPT system from solar radiation than that from ISCC-PTC (47.44 GWh against 38.69 GWh). Hence, ISCC-SPT is the most efficient system to convert solar into electricity ($\eta_{sol,elec}$) with an efficiency value of 20.8% higher than that from ISCC-PTC which is about 15.4 %. Furthermore, ISCC-SPT exhibits a higher value of the annual overall thermal efficiency (η_{ISCC}) than that shown by ISCC-PTC (57.19 % against 56.23 %). As a consequence, we conclude that the solar thermal plant with ISCC-SPT configuration is the most efficient system as solar heat is integrated as supplementary firing via the volumetric receiver and led HRSG to operate in fired mode while it converts solar into electricity with high thermodynamic efficiency.

5.5. Economic assessment

Improving the performances of any solar thermal plant system or finding the most efficient one based on thermal investigations obviously it is very important. However, before starting any realization of such system it is vital to demonstrate its economic feasibility and viability.

Table 5.3. Economic assumption and data

Assumptions and data	Value
Life expectancy of solar field (year) [172]	30
Life expectancy of steam unit (year) [98]	30
Life expectancy of gas unit (year) [98]	15
Annual discount rate R (year) [98]	10
Capacity factor	0.8
Direct costs	
Specific cost of PTC solar field with HTF system $C_{sol,PTC}$ ($/kW) [182]	786.55
Specific cost of Heliostats solar field $C_{sol,Helio}$ ($/kW) [127]	818
Specific cost of tower with receiver $C_{sol,Tow}$ ($/kW) [127]	286
Specific cost of steam unit C_s ($/kW) [173]	1052
Specific cost of gas unit C_g ($/kW) [173]	314
Contingency (% of direct costs)	7
Indirect costs	
Engineering, procurement and construction (% of direct costs) [182]	11
O&M cost factor of solar field k_{sol} (%) [98]	1.5
O&M cost factor of steam unit of CC k_s (%) [98]	2
O&M cost factor of gas unit k_g (%) [98]	5
Q_{cv}= Lower Heating Value of natural gas (kJ/kg) [98]	46595.3
Fuel price ($/MMBTU) based on average 2018 [174]	3.16
Emissions ($/ton) [98]	9.9

Thereby, estimation of the electricity cost defined in terms of Levelized cost of energy (LCOE) is the key of the economic assessment for the present ISCC-PTC and ISCC-SPT plants and find out the system corresponding to the lowest LCOE.

The current economic analysis is based on the design parameters and this is for the 21st of March with a capacity operation factor of 0.8 for both plants. Also, LCOE comparisons are made between GT, CC, ISCC-PTC, and ISCC-SPT where the conventional CC is taken as a reference plant. The evaluation of electricity production cost LCOE is based on the economical assumptions and data required in this economic analysis are presented in Table 5.3. As a result, the comparison between the four different power plants in terms of LCOE are given in Table 5.4 including the fuel saving and CO_2 emission, while considering CC as the reference power plant for the purpose of comparison.

The estimated cost of electricity expressed by LCOE is reported in the Table 5.4 below for four different power plants GT, CC, ISCC-PTC, and ISCC-SPT. LCOE is subdivided into three parts: investment cost, fuel cost, and O&M cost, and into four parts includes environmental cost when it is taken into account as detailed by Fig. 5.16 and Fig. 5.17. Thus, it is seen that ISCC systems are greatly affected by the capital cost especially the solar power tower component since its cost is very high compared to the other components.

Table 5.4. Estimated LCOE for different power plants

parameters	GT	CC	ISCC-PTC	ISCC-SPT
DNI_an (KWh/m2 yr)	-	-	1611.6	1611.6
Annual electricity production (MWh)	329,376	435,509	471,436	473,867
LCOE[a] ($/kWh)	0.0248	0.0216	0.0269	0.0297
LCOE[b]($/kWh)	0.0305	0.0259	0.0309	0.0326
Fuel saving in 30 years Million $)	-	-	9.82	10.49
Avoided CO2 emission in 30 years (Million ton)	-	-	0.46	0.50

[a] Without considering environmental cost.

[b] Considering environmental cost.

The economic assessment shows that the CC power plant has the lowest LCOE followed by GT which is about 0.0216 $/kWh (Fig. 5.16) and 0.0259 $/kWh with emission consideration (Fig. 5.17). Conversely, ISCC systems both are having the highest LCOE (Fig. 5.16 and Fig. 5.17).

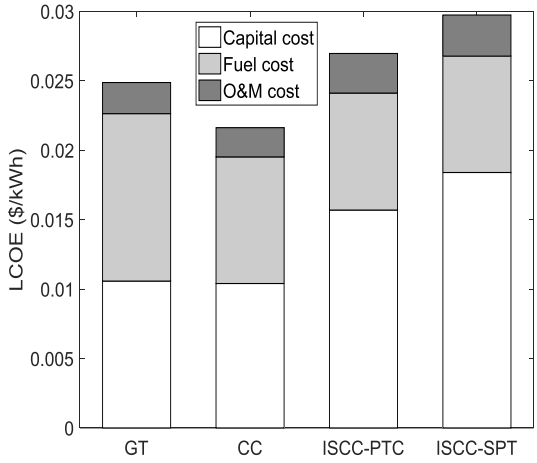

Figure 5.16. LCOE without environmental cost

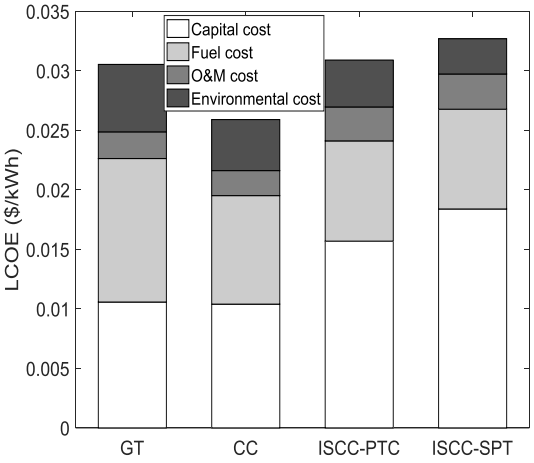

Figure 5.17. LCOE with environmental cost

When environment cost is not taken into consideration (Fig. 5.16), the LCOE of ISCC-SPT and ISCC-PTC are about 0.0297 $/kWh and 0.0269 $/kWh which are about 19%, 8% higher than GT and 37%, 24% higher than CC respectively. In case the environmental issue is considered, the LCOE of ISCC-SPT and ISCC-PTC becomes 0.0326 $/kWh and 0.0309 $/kWh (Fig. 5.17), which are about 6%, 1% higher than GT and 25%, 19% higher than CC respectively. Consequently, LCOE of CC is still the lowest.

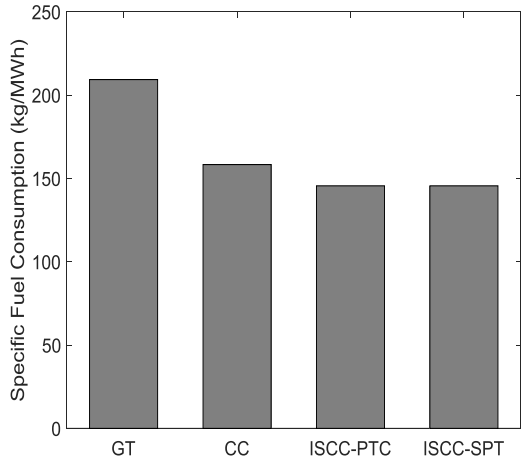

Figure 5.18. Specific fuel consumption

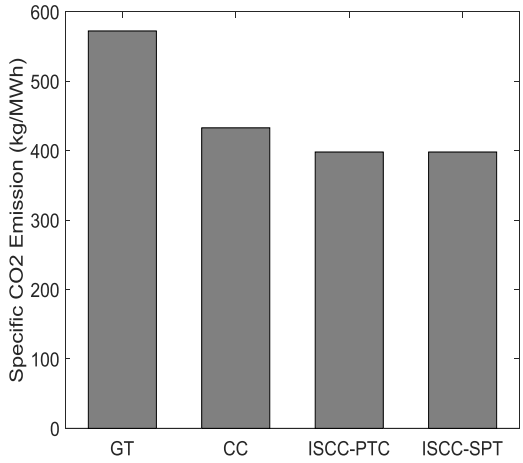

Figure 5.19. Specific emission of CO_2

The exhaust gases from the GT are responsible for the carbon dioxide (CO_2) and lead to an increase of the greenhouse in the atmosphere, hence it's evaluated from the fuel consumption with assuming an emission factor of 249 kg/MWh_{fuel} [177]. Fig. 5.18 and Fig. 5.19 show the specific fuel consumption (SFC) in (kg/MWh) and the CO_2 emission in (kg/MWh) respectively where it is shown that ISCC systems have the lowest SFC and the lowest CO_2 emission compared to GT and CC power plants and both share the same values. The SFC is

about 44% lower than GT and 9% lower than CC (Fig. 5.18). Consequently the two ISCC systems will save about 10 million $ of fuel consumption over 30 years of operation but ISCC-SPT saves slightly more about 6% higher than ISCC-PTC. We can conclude through Fig. 5.19 that the CO_2 emission is proportional to the fuel consumption by the power plant which is extremely high in GT followed by the CC power plant. Thanks to the solar energy available during the day that makes ISCC systems have the lowest CO_2 production and hence avoiding emissions of 0.5 million tons of CO_2 in the case of ISCC-SPT and 0.46 million tons for ISCC-PTC during 30 years of the operational life.

The economic analysis for two ISCC configurations based on two different CSP technologies was conducted in the present work. The comparison of the cost of electricity generated from these two plants shows that despite the high LCOE value for both ISCC systems due to the high capital cost of the solar part, it is still competitive to that from conventional fossil plants mainly to that from GT when the environmental effect is considered. As a result, even though integrated solar systems with PTC technology is the most mature and commercialized thermal plants, ISCC incorporating the SPT technology (ISCC-SPT) presents an approximate LCOE value to that from ISCC-PTC. Consequently, according to the present investigation, ISCC based on the SPT could be sufficiently mature power plant in the near future in addition to ISCC running with PTC as considered the most commercialized and power plants in operation today. This is explained as the ISCC-SPT offers the best thermal performances throughout the year mainly in terms of solar-to-electric conversion and economically viable and feasible. Thus, more research and development should be devoted on the development of such ISCC incorporating a SPT system as this CSP technology reaches high temperature levels and offers the best optical efficiency over the PTC.

5.6. Conclusion

Instantaneous and annual thermal performance investigations of two ISCC systems adopting two different CSP technologies were conducted in the present study and complemented with an economic assessment. One system is with PTC technology to constitute an ISCC-PTC configuration and the other one is based on the SPT system to compose an ISCC-SPT configuration. The former integrates solar heat to generate saturated steam in parallel to the HRSG evaporator and the latter uses solar thermal energy as supplementary firing leading HRSG to operate in fired mode. The achieved results show that both ISCC systems exhibit a high value of electricity production and high overall thermal efficiency; while ISCC-SPT exhibits the best annual performance efficiency value of about 57.2 %. In terms of solar

conversion into electricity, ISCC-SPT configuration is the most efficient system while it reveals a noticeable enhancement in solar-to-electric efficiency with a steady value over the seasons; conversely to the ISCC-PTC where its efficiency value is unsteady and drops dramatically in cold periods. Thus, ISCC-SPT configuration has an annual solar-to-electric efficiency of about 20.8 % much higher than that from ISCC-PTC which is about 15.4 %. Furthermore, the annual global output of the ISCC-SPT plant is slightly higher than the ISCC-PTC output (585.9 GWh against 581.61 GWh). Consequently, the proposed ISCC-SPT configuration exhibits incontestable improvement in terms of thermal performances mainly in solar-to-electric conversion. The economic assessment of the electricity production cost shows that both ISCC configurations has an approximate value of LCOE which are of about 0.0297 $/kWh and 0.0269 $/kWh for ISCC-SPT and ISCC-PTC respectively, while the latter is considered the most mature and commercialized integrated solar system. When the environmental issue is considered, both ISCC systems become competitive with CC and GT power plants. In addition, the two ISCC systems both offer the advantage of fuel-saving and emissions reduction but the ISCC-SPT system offers slightly more advantage during 30 years of operation. Finally, besides to ISCC systems integrating PTC technology of being the most mature and commercialized power plants, it may be concluded that hybridization of SPT system with a conventional CC system where solar energy allows HRSG operate in fired mode offers high thermal performances with high solar-to-electric efficiency, and economically is considered feasible and viable.

Conclusion and future works

A detailed thermal performance of the most two mature concentrating solar power technologies in the integrated solar combined cycle (ISCC) has been carried out under Algerian climate. These two solar thermal plants are the ISCC-PTC based on the integration of a parabolic trough collector (PTC) technology into the combined cycle (CC) and the ISCC-SPT is a novel hybridization of the solar power tower (SPT) system with a CC. An economic assessment for such solar projects is completed to demonstrate their technical feasibility and viability.

The modeling of these two ISCC plants is based on MATLAB programming. A developed code for each subsystem include solar system, gas turbine and steam cycle is carried out and run with the global program to analyze and simulate the performance of the present solar thermal power plants under the Hassi R'mel weather conditions located in the Algeria desert.

The thermal analysis of the ISCC-PTC system based on Hassi R'mel configuration exhibits high thermal performances efficiency during the day when the solar radiation is available and reaches a value of 59% which is much higher than night when it is working as a CC. At this point, the electricity generation corresponds to a value of 150.5 MW much higher than the produced value during night while the plant works as a CC. The economic assessment of such project is crucial to demonstrate its technical feasibility since it is registered among the ambitious renewable energy program of Algeria at the horizon 2030 for future installations. It is found that when considering the environment cost effect the ISCC-PTC system becomes competitive with a levelized cost of energy (LCOE) equals to 0.0222 $/kWh which is about 20 % higher than for CC and allows also to make save in fuel consumption about 18.45 million $ through 30 years of operation with reducing 0.89 million ton of CO_2 rejected.

The second ISCC plant is a new configuration of integrating a SPT technology to a CC to constitute the ISCC-SPT system. This proposed ISCC-SPT thermal plant offers some advantages compared to the solarized gas turbine: no modifications are required in GT or in the volumetric receiver to resist at pressure more than 15 bar since the exhaust gases from GT are at low pressure, the temperature difference across receiver is not too high, there is no need for another SSG and the use of a HRSG single-pressure level makes it simpler and less expensive compared with a multi-pressure levels HRSG. Its thermodynamic analysis shows high thermal performances, for a GT size of 30 MW and with the same heliostat solar field size of PS10 the overall thermal efficiency may reach up to 64.40 % and revealing a high production about 52.6MW. In addition, a good agreement in the solar energy conversion into electricity with an efficiency value of about 22 % when it is compared to PS10 power plant

working in solar-only plant. The economic analysis shows that the LCOE is about 0.0335 $/kWh and becomes competitive when the environmental issue is considered. While optimization is implemented to set the optimal design and parameters of the present proposed ISCC-SPT, the global thermal performances are improved and total cost is reduced. Consequently, The ISCC-SPT system permits an advantage of fuel saving about 7.07 Million $ and pollutant reduction to 0.33 Million ton during 30 years of operation.

The comparison analysis between these two different ISCC systems studied above which are ISCC-PTC and ISCC-SPT was carried out. The results allow concluding that instantaneous and annual performances of the proposed ISCC-SPT layout exhibits incontestable improvement in thermal performance efficiency mainly in solar-to-electric conversion when compared to that ISCC-PTC system. Furthermore, the economic analysis both power plants show approximately the same Levelized cost of energy (LCOE) of 0.0297$/kWh and 0.0269 $/kWh for ISCC-SPT and ISCC-PTC respectively.

We conclude integrating a CSP technology into a CC is the best way of converting solar radiation to electricity and reducing pollutant emissions. The cost of electricity produced by such solar thermal systems is competitive and demonstrates their technical feasibility. In addition, it is also known that, in an ISCC, the inefficiencies resulting from daily start-up and shut-down of steam turbines are eliminated. Consequently, more research and development activities have to be devoted to the development of the ISCC powered by PTC and SPT technologies where at the moment the PTC is the only proven CSP technology that has found the most application in the combined cycle hybridization with solar thermal technology.

It is possible that the ISCC system will dominate the giant electric generating industry in the near future; thereby we suggest some integrating techniques that should be improved like:

- Thermal energy storage (TES) could be an alternative to improve the solar share and increase the dispatchability of the ISCC system during the night or cloudy periods. TES converts the intermittent solar energy into a reliable, dispatchable resource, thus it becomes of great importance to design an efficient energy storage system while there are three main aspects that need to be considered in the design of a solar thermal energy storage system: technical properties, cost effectiveness and environmental impact.
- Incorporation of Kalina cycle in Rankine cycle of an ISCC could be as well a good solution to enhance the thermal performances of such system. The working fluid is a mixture of ammonia and water. The ammonia–water mixture has a varying boiling and condensing temperature instead of water, which has a constant boiling point.

During evaporation the mixing ratio of the binary working fluid changes because of the lower boiling temperature of ammonia which evaporates predominantly. Kalina cycle is generally used as a bottoming cycle to enhance energy conversion efficiency by recovering waste heat from exhaust gases are low-temperature heat sources that are not used efficiently. As the case, Kalina cycle could be used as the process to cool down more the exhaust gases from HRSG to enhance energy conversion efficiency by recovering waste heat from the exhaust gases as a result improving solar-to-electric efficiency. Therefore, investigation of such idea of integrating Kalina cycle into an ISCC is necessary in the further works.

References

[1] Goswami DY, Kreith F. Energy conversion. USA: Taylor & Francis Group; 2007.

[2] Okoroigwe E, Madhlopa A. An integrated combined cycle system driven by a solar tower: A review.Renewable and Sustainable Energy Reviews 2016 ;57:337–350.http://dx.doi.org/10.1016/j.rser.2015.12.092.

[3] Goswami DY, Zhao Y. Proceedings of ISES World Congress 2007. China: Springer; 2008.

[4] Zoschak RJ, Wu SF. Studies of the direct input of solar energy to a fossil fueled central station steam power plant. Solar Energy 1975;17:297-305. https://doi.org/10.1016/0038092X(75)90047-X

[5] Zachary J. Integrated solar combined cycle (ISCC) systems. USA: Bechtel Corp; 2013.

[6] Sun J, Liu Q, Hong H. Numerical study of parabolic-trough direct steam generation loop in recirculation mode: characteristics, performance and general operation strategy. Energy Conversion and Management 2015; 96:287–302. https://doi.org/10.1016/j.enconman.2015.02.080

[7] SolarPACES. Solar thermal electricity global outlook 2016. Available from https://www.solarpaces.org/solar-thermal-electricity-global-outlook-2016/; 2016 [accessed 07 May 2019].

[8] Izquierdo S, Montanes C, Dopazo C, Fueyo N. Analysis of CSP plants for the definition of energy policies: the influence on electricity cost of solar multiples, capacity factors and energy storage. Energy Policy 2010; 38:6215–6221. https://doi.org/10.1016/j.enpol.2010.06.009

[9] Teske S, Leung J, Crespo L, Bial M, Dufour E, Richter C. Solar thermal electricity: Global outlook 2016.

[10] Trieb F, Schillings C, O'Sullivan M, Pregger T, Hoyer-Klick C. Global potential of concentrating solar power. Berlin, Germany: Proceedings of the SolarPACES 2009.

[11] Brenna M, Foiadelli F, Roscia M, Zaninelli D. Evaluation of solar collector plant to contribute climate change mitigation. Singapore: In Proceedings of the IEEE international conference on sustainable energy technologies, ICSET. 2008.

[12] Philibert C. Technology roadmap: concentrating solar power. France: OECD/IEA; 2010.

[13] FirstGreen. Comparison of CSP technologies, https://firstgreenconsulting.wordpress.com/2012/06/04/comparison-of-csp-technologies/; 2012 [accessed 18 October 2018].

[14] CEC. California Energy Commission solar power plant licensing projects, http://www.energy.ca.gov/maps/renewable/Solar_Power_Plant_Licensing_Projects.pdf; 2014 [accessed 04 May 2017].

[15] Richter C, Teske S, Nebrera J. Concentrating solar power global outlook 09. Greenpeace International/European Solar Thermal Electricity Association (ESTELA)/IEA SolarPACES, Report; 2009.

[16] Tasbirul I, Nazmul H, A.B. Abdullah, R. Saidur. A comprehensive review of state-of-the-art concentrating solar power (CSP) technologies: Current status and research trends. Renewable and Sustainable Energy Reviews 2018 ;91:987–1018. https://doi.org/10.1016/j.rser.2018.04.097.

[17] Pavlović TM, Radonjić IS, Milosavljević DD, Pantić LS. A review of concentrating solar power plants in the world and their potential use in Serbia. Renewable and Sustainable Energy Reviews 2012 ;16:3891–902. https://doi.org/10.1016/j.rser.2012.03.042

[18] Peters M, Schmidt TS, Wiederkehr D, Schneider M. Shedding light on solar technologies—a techno economic assessment and its policy implications. Energy Policy 2011;39:6422–39. https://doi.org/10.1016/j.enpol.2011.07.045

[19] Santos-Alamillos FJ, Pozo-Vázquez D, Ruiz-Arias JA, Von Bremen L, Tovar- Pescador J. Combining wind farms with concentrating solar plants to provide stable renewable power. Renewable Energy 2015; 76:539–50. https://doi.org/10.1016/j.renene.2014.11.055

[20] Sharma A. A comprehensive study of solar power in India and World. Renewable and Sustainable Energy Reviews 2011;15:1767–76. https://doi.org/10.1016/j.rser.2010.12.017

[21] Kaygusuz K. Prospect of concentrating solar power in Turkey: the sustainable future. Renewable and Sustainable Energy Reviews 2011;15:808–14. https://doi.org/10.1016/j.rser.2010.09.042

[22] CSP Projects Around the Worldhttps://www.solarpaces.org/csp-technologies/csp-projects-around-the-world/; 2020 [accessed 06 December 2021]

[23] Ummadisingu A, Soni M. Concentrating solar power–technology, potential and policy in India. Renewable and Sustainable Energy Reviews 2011 ;15:5169–75. https://doi.org/10.1016/j.rser.2011.07.040

[24] Kuravi S, Trahan J, Goswami DY, Rahman MM, Stefanakos EK. Thermal energy storage technologies and systems for concentrating solar power plants. Progress in Energy and Combustion Science 2013; 39:285–319. https://doi.org/10.1016/j.pecs.2013.02.001

[25] Nixon J, Dey P, Davies P. Which is the best solar thermal collection technology for electricity generation in north-west India? Evaluation of options using the analytical hierarchy process. Energy 2010 ;35:5230–40. https://doi.org/10.1016/j.energy.2010.07.042

[26] Liu M, Steven Tay NH, Bell S, Belusko M, Jacob R, Will G, et al. Review on concentrating solar power plants and new developments in high temperature thermal energy storage technologies. Renewable and Sustainable Energy Reviews 2016 ;53:1411–32. https://doi.org/10.1016/j.rser.2015.09.026

[27] Zhang W. Institut für Energiewirtschaft und Rationelle Energieanwendung. Concentrating solar power–state of the art, cost analysis and pre-feasibility study for the implementation in China. https://www.efchina.org/Attachments/Report/reports-efchina-20101222-2-en/Concentrating%20Solar%20Power%20-%20State%20of%20the%20Art,%20Cost%20Analysis%20and%20Pre-Feasibility%20Study%20for%20the%20Implementation%20in%20China.pdf; 2009 [accessed 18 October 2018].

[28] Steinmann W-D, Laing D, Tamme R. Latent heat storage systems for solar thermal power plants and process heat applications. J Sol Energy Eng 2010 ;132(2):021003. https://doi.org/10.1115/1.4001405

[29] SolarPACES. CSP projects around the world. Available from http://www.solarpaces.org/csp-technology/csp-projects-around-the-world; 2016 [accessed 07 May 2016].

[30] Mohamad A, Orfi J, Alansary H. Heat losses from parabolic trough solar collectors. International Journal of Energy Research 2014 ;38:20–8. https://doi.org/10.1002/er.3010

[31] Fernández-García A, Zarza E, Valenzuela L, Pérez M. Parabolic-trough solar collectors and their applications. Renewable and Sustainable Energy Reviews 2010 ;14:1695–721. https://doi.org/10.1016/j.rser.2010.03.012

[32] IEA. International Energy Agency Technology Roadmap – concentrating solar power. Available from https://www.iea.org/publications/freepublications/publication/csp_roadmap.pdf; 2010 [accessed 12 October 2016].

[33] Ab Kadir MZA, Rafeeu Y, Adam NM. Prospective scenarios for the full solar energy development in Malaysia. Renewable and Sustainable Energy Reviews 2010 ;14:3023–31. https://doi.org/10.1016/j.rser.2010.07.062

[34] Tyagi V, Kaushik S, Tyagi S. Advancement in solar photovoltaic/thermal (PV/T) hybrid collector technology. Renewable and Sustainable Energy Reviews 2012 ;16:1383–98. https://doi.org/10.1016/j.rser.2011.12.013

[35] Braun FG, Hooper E, Wand R, Zloczysti P. Holding a candle to innovation in concentrating solar power technologies: a study drawing on patent data. Energy Policy 2011 ;39:2441–56. https://doi.org/10.1016/j.enpol.2011.02.008

[36] Cavallaro F. Multi-criteria decision aid to assess concentrated solar thermal technologies. Renewable Energy 2009 ;34:1678–85. https://doi.org/10.1016/j.renene.2008.12.034

[37] Manzolini G, Giostri A, Saccilotto C, Silva P, Macchi E. Development of an innovative code for the design of thermodynamic solar power plants part A: code description and test case. Renewable Energy 2011 ;36:1993–2003. https://doi.org/10.1016/j.renene.2010.12.027

[38] https://helioscsp.com/moroccos-noor-concentrated-solar-power-projects-support-africas-energy-transition/ [accessed 27 April 2021].

[39] https://www.solarpaces.org/csp-technologies/csp-potential-solar-thermal-energy-by-member-nation/egypt/ [accessed 27 April 2021].

[40] El Gharbi N, Derbal H, Bouaichaoui S, Said N. A comparative study between parabolic trough collector and linear Fresnel reflector technologies. Energy Procedia 2011 ;6:565–572. doi.org/10.1016/j.egypro.2011.05.065

[41] Chemisana D. Building integrated concentrating photovoltaics: a review. Renewable and Sustainable Energy Reviews 2011 ;15:603–611. https://doi.org/10.1016/j.rser.2010.07.017

[42] Zhang H, Baeyens J, Degrève J, Cacères G. Concentrated solar power plants: review and design methodology. Renewable and Sustainable Energy Reviews 2013 ;22:466–481. https://doi.org/10.1016/j.rser.2013.01.032

[43] Kalogirou SA. Solar thermal collectors and applications. Progress Energy and Combust Science 2004 ;30:231–95. https://doi.org/10.1016/j.pecs.2004.02.001

[44] Müller-Steinhagen H, Trieb F, Trieb F. Concentrating solar power: a review of the technology. http://www.dlr.de/tt/Portaldata/41/Resources/dokumente/institut/system/publications/Concentrating_Solar_Power_Part_1.pdf⟩; 2004 [accessed 16 October 2016].

[45] STELA. Fresnel collector – PSA. Available from http://www.stelaworld.org/ linear-fresnel reflectors/; 2018 [accessed 25 March 2019].

[46] Behar O, Khellaf A, Mohammedi K. A review of studies on central receiver solar thermal power plants. Renewable and Sustainable Energy Reviews 2013 ;23:12–39. https://doi.org/10.1016/j.rser.2013.02.017

[47] Brakmann G, Aringhoff R, Geyer M. ESTIA, Brussels: Greenpeace International, Amsterdam, IEA SolarPACES Implementing Agreement. Concentrated solar thermal power – now! http://www.preppers.info/uploads/ Concentrated-Solar-Thermal-Power.pdf; 2005 [accessed 04 May 2017].

[48] USDOE. Office of Energy Efficiency & Renewable Energy concentrating solar power. http://energy.gov/eere/sunshot/concentrating-solarpower; 2016 [accessed 16 October 2016].

[49] Richter P, Frank M, Ábrahám E. Multi-Objective Optimization of Solar Tower Heliostat Fields. In Conference. Italy: European Consortium for Mathematics in Industry (ECMI); 2016. DOI:10.1007/978-3-319-23413-7_107

[50] SolarPACES. SolarPACES technology characterization solar dish systems. http://www.solarpaces.org/images/pdfs/solar_dish.pdf; 2016 [accessed 10 October 2016].

[51] Poullikkas A, Kourtis G, Hadjipaschalis I. Parametric analysis for the installation of solar dish technologies in Mediterranean regions. Renewable and Sustainable Energy Reviews 2010 ;14:2772–83. https://doi.org/10.1016/j.rser.2010.07.021

[52] Solar M. Tessera Solar North America. Available from http://www.mortenson.com/solar/projects/maricopa-solar; 2018 [accessed 25 March 2019].

[53] Milow B, Trieb F. State of the art 2000: Solar thermal power stations. Germany, 2000.

[54] Goswami DY, Kreith F, Kreider J. Principles of Solar Engineering. USA, Philadelphia, PA: Taylor & Francis; 2000.

[55] Price H, Lüpfert E, Kearney D, Zarza E, Cohen G., Gee R, Mahoney R. Advances in parabolic trough solar power technology. Journal of Solar Energy Engineering, Transactions of the ASME 2002;124(2):109–125. https://doi.org/10.1115/1.1467922.

[56] Geyer M, Lüpfert E, Osuna R, Esteban A, Schiel W, Schweitzer A, Zarza E, Nava P, Langenkamp J, Mandelberg E. EUROTROUGH-Parabolic Trough Collector Developed for Cost Efficient Solar Power Generation. Zurich, Switzerland In Proceedings 11th SolarPACES Int. Symp. Conc. Solar Power and Chemical Energy Technologies, September, Sept 4-6, 2002.

[57] Thirumalai NC, Ramaswamy MA, Srilakshmi G, Badri VV, Rao S. Global review of solar tower technology. India: CSTEP; 2014.

[58] Pfahl A, Coventry J, Roger M. Progress in heliostat development. Solar energy 2017 ;152:3-37. doi.org/10.1016/j.solener.2017.03.029

[59] Report Article: The Solar Tower Julich -A research and demonstration plant for central receiver systems.

[60] European Commission Report: Solar hybrid gas turbine electric power system

[61] Steinmann W-D, Eck M. Buffer storage for direct steam generation. Solar Energy 2006 ;80: 1277–1282. https://doi.org/10.1016/j.solener.2005.05.013

[62] Tian Y, Zhao CY. A review of solar collectors and thermal energy storage in solar thermal applications. Applied Energy 2013 ;104: 538–553. https://doi.org/10.1016/j.apenergy.2012.11.051

[63] http://www.nrel.gov/csp/solarpaces/project_detail.cfm/projectID=246.

[64] Quero M, Korzynietz R, Ebert M , Jiménez AA , del Río A , Brioso JA. Solugas–Operation experience of the first solar hybrid gas turbine system at MW scale. Energy Procedia 2014 ;49:1820–1830. doi: 10.1016/j.egypro.2014.03.193

[65] Augsburger G. Thermo-economic optimisation of large solar tower power, PhD Dissertation, Ecole Polytechnique Fédérale de Lausanne; 2013. 10.5075/epfl-thesis-5648

[66] del Río A, Korzynietz R, Brioso JA, Gallasa M, Ordóñez I, Quero M. Soltrec - Pressurized volumetric solar air receiver technology. Energy Procedia 2015 ;69:360–368. doi: 10.1016/j.egypro.2015.03.042

[67] Drouot LP, Hillairet MJ. Themis program and the 2500-kW Themis solar power station at Targasonne. *J. Sol. Energy Eng*. 1984 ;106(1):83-89. doi:10.1115/1.3267567.

[68] Bezian JJ. Themis solar power plant first evaluation results. Proceedings of the Ninth Biennial Congress of the International Solar Energy Society 1986 ;1408-1412 . https://doi.org/10.1016/B978-0-08-033177-5.50269-6

[69] Can Gülen S. Second Law Analysis of Integrated Solar Combined Cycle Power Plants. J. Eng. Gas Turbines Power. 2015 ;137(5): 051701. https://doi.org/10.1115/1.4028741.

[70] Kalogirou S.A. A detailed thermal model of a parabolic trough collector receiver. Energy 2012 ; 48:298-306. http://dx.doi.org/10.1016/j.energy.2012.06.023

[71] Tzivanidis C, Bellos E, Korres D, Antonopoulos K.A, Mitsopoulos G. Thermal and optical efficiency investigation of a parabolic trough collector. Case Studies in Thermal Engineering 2015; 6:226–237. http://dx.doi.org/10.1016/j.csite.2015.10.005

[72] Agagna B, Smaili A, Behar O. An improved model for predicting the performance of parabolic trough solar collectors. International Journal of Energy Research 2018 ;42: 4512-4521. https://doi.org/10.1002/er.4165

[73] Agagna B, Smaili A, Falcoz Q, Behar O. Experimental and numerical study of parabolic trough solar collector of MicroSol-R tests platform. Experimental Thermal and Fluid Science 2018; 98:251-266. https://doi.org/10.1016/j.expthermflusci.2018.06.001

[74] Binotti M, Zhu G, Gray A, Manzolini G, Silva P. Geometric analysis of three-dimensional effects of parabolic trough collectors. Solar Energy 2013 ; 88:88–96. http://dx.doi.org/10.1016/j.solener.2012.10.025

[75] Giostri A, Binotti M, Silva P, Macchi E, Manzolini G. Comparison of Two Linear Collectors in Solar Thermal Plants: Parabolic Trough Versus Fresnel. *J. Sol. Energy Eng*. 2013 ;135(1):011001. https://doi.org/10.1115/1.4006792

[76] M.H Ahmed, M Rady, Amin A.M.A, Montagnino F.M, Paredes F, Comparison of thermal and optical performance of Linear Fresnel and Parabolic Trough Concentrator. Italy: 4th International Conference on Renewable Energy Research and Applications (ICRERA) ; 2015. DOI: 10.1109/ICRERA.2015.7418488

[77] Herrmann U, Kelly B, Price H. Two-tank molten salt storage for parabolic trough solar power plants. Energy 2004 ;29:883–893. doi:10.1016/S0360-5442(03)00193-2.

[78] Kumaresan G, Sridha R, Velraj R. Performance studies of a solar parabolic trough collector with a thermal energy storage system. Energy 2012 ;47:395-402.http://dx.doi.org/10.1016/j.energy.2012.09.036

[79] Sivaram P.M, Nallusamy N, Suresh M. Experimental and numerical investigation on solar parabolic trough collector integrated with thermal energy storage unit. Int. J. Energy Res. 2016 ;1564-1575. https://doi.org/10.1002/er.3544

[80] Bataineh K, Gharaibeh A. Optimal design for sensible thermal energy storage tank using natural solid materials for a parabolic trough power plant. Solar Energy 2018 ;171:519–525. https://doi.org/10.1016/j.solener.2018.06.108.

[81] Boukelia T.E, Mecibah M.S. Parabolic trough solar thermal power plant: Potential, and projects development in Algeria. Renewable and Sustainable Energy Reviews 2013 ;21:288–297. http://dx.doi.org/10.1016/j.rser.2012.11.074.

[82] Al-Maliki W.D K, Alobaid F, Starkloff R, Kez V, Epple B. Investigation on the dynamic behaviour of a parabolic trough power plant during strongly cloudy days. Applied Thermal Engineering 2016 ;99:114-132. https://doi.org/10.1016/j.applthermaleng.2015.11.104

[83] Alsagri A.S. Energy performance enhancement of solar thermal power plants by solar parabolic trough collectors and evacuated tube collectors-based preheating units. Int J Energy Res. 2020 ;44:6828-6842. https://doi.org/10.1002/er.5431

[84] Dersch J, Geyer M, Geyer M, Herrmann U, Jones SA, Kelly B, Kistner R, Ortmanns W, Pitz-Paal R, Price H.; 2004. Trough integration into power plants-a study on the performance and economy of integrated solar combined cycle systems. Energy 2004 ;29:947–959. Doi:10.1016/S0360-5442(03)00199-3

[85] Montes MJ, Rovira A, Muñoz M, Martínez-Val JM.; 2011. Performance analysis of an integrated solar combined cycle using direct steam generation in parabolic trough collectors, Applied Energy 2011 ;88:3228–3238. doi:10.1016/j.apenergy.2011.03.038.

[86] Antonanzas J, Jimenez E, Blanco J, Antonanzas-Torres F. Potential solar thermal integration in Spanish combined cycle gas turbines, Renewable and Sustainable Energy Reviews 2014 ;37:36–46. doi.org/10.1016/j.rser.2014.05.006.

[87] Zhu G, Neises T, Turchi C, Bedilion R.; 2015. Thermodynamic evaluation of solar integration into a natural gas combined cycle power plant. Renewable Energy 2015 ;74:815–824. doi.org/10.1016/j.renene.2014.08.073.

[88] Nezammahalleh H, Farhadi F, Tanhaemami M.; 2010. Conceptual design and techno-economic assessment of integrated solar combined cycle system with DSG technology. Solar Energy 2010 ;84:1696–1705. DOI:10.1016/j.solener.2010.05.007.

[89] Behar O, Khellaf A, Mohammedi K, Ait-Kaci S. A review of integrated solar combined cycle system (ISCCS) with a parabolic trough technology. Renewable and Sustainable Energy Reviews 2014 ;39:223–250. http://dx.doi.org/10.1016/j.rser.2014.07.066.

[90] Derbal-Mokrane H, Bouaichaoui S, El Gharbi N, Belhamel M, Benzaoui A. Modeling and numerical simulation of an Integrated Solar Combined Cycle System in Algeria. Procedia Engineering 2012 ;3:199 – 208. https://doi.org/10.1016/j.proeng.2012.01.1194

[91] Behar O, Kellaf A, Mohamedi K, Belhamel M. Instantaneous performance of the first Integrated Solar Combined Cycle System in Algeria. Energy Procedia 2011 ;6:185–193. https://doi.org/10.1016/j.egypro.2011.05.022.

[92] Rovira A, Montes MJ, Varela F, Gil M. Comparison of heat transfer fluid and direct steam generation technologies for integrated solar combined cycles. Applied Thermal Engineering 2013 ;52:264-274. DOI: 10.1016/j.applthermaleng.2012.12.008.

[93] Franchini G, Perdichizzi A, Ravelli S, Barigozzi G. A comparative study between parabolic trough and solar tower technologies in Solar Rankine Cycle and Integrated Solar

Combined Cycle plants. Solar Energy 2013 ;98:302-314. doi.org/10.1016/j.solener.2013.09.033.

[94] Abdel-Dayem AM, Metwally MN, Alghamdi AS, Marzouk EM. Numerical simulation and experimental validation of integrated solar combined power plant. Energy Procedia 2014 ;50:290 – 305. DOI: 10.1016/j.egypro.2014.06.036.

[95] Aldali Y, Morad K. Numerical simulation of the integrated solar/North Benghazi combined power plant. Applied Thermal Engineering 2016 ;108:785–792. doi.org/10.1016/j.applthermaleng.2016.07.178.

[96] Price H, Kearney D.; 2003. Reducing the cost of energy from parabolic trough solar power plants, National Renewable Energy Laboratory. USA: NREL/CP-550-33208; 2003.

[97] Horn M, Fuhring H, Rheinlander J. Economic analysis of integrated solar combined cycle power plants. Energy 2004 ;29:935–945. Doi: 10.1016/S0360-5442(03)00198-1.

[98] Hosseini R, Soltani M, Valizadeh G. Technical and economic assessment of the integrated solar combined cycle power plants in Iran. Renewable Energy 2005 ;30:1541–1555. DOI:10.1016/j.renene.2004.11.005.

[99] Mokheimer EMA, Dabwan Y N, Habib M A. Optimal integration of solar energy with fossil fuel gas turbine cogeneration plants using three different CSP technologies in Saudi Arabia. Journal of Applied Energy 2017 ;185(2,1):1268-1280. https://doi.org/10.1016/j.apenergy.2015.12.029

[100] Duan L, Qu W, Jia S, Feng T. Study on the integration characteristics of a novel integrated solar combined cycle system. Energy 2017 ;130 :351–364, http://dx.doi.org/10.1016/j.energy.2017.04.118.

[101] Li Y, Xiong Y.; 2018. Thermo-economic analysis of a novel cascade integrated solar combined cycle system, Energy 2018 ;145:116–127. https://doi.org/10.1016/j.energy.2017.12.128.

[102] Achour L, Bouharkat M, Behar O. Performance assessment of an integrated solar combined cycle in the southern of Algeria. Energy Reports 2018 ;4:207–217. https://doi.org/10.1016/j.egyr.2017.09.003

[103] Abdelhafidi N, Yılmaz İ.H, Bachari N. An innovative dynamic model for an integrated solar combined cycle power plant under off-design conditions. Energy Conversion and Management 2020 ;220:113066. https://doi.org/10.1016/j.enconman.2020.113066.

[104] Temraz A, Alobaid F, Link J, Elweteedy A, Epple B. Development and Validation of a Dynamic Simulation Model for an Integrated Solar Combined Cycle Power Plant. Energies 2021; 14(11):3304. https://doi.org/10.3390/en14113304

[105] Wang G, Cao Y, Wang S, Chen Z, Hu P. Design and preliminary performance analysis of a novel solar-gas combined cycle system. Applied Thermal Engineering 2020 ;172:115184. https://doi.org/10.1016/j.applthermaleng.2020.115184

[106] Rovira A, Abbas R, Sánchez C, Muñoz M. Proposal and analysis of an integrated solar combined cycle with partial recuperation. Energy 2020 ;198:117379. https://doi.org/10.1016/j.energy.2020.117379

[107] Manesh MHK, Aghdam MH, Modabber HV, Ghasemi A, Talkhoncheh MK. Techno economic, environmental and emergy analysis and optimization of integrated solar parabolic trough collector and multi effect distillation systems with a combined cycle power plant. Energy 2021; X:122499. https://doi.org/10.1016/j.energy.2021.122499

[108] Zhang ZW, Sun J, Wang RL, Wei JJ. Comprehensive evaluation of integrated solar combined cycle system regarding fuel-savability under unified framework. Applied Thermal Engineering 2021; 199:117539. https://doi.org/10.1016/j.applthermaleng.2021.117539

[109] Dabwan YN, Pei G, Kwan TH, Zhao B. An innovative hybrid solar preheating intercooled gas turbine using parabolic trough collectors, Renewable Energy 2021; 179:1009-1026. https://doi.org/10.1016/j.renene.2021.07.057

[110] Besarati SM, Goswami DY. A computationally efficient method for the design of the heliostat field for solar power tower plant. Renewable Energy 2014 ;69:226-232.doi.org/10.1016/j.renene.2014.03.043.

[111] Lee H. J, Kim J. K, Lee S.N, Kang Y. H. Numerical study on optical performances of the first central-receiver solar thermal power plant in Korea. Journal of Mechanical Science and Technology 2016 ;30(4):1911-1921.doi.org/10.1007/s12206-016-0350-z.

[112] Eddhibi F, Ben Amara M, Balghouthi M, Guizani A. Design and analysis of a heliostat field layout with reduced shading effect in southern Tunisia. International Journal of Hydrogen Energy 2017 ;42:28973-28996.doi.org/10.1016/j.ijhydene.2017.07.217.

[113] Hoffschmidt B, Téllez F. M, Valverde A, Fernandez J, Fernandez V. Performance evaluation of the 200-kWth HiTRec-II open volumetric air receiver. Journal of Solar Energy Engineering 2003 ;125:87-94.DOI: 10.1115/1.1530627.

[114] Marcos M. J, Romero M, Palero S. Analysis of air return alternatives for CRS-type open volumetric receiver. Energy 2004 ;29:677-686.doi:10.1016/S0360-5442(03)00176-2.

[115] Hischier I, Pozivil P, Steinfeld A. Optical and thermal analysis of a pressurized-air receiver cluster for a 50 MWe solar power tower. Journal of Solar Energy Engineering 2015 ;137:1-7.DOI: 10.1115/1.4031210

[116] Schwarzbozl P, Buck R, Sugarmen C, Ring A, Crespo M. J. M, Altwegg P, Enrile J. Solar gas turbine systems: Design, cost and perspectives. Solar Energy 2006 ;80:1231-1240.doi:10.1016/j.solener.2005.09.007.

[117] Spelling J, Favrat d, Martin A, Augsburger G. Thermo-economic optimization of a combined-cycle solar tower power plant. Energy 2012 ;41:113-120. https://doi.org/10.1016/j.energy.2011.03.073

[118] Xu C, Wang Z, Li X, Sun F. Energy and exergy analysis of solar power tower plants. Applied Thermal Engineering 2011 ;31:3904-3913. doi:10.1016/j.applthermaleng.2011.07.038

[119] Luo Y, Lu T, Du X. Novel optimization design strategy for solar power tower plants. Energy Conversion and Management 2018 ;177:682–692. https://doi.org/10.1016/j.enconman.2018.09.089.

[120] Xu E, Wang Z, Wei G, Zhuang J. Dynamic simulation of thermal energy storage system of Badaling 1 MW solar power tower plant. Renewable Energy 2012 ;39:455-462. doi:10.1016/j.renene.2011.08.043

[121] Rovense F, Amelio A, Ferraro V, Scornaienchi N.M. Analysis of a Concentrating Solar Power Tower Operating with a Closed Joule Brayton Cycle and Thermal Storage. International Journal of Heat and Technology 2016 ;34(3):485-490. https://doi.org/10.18280/ijht.340319

[122] de la Beaujardiere J-F P. P, Reuter H. C.R, Klein S. A, Reindl D. T. Impact of HRSG characteristics on open volumetric receiver CSP plant performance. Solar Energy 2016 ;127:159-174. doi.org/10.1016/j.solener.2016.01.030.

[123] Yamani N, Khellaf A, Mohammedi K, Behar O. Assessment of solar thermal tower technology under Algerian climate. Energy 2017 ;126:444-460. doi.org/10.1016/j.energy.2017.03.022.

[124] Stein W H, Buck R. Advanced power cycles for concentrated solar power. Solar Energy 2017 ;152:91-105. doi.org/10.1016/j.solener.2017.04.054.

[125] Ma Z, Turchi CS, editors. Advanced supercritical carbon dioxide power cycle configurations for use in concentrating solar power systems. USA: In Proceedings of

Supercritical CO2 Power Cycle Symposium; 2011 May 24-25; NREL/CP-5500-50787; 2011.

[126] Wang K, He YL, Thermodynamic analysis and optimization of a molten salt solar power tower integrated with a recompression supercritical CO_2 Brayton cycle based on integrated modeling. Energy Conversion and Management 2017 ;135:336–350. http://dx.doi.org/10.1016/j.enconman.2016.12.085.

[127] Zhu HH, Wang K, He YL, Thermodynamic analysis and comparison for different direct-heated supercritical CO2 Brayton cycles integrated into a solar thermal power tower system. Energy 2017 ;140:144–157https://doi.org/10.1016/j.energy.2017.08.067.

[128] Kang Q, Dewila R, Degrève J, Baeyens J, Zhang H. Energy analysis of a particle suspension solar combined cycle power plant. Energy Conversion and Management 2018 ;163:292–303.https://doi.org/10.1016/j.enconman.2018.02.067.

[129] Li C, Zhai R, YangY, Patchigolla K, Oakey JE. Thermal performance of different integration schemes for a solar tower aided coal-fired power system. Energy Conversion and Management 2018 ;171:1237–1245.https://doi.org/10.1016/j.enconman.2018.06.064.

[130] Price H, Kearney K, Parabolic-Trough Technology Roadmap: A Pathway for Sustained Commercial Development and Deployment of Parabolic-Trough Technology. USA: ROADMAP WORKSHOP PARTICIPANTS; 1998.

[131] KRIBUS A, KRIBUS R, CAREY D, SEGAL A, KARNI J. A SOLAR-DRIVEN COMBINED CYCLE POWER PLANT. Solar Energy 1988 ;62(2):121-129. https://doi.org/10.1016/S0038-092X(97)00107-2.

[132] Heide S, Gampe U, Orth U, Beukenberg M, Gericke B, Freimark M, Langnickel U, Pitz-Paal R, Buck R, Giuliano S. Design and Operational Aspects of Gas and Steam Turbines for the Novel Solar Hybrid Combined Cycle SHCC. Power for Land, Sea, and Air. UK: Proceedings of ASME Turbo Expo 2010 June 14–18; 2010. https://doi.org/10.1115/GT2010-22124.

[133] Zare V, Hasanzadeh M. Energy and exergy analysis of a closed Brayton cycle-based combined cycle for solar power tower plants. Energy Conversion and Management 2016 ;128:227–237. http://dx.doi.org/10.1016/j.enconman.2016.09.080

[134] Zaversky F, Les I, Sorbet P, Sánchez M, Valentin B, Brau J, Siros F. The challenge of solar powered combined cycles-Providing dispatchability and increasing efficiency by integrating the open volumetric air receiver technology. Energy 2020 ;194:116796. https://doi.org/10.1016/j.energy.2019.116796.

[135] Khatoon S, Kim M. Performance analysis of carbon dioxide based combined power cycle for concentrating solar power. Energy Conversion and Management 2020 ;205:112416. https://doi.org/10.1016/j.enconman.2019.112416

[136] Behar O, Grange B, Flamant G. Design and performance of a modular combined cycle solar power plant using the fluidized particle solar receiver technology. Energy Conversion and Management 2020 ;220:113108. https://doi.org/10.1016/j.enconman.2020.113108

[137] Zoghi M, Habibi H, Chitsaz A, Shamsaiee M. Exergoeconomic and environmental analyses of a novel trigeneration system based on combined gas turbine-air bottoming cycle with hybridization of solar power tower and natural gas combustion. Applied Thermal Engineering 2021; 188:116610.

[138] Javadi MA, Abhari MK, Ghasemias R, Ghomashi H. Energy, exergy and exergy-economic analysis of a new multigeneration system based on double-flash geothermal power plant and solar power tower. Sustainable Energy Technologies and Assessments 2021; 47:101536. https://doi.org/10.1016/j.seta.2021.101536

[139] Boukelia TE, Arslan O, Bouraoui A. Thermodynamic performance assessment of a new solar tower-geothermal combined power plant compared to the conventional solar tower power plant, Energy 2021; 232:121109. https://doi.org/10.1016/j.energy.2021.121109

[140] Mokheimer EMA, Dabwan YN, Habib MA, Said SAM, Al-Sulaiman FA. Techno-economic performance analysis of parabolic trough collector in Dhahran, Saudi Arabia. Energy Conversion and Management 2014 ;86:622–633. http://dx.doi.org/10.1016/j.enconman.2014.06.023.

[141] Burkholder F, Kutscher C. Heat Loss Testing of Schott's 2008 PTR70 Parabolic Trough Receiver. USA: National Renewable Energy Laboratory; 2009.

[142] Mabrouk M.T, Kheiri A, Feidt M. A systematic procedure to optimize Integrated Solar Combined Cycle power plants (ISCCs). Applied Thermal Engineering 2018 ;136:97–107. https://doi.org/10.1016/j.applthermaleng.2018.02.098.

[143] Behar O, Khellaf A, Mohammedi K. A novel parabolic trough solar collector model – Validation with experimental data and comparison to Engineering Equation Solver (EES). Energy Conversion and Management 2015 ;106:268–281. http://dx.doi.org/10.1016/j.enconman.2015.09.045.

[144] Elmohlawy AE, Ochkova VF, Kazandzhan BI. Thermal performance analysis of a concentrated solar power system (CSP) integrated with natural gas combined cycle (NGCC) power plant. Case Studies in Thermal Engineering 2019 ;14:100458. https://doi.org/10.1016/j.csite.2019.100458.

[145] Elmohlawy AE, Kazanjan BI, Ochkov VF. Solar parabolic trough collector for hybrid thermal power generation plant under different weather conditions. 17th Conference of Power System Engineering, Thermodynamics and Fluid Mechanics. Czech Republic: AIP Conference Proceedings 13–14 June; 2018. https://doi.org/10.1063/1.5081635

[146] Horlock JH. Advanced gas turbine cycles. UK: Elsevier Science Ltd; 2003.

[147] Wilcock RC, Young JB, Horlock JH. The effect of turbine blade cooling on the cycle efficiency of gas turbine power cycles. Journal of Engineering for Gas turbines and Power 2005 ;127:109–120. https://doi.org/10.1115/1.1805549

[148] Razak AMY. Industrial gas turbines 'Performance and operability'. USA: Taylor & Francis Group; 2007.

[149] Kim TS, Ro ST. Comparative evaluation of the effect of turbine configuration on the performance of heavy-duty gas turbines. USA: International Gas Turbine and Aeroengine Congress and Exposition June 5-8; 1995. https://doi.org/10.1115/95-GT-334

[150] Wilcox M, Baldwin R, Garcia-Hernandez A, Brun K. Guideline for gas turbine inlet air filtration systems. USA: Gas Machinery Research Council Southwest Research Institute; 2010.

[151] Behar O. A novel hybrid solar preheating gas turbine. Energy Conversion and Management 2018 ;158:120–132. https://doi.org/10.1016/j.enconman.2017.11.043.

[152] Çengel AY. Introduction to Thermodynamics and Heat Transfer.2nd edition. USA: McGraw−Hill Primi; 2008.

[153] Barigozzi G, Bonetti G, Franchini G, Perdichizzi A, Ravelli S. SOLAR HYBRID COMBINED CYCLE PERFORMANCE PREDICTION: INFLUENCE OF GT MODEL AND SPOOL ARRANGEMENT. Turbine Technical Conference and Exposition. Denmark: Proceedings of ASME Turbo Expo 2012 GT2012 June 11-15; 2012. https://doi.org/10.1115/GT2012-68881

[154] Steam turbines for CSP plants. Germany: Siemens AG Energy Sector; 2011.

[155] Ganapathy V. Steam generators and waste heat boilers for process and plant engineers. USA: Taylor & Francis Group; 2015.

[156] Ganapathy V. Industrial boilers and heat recovery steam generators. USA: Marcel Dekker; 2003.

[157] National meteorological Office (ONM). 2014, Report, Algeria.

[158] Gueymard CA. A review of validation methodologies and statistical performance indicators for modeled solar radiation data: Towards a better bankability of solar projects.

Renewable and Sustainable Energy Reviews 2014 ;39:1024–34. https://doi.org/10.1016/j.rser.2014.07.117

[159] Duffie AJ, Beckman AW. Solar engineering of thermal processes. 2nd edition. New York: Wiley; 1991.

[160] Wong LT, Chow WK. Solar radiation model. Appl Energy 2001 ;69(3):191–224. https://doi.org/10.1016/S0306-2619(01)00012-5

[161] Geuymard CA. Direct solar transmittance and irradiance predictions with broadband models. Part I: detailed theoretical performance assessment. Solar Energy 2003 ;74:381–95. https://doi.org/10.1016/S0038-092X(03)00195-6

[162] ASHRAE. Handbook of HVAC Applications. USA: ASHRAE; 2007

[163] Geuymard CA. Direct solar transmittance and irradiance predictions with broadband models. Part II: validation with high-quality measurements. Solar Energy 2003 ;74:355–79. https://doi.org/10.1016/S0038-092X(03)00196-8

[164] Gueymard CA. Clear-sky irradiance predictions for solar resource mapping and large-scale applications: Improved validation methodology and detailed performance analysis of 18 broadband radiative models. Solar Energy 2012 ;86:2145–69. https://doi.org/10.1016/j.solener.2011.11.011

[165] Merich IE, Baghidja A, Boukelia T. Design and Performance Evaluation of Solar Gas Turbine Power Plant in South Western Algeria. International Journal of Renewable Energy Research 2014 ;4(1): 224-232.

[166] Noone CJ, Torrilhon M, Mitsos A. Heliostat field optimization: A new computationally efficient model and biomimetic layout. Solar Energy 2012 ;86:792–803. doi:10.1016/j.solener.2011.12.007.

[167] Tehrani SSM, Taylor RA. Off-design simulation and performance of molten salt cavity receivers in solar tower plants under realistic operational modes and control strategies. Applied Energy 2016 ;179:698–715. http://dx.doi.org/10.1016/j.apenergy.2016.07.032.

[168] Li X, Kong W, Wang Z, Chang C, Bai F. Thermal model and thermodynamic performance of molten salt cavity receiver. Renewable Energy 2010 ;35:981–988.doi:10.1016/j.renene.2009.11.017.

[169] Spelling J, Laumert B, Fransson T. Optimal Gas-Turbine Design for Hybrid Solar Power Plant Operation. J. Eng. Gas Turbines Power 2012 ;134:092301-1–092301-9. DOI: 10.1115/1.4006986.

[170] Fernández V. PS10: a 11.0-MWe Solar tower power plant with saturated steam receiver. Solúcar: Corporate presentation; 2002.

[171] Colzia F, Petrucci S, Manzolini G, Chacartegui R, Silva P, Campanari S, Sánchez D. Modeling on/off-design performance of solar tower plants using saturated steam. Proceedings of the ASME 2010. USA: 4th International Conference on Energy Sustainability; 2010. doi:10.1115/ES2010-90399.

[172] Meybodi MA, Beath AC. Impact of cost uncertainties and solar data variations on the economics of central receiver solar power plants: An Australian case study. Renewable Energy 2016 ; 93:510–524.doi.org/10.1016/j.renene.2016.03.016.

[173] Bakos GC, Parsa D. Techno-economic assessment of an integrated solar combined cycle power plant in Greece using line-focus parabolic trough collectors. Renewable Energy 2013 ;60:598–603.doi.org/10.1016/j.renene.2013.05.025.

[174] U.S. Energy Information Administration: Jun 25, 2019, https://www.eia.gov/naturalgas/monthly/pdf/table_03.pdf

[175] Sharma N, Siddhartha V. Stochastic techniques used for optimization in solar systems: A review. Renewable and Sustainable Energy Reviews 2012 ;16:1399–1411. doi:10.1016/j.rser.2011.11.019

[176] Koutroulis E, Kolokotsa D, Potirakis A, Kalaitzakis K. Methodology for optimal sizing of stand-alone photovoltaic/wind-generator systems using genetic algorithms. Solar Energy 2006 ;80:1072–1088. doi:10.1016/j.solener.2005.11.002

[177] Besarati SM, Goswami DY, Stefanakos EK. Optimal heliostat aiming strategy for uniform distribution of heat flux on the receiver of a solar power tower plant. Energy Conversion and Management 2014 ;84:234–243. doi.org/10.1016/j.enconman.2014.04.030

[178] Emmerich MT, Deutz AH. Tutorial on multi-objective optimization: fundamentals and evolutionary methods. Natural Computing 2018 ;17(3):585-609. doi.org/10.1007/s11047-018-9685-y

[179] Desalination and water resources: Renewable energy systems and desalination – volume III. UK: Eolss Publisher Co.Ltd; 2010.

[180] https://www.mathworks.com/

[181] Dersch J, Geyer M, Hermann U, Jones S.A, Kelly B, Kistner R, Ortmanns W, Pitz-Paal R, Price H. Solar Trough Integration Into Combined Cycle Systems. Proceedings of the ASME June 15-20. USA: Poceedings of SED2002: International Solar Energy Conference.; 2002. https://doi.org/10.1115/SED2002-1072

[182] Kurup P, Turchi CS. Parabolic Trough Collector Cost Update for the System Advisor Model (SAM). USA: National Renewable Energy Laboratory; 2015.

Appendix

A.1. Solar Radiation

Solar energy is in the form of electromagnetic radiation with the wavelengths ranging from about 0.3 μm (10^{-6} m) to over 3μm, which correspond to ultraviolet (less than 0.4 μm), visible (0.4 μm and 0.7 μm), and infrared (over 0.7μm); most of this energy is concentrated in the visible and the near-infrared wavelength range. The incident solar radiation, sometimes called insolation, is measured as irradiance, or the energy per unit time per unit area (kW/m^2) [1].

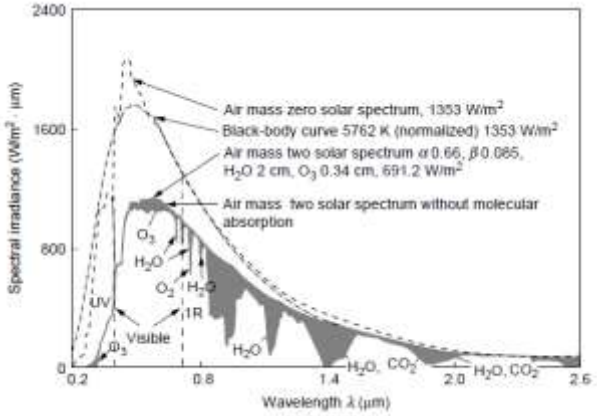

Figure A.1. Spectral distribution of solar energy at sea level [1]

It is useful to define a standard atmosphere clear sky and calculate the hourly and daily radiation that would be received on a horizontal surface under these standard conditions. (Hottel, 1976) has presented a method of estimating the beam radiation transmitted through a clear atmosphere and he introduced four climate types as in Table A.1. The atmospheric transmittance for beam radiation (τ_b) is given in an exponentially decreasing form depending on the altitude (α_s) and zenith angle (θ_z) as [1, 152]:

$$\tau_b = a + b \exp\left(-\frac{c}{\cos(\theta_z)}\right) \tag{A.1}$$

The estimations of constants a, b, and c for the standard atmosphere with 23 km visibility is given by:

$$a = \left(0.4237 - 0.00281\,(6 - {\alpha_s}^2)\right) a_0 \tag{A.2}$$

$$b = \left(0.5055 - 0.00595\,(6.5 - {\alpha_s}^2)\right) b_0 \tag{A.3}$$

$$c = \left(0.2711 - 0.01858\,(2.5 - {\alpha_s}^2)\right) c_0 \tag{A.4}$$

Where α_s is the altitude of the observer in kilometers. The correction factors a_o, b_o and c_o are given for four climate types in the flowing table:

Table A.1. Correction factors for four climate types

Climate type	a_0	b_0	c_0
Tropical	0.95	0.98	1.02
Midlatitude summer	0.97	0.99	1.02
Subarctic summer	0.99	0.99	1.01
Midlatitude winter	1.03	1.01	1.00

- The sun

The sun is a sphere of intensely hot gaseous matter with a diameter of 1.39 x 10^9 m. The sun is about 1.5 10^8 km away from earth, so, because thermal radiation travels with the speed of light in a vacuum (300,000 km/s), after leaving the sun solar energy reaches our planet in 8 min and 20 s. As observed from the earth, the sun disk forms an angle of 32 min of a degree. This is important in many applications, especially in concentrator optics, where the sun cannot be considered as a point source and even this small angle is significant in the analysis of the optical behavior of the collector. The sun has an effective black-body temperature of 5760 K. The temperature in the central region is much higher. In effect, the sun is a continuous fusion reactor in which hydrogen is turned into helium. The sun's total energy output is 3.8 x10^{20} MW, which is equal to 63 MW/m^2 of the sun's surface. This energy radiates outward in all directions. The earth receives only a tiny fraction of the total radiation emitted, equal to 1.7 x 10^{14} kW; however, even with this small fraction, it is estimated that 84 min of solar radiation falling on earth is equal to the world energy demand for one year (about 900 EJ). As seen from the earth, the sun rotates around its axis about once every four weeks [1, 152].

- Solar constant (I_{sc})

the solar constant denoted by I_{sc} is the energy from the sun per unit time received on a unit surface area perpendicular of the direction of propagation of radiation at the earth mean distance from the sun outside the atmosphere. The World Radiation Center has adapted a value of 1367 Watts per square meter, with an uncertainty of the order of 1% [1, 152].

- Extraterrestrial radiation (I_{so})

is the radiation that would be received in the absence of the atmosphere. The change in the extraterrestrial radiation can be caused by two sources: Variation in radiation emitted by the sun: there are conflicting reports in the literature on periodic variation of intrinsic solar

radiation. It has been suggested that there is small variation with different periodicities and variation related to sunspot activities. Hence, data from Nimbus and Mariner satellites over several months were used. For instance, (Hickey et al., 1982) during two years and a half found that the solar constant is decreasing slowly, at the rate of approximately 0.02% per year. In this research the solar constant is considered invariable [1, 152].

Variation of earth-sun distance: the earth rotates around the sun in an elliptical orbit. This movement results in variation in an earth-sun distance by 1.7%. Therefore, the extraterrestrial radiation varies in a range of ±3%. The change in I_{so} can be calculated by taking into account the astronomical facts according to the following approximation formula [1, 152]:

$$I_{so} = I_{sc}\left(1 + 0.033\cos\left(\frac{360\,n}{365}\right)\right) \quad (A.5)$$

Where n_j is the number of the day corresponding to a given date. It is defined as the number of days elapsed in a given year up to a particular date starting from 1 on 1 January to 365 on 31December.

- Direct normal irradiation (DNI)

Direct normal irradiation as described in figure A.2, is the amount of solar radiation received at any place on the earth directly from the sun without any disturbances. In practical terms, this is the radiation which creates sharp shadows of the subjects. There is no interference by dust, gas, and cloud or any other intermediate material on the direct solar radiation. Hence, the terrestrial solar radiation on a horizontal plane can be estimated as (Hottel,1976) [1, 152]:

$$DNI = I_{so}\tau_b\cos(\theta_z) \quad (A.6)$$

Where I_{so} and DNI are the extraterrestrial and terrestrial intensities of direct radiation. As shown in figure A.2, only the direct normal irradiation can be collected by the solar concentrators.

- Diffuse radiation (I_d)

the solar radiation component which has been scattered by the atmosphere.

- Terrestrial solar radiation **(**IT)

the sum of the beam and diffuse radiation at the surface of the earth is called terrestrial or global radiation. Its value at any location is roughly proportional to direct solar radiation, and varies with the geometry of the receiving surface. The other components, such as diffuse radiation, vary only slightly from slope to slope within a small area and the variations can be linked to slope gradient [1, 152]

$$I_{so} = DNI + I_d \quad (A.7)$$

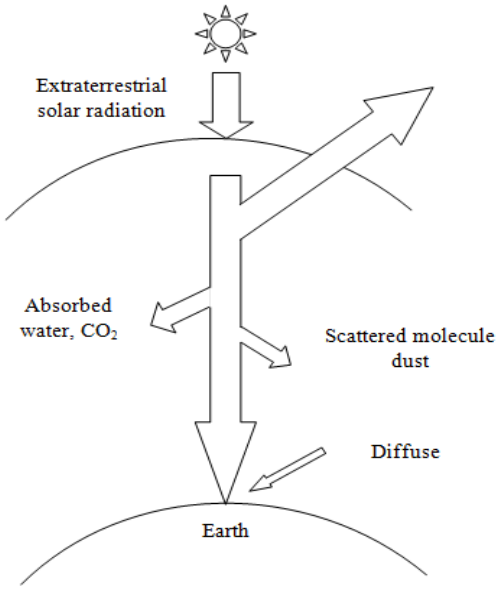

Figure A.2. Attenuation of solar radiation as it passes through the atmosphere

- Equation of Time

Due to factors associated with the earth's orbit around the sun, the earth's orbital velocity varies throughout the year, so the apparent solar time varies slightly from the mean time kept by a clock running at a uniform rate. The variation is called the equation of time (ET). The equation of time arises because the length of a day, that is, the time required by the earth to complete one revolution about its own axis with respect to the sun, is not uniform throughout the year. Over the year, the average length of a day is 24 h; however, the length of a day varies due to the eccentricity of the earth's orbit and the tilt of the earth's axis from the normal plane of its orbit. Due to the ellipticity of the orbit, the earth is closer to the sun on January 3 and furthest from the sun on July 4. Therefore the earth's orbiting speed is faster than its average speed for half the year (from about October through March) and slower than its average speed for the remaining half of the year (from about April through September). The values of the equation of time as a function of the day of the year (n) can be obtained approximately from the following equations:

$$E = 9.87 \sin(2B) - 7.53 \cos(B) - 1.5 \sin(B) \quad \text{(A.8)}$$

$$\text{with} \quad B = (n - 81)\frac{360}{364} \quad \text{(A.9)}$$

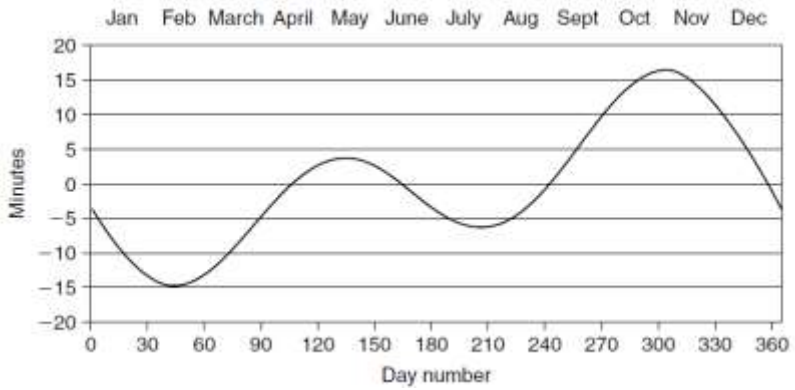

Figure A.3. Equation of time [1, 152].

- Solar time

Solar time (ST) is the time based on apparent angular motion of the sun across the sky. Solar noon is the time where the sun crosses the meridian of the observer. There is a difference between clock time and solar time which varies at any instant depending on the east-west displacement. The relation between the local standard time and the solar time is given by [1, 152]:

$$\mathrm{ST} = \mathrm{LST} + \mathrm{ET} \pm 4(\mathrm{SL} - \mathrm{LL}) - \mathrm{DS} \tag{A.10}$$

Where

LST: local standard time.

ET: Equation of time.

SL: Standard longitude.

LL: Local longitude.

DS: Daylight saving (it is either 0 or 60 min).

If a location is east of Greenwich, the sign of Eq. is minus (-), and if it is west, the sign is plus (+). If a daylight saving time is used, this must be subtracted from the local standard time. The term DS depends on whether day-light saving time is in operation (usually from end of March to end of October) or not. This term is usually ignored from this equation and considered only if the estimation is within the DS period.

- Hour angle (ω)

The angular displacement of the sun east or west of the local meridian due to rotation of the earth on its axis at 15 degrees per hour angle. It express the time of the day with respect to the solar noon. It can be expressed by [1, 152]:

$$\omega = 15^\circ\,(\text{solar time} - 12) \tag{A.11}$$

- Declination angle (**δ**)

The angle between the earth–sun line and the equatorial plane is called the declination angle which changes with the date and it is independent of the location. The declination is maximum 23°45'/ minimum -23°45' on the summer / winter solstice and 0° on the equinoxes as shown in figure A.4 [1, 152].

The declination angle can be calculated as [1, 152]:

$$\delta = 23.45 \sin\left(\frac{360(284 + n)}{365}\right) \tag{A.12}$$

It is also possible to consider the following expression for the accurate calculations of the declination angle in radians:

$$\delta = 0.006918 - 0.399912 \cos B + 0.07257 \sin B - 0.006758 \cos 2B + 0.000907 \sin 2B - 0.002697 \cos 3B + 0.00148 \sin 3B \tag{A.13}$$

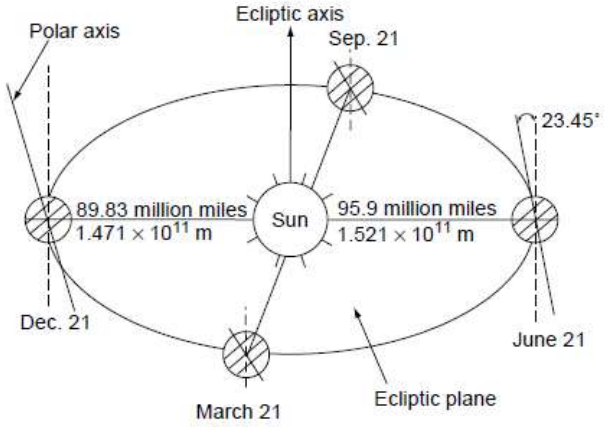

Figure A.4. Annual motion of the Earth around the sun [1].

- Earth's Eccentricity (ε)

It is desirable to have the distance and the earth's eccentricity in mathematical forms for simple calculations. Although a number of such forms are available of varying complexities, it is better to have simple and manageable expressions such as the one suggested by (Duffie and Beckman, 1991), who gave the eccentricity, ε, correction factor of the earth's orbit as [1, 152]:

$$\varepsilon = 1 + 0.033 \cos\left(\frac{360\ n}{365}\right) \tag{A.14}$$

The average distance between the sun and the earth is R = 150×10^6 km. Due to the eccentricity of the earth's orbit, the distance varies by 1.7%.

- Geographic locations

The basic angles that are necessary in the definition of the geographic locations are latitude and longitude [1, 152].

- Latitude (Φ)

Latitude is the angular distance measured along a meridian from the equator (north or south) to a point on the earth's surface. Any location towards the north (south) has positive (negative) latitude with maximum (minimum) degrees as +90° (−90°) in the north (south) pole [1, 152].

- Longitude (L_{loc})

Longitude is the angular distance measured from the prime (solar noon) meridian through Greenwich west or east to a point on the earth's surface. Any location west (east) of the prime meridian is positive (negative) location [1, 152].

- Sun position in the sky

The position of the sun can be calculated for any location and any time. Figure A.5 represents the angle to describe the position of the sun in the sky. Angles are described in the following way [1, 152]:

- Solar altitude angle (αs)

It is the angle between the projection of the sun's rays on the horizontal plane and the direction of the sun rays (the complement angle of the zenith angle).

- Solar zenith angle (θz)

It is the angle between the vertical and the line connecting to the sun.

- Solar azimuth angle (γs)

It is the angular displacement from the south of the projection of beam radiation on the horizontal plane.

- Sunrise and sunset of the sun

The sunrise and sunset times at for any date and location can be calculated, respectively, from the following equations [1, 152].

$$S_r = 12 - \left(\frac{\omega_s}{15}\right) \tag{A.15}$$

$$S_s = 12 + \left(\frac{\omega_s}{15}\right) \tag{A.16}$$

Where ω_s is the sunset hour angle in degrees. It is given by [1, 152]:

$$\omega_s = \cos^{-1}[-\tan\phi \tan(\delta)] \tag{A.17}$$

- Length of day

The number of daylight hours L_d can be calculated from the hour angle, since the hour angle changes by 15° every hour. The factor 2 results from taking into consideration morning and afternoon hours [1, 152].

$$L_d = \left(\frac{2}{15°}\right)\cos^{-1}[\tan\phi\tan(\delta)] \quad (A.18)$$

- Angles incidence on a plane

Angles describing the position of the surface in relation to the sun's rays and the earth are defined in this section and described by the figure A.5.

- Slop of the surface (β)

It is the angle between the plane of the surface and the horizontal plane.

- Surface azimuth angle (γ)

Surface azimuth angle is the angle made in the horizontal plane between the line due south and the projection of the normal to the surface on the horizontal plane. -180°< γ<+180°

- Angle of incidence (θ)

Angle of incidence is the angle between the beam radiation on a surface and the normal to that surface.

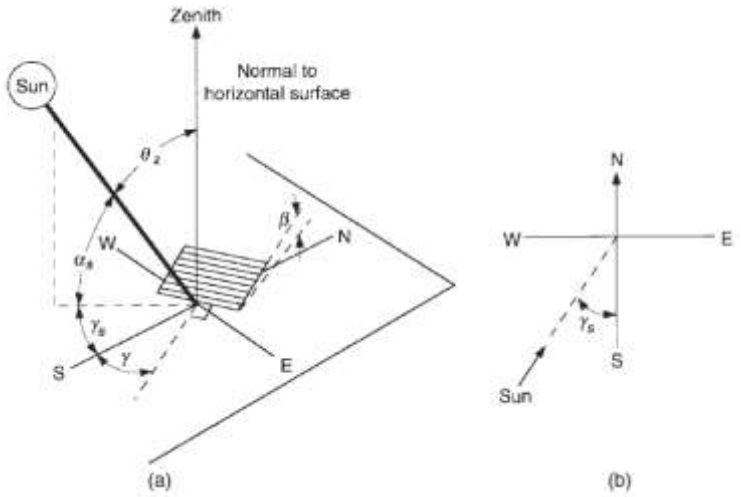

Figure A.5. (a) Zenith angle, slope, surface azimuth angle, and solar azimuth angle for a tilted surface. (b) Plan view showing solar azimuth angle [1, 152].

The relation between the angle of incidence, the solar position angles is given by [1, 152]:

$$\cos(\theta) = \sin(\delta)\sin(\phi)\cos\beta - \sin(\delta)\cos(\phi)\sin(\beta)\cos\gamma + \cos(\delta)\cos(\phi)\cos(\omega)\cos\beta + \cos(\delta)\sin(\phi)\sin(\beta)\cos(\omega)\cos(\gamma) + \sin(\omega)\sin(\beta)\sin(\gamma)\cos\delta \quad (A.19)$$

For horizontal surface β=0°, the incidence angle equal to the zenith angle.

$$\cos(\theta_z) = \cos(\delta)\cos(\phi)\cos(\omega) + \sin(\delta)\sin(\phi) \quad (A.20)$$

- Solar angles for tracking parabolic trough collector

Parabolic trough concentrators track the sun by moving prescribed ways to minimize the angle of incidence of beam radiation on their parabola and thus maximize the useful energy. Hence, the angle of incidence and the surface azimuth angle are needed.

Tracking system can drive the collector to rotate around a single axis or around two axes. For parabolic through collectors, horizontal east-west and north-south axes are usually used [1, 152].

- Horizontal east-west rotation axis

For collectors rotating about a horizontal east-west axis with continuous adjustment to minimize the angle of incidence [1, 152].

$$\cos(\theta) = \left(1 - \cos^2(\delta)\sin^2(\omega)\right)^{0.5} \quad (A.21)$$

This mode tracks the sun's position to achieve the optimum slope angle for the collector's aperture. The slope angle is given by [1, 152]:

$$\tan\beta = \tan(\theta_z)\cos(\gamma_s) \quad (A.22)$$

- Horizontal north-south rotation axis

For collectors rotated about a horizontal north-south axis with continuous adjustment to minimize the angle of incidence. The employed control system tracks the sun's position by this mode, to achieve the optimum slope angle for the collector's aperture. The optimum angle is given by [1, 152]:

$$\beta_{opt} = \tan^{-1}\left(\frac{\sin\omega\cos\delta}{\cos(\theta_z)}\right) \quad (A.23)$$

The angle of incidence can be expressed by:

$$\cos(\theta) = \sin\delta\sin\beta\sin\phi + \cos(\delta)\cos(\phi)\cos(\omega)\cos\beta + \sin(\beta)\cos\delta\sin\omega \quad (A.24)$$

The aperture turns towards the east before noon (γ =-90°) and turns towards the west after midday (γ =+90°). At midday (ω =0°) the collector aperture is in horizontal position ($\boldsymbol{\gamma}$ =0°).

The slop angle can also given be by the following expression [1, 152]:

$$\tan\beta = \tan(\theta_z)\cos(\gamma - \gamma_s) \quad (A.25)$$

In this case the incidence angle is:

$$\cos(\theta) = (\cos(\theta_z)^2 + \cos(\delta)^2\sin(\omega)^2)^{0.5} \quad (A.26)$$

The surface azimuth angle will be +90° or -90° depending on the sign of azimuth angle. i.e.

$$\text{if } \gamma_s > 0°, \gamma = +90°$$

$$\text{if } \gamma_s < 0°, \gamma = -90°$$